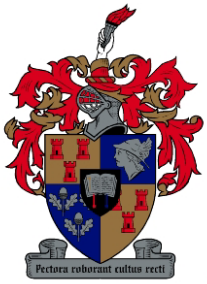

UNIVERSITEIT • STELLENBOSCH • UNIVERSITY

The Effect of the Crystalline State on the Properties of the Dative Bond

by

Gerhard Venter

Dissertation presented at the University of Stellenbosch for the degree of

Doctor of Philosophy

Department of Chemistry and Polymer Science
University of Stellenbosch
Private Bag X1, 7602 Matieland, South Africa

Promoter: Prof J. Dillen

December 2005

Declaration

I, the undersigned, hereby declare that the work contained in this dissertation is my own original work and that I have not previously in its entirety or in part submitted it at any university for a degree.

Signature: .....
G.A. Venter

Date: .....

Summary

Density functional theory (DFT) has been used to investigate the effect of the surrounding molecules on the structure of selected boron-nitrogen compounds. It was found that a very limited number of molecules, orientated according to the experimental crystal structure, are needed to successfully reproduce the large changes in structure witnessed when $HCN–BF_3$ and $CH_3CN–BF_3$ crystallises. Specifically, the addition of seven molecules shortens the B–N distance by 0.735 Å in $(HCN–BF_3)_8$ and 0.654 Å in $(CH_3CN–BF_3)_8$.

Accompanying the large changes in B–N bond length are equally large changes in the N–B–F angle. Investigation of the structure of these complexes in terms of localised electron pairs shows that the availability of lone pairs, in close proximity to the B–N bond axis, plays an important role in the bond change. Through delocalisation of the fluorine lone pairs the antibonding σ^*(B–N) orbital becomes increasingly occupied as the N–B–F angle lessens and vice versa.

Further, an investigation of the specific effects of dipole-dipole interactions was performed by applying uniform electric fields of varying strength along the donor-acceptor bond axis of a series of compounds of the form X–Y; X = H_3N, HCN, CH_3CN; Y = BF_3, BH_3, SO_3. All complexes investigated show sensitivity to the external electric field, however, only the compounds having nitrile donors and acceptors with fluorine atoms produce large changes, which in turn are dominated by a very sudden large change in B–N bond length occurring in a very narrow range of changing field strength. Analysis of the changes in bond character reveals that $HCN–BF_3$ and $CH_3CN–BF_3$ have long bonds in the gas phase, formed primarily through electrostatic interaction between the donor and acceptor. In the short bond in the condensed phase the bond character changes considerably through the introduction of strong electron sharing interactions, i.e. covalent or orbital interactions.

Fundamental changes in the nature of the bond, catalysed by surrounding molecules, thus lie at the heart of the large phase-dependent changes in these species.

Opsomming

'n Kohn-Sham elektrondigtheidsteorie (DFT) studie is gedoen op die effek van die omliggende molekules in die kristalstruktuur van sekere molekules wat boor-stikstof bindings bevat. Daar is gevind dat 'n klein aantal molekules, georienteer soos in die eksperimentele kristalstruktuur, benodig word om die groot veranderinge in stuktuur te veroorsaak wat eksperimenteel waargeneem word wanneer $HCN–BF_3$ en $CH_3CN–BF_3$ kristaliseer. Spesifiek, die byvoeging van sewe molekules verminder die B–N bindingslengte met 0.735 Å in $(HCN–BF_3)_8$ en 0.654 Å in $(CH_3CN–BF_3)_8$.

Die groot veranderinge in B–N bindingslengte gaan saam met ewe groot veranderinge in die N–B–F hoek. 'n Ondersoek van die struktuur van die molekules in terme van gelokaliseerde elektronpare wys dat die beskikbaarheid van alleenpare, wat naby die B–N bindingsas lê, 'n belangrike rol speel in the verandering in bindingslengte. Deur delokalisasie van die fluoor alleenpare word die antibindende σ^*(B–N) orbitaal toenemend beset soos die N–B–F hoek afneem en omgekeerd.

Verder is die spesifieke effek van dipool-dipool interaksies ondersoek deur uniforme elektriese velde aan te lê langs the donor-akseptor bindingsas van 'n reeks komplekse van die vorm X–Y; X = H_3N, HCN, CH_3CN; Y = BF_3, BH_3, SO_3. Al die komplekse toon sensitiwiteit teenoor die eksterne elektriese veld, maar net die verbindings wat nitriel akseptore en fluoor atome aan the donor fragmente het, toon groot veranderinge, wat op hulle beurt weer oorskadu word deur 'n skielike verandering in the B–N bindingslengte in 'n nou band van veranderende veldsterkte. Analise van die veranderinge in bindingskarakter toon dat $HCN–BF_3$ en $CH_3CN–BF_3$ lang bindings in die gasfase het, wat hoofsaaklik gevorm word deur elektrostatiese interaksies tussen die donor en akseptor fragmente. In die kort binding in die kristalfase is daar 'n aansienlike verandering in the karakter as gevolg van die intrede van sterk elektrondelingsinteraksies, m.a.w. kovalente of orbitaalinteraksies.

Fundamentele veranderinge in the manier wat die binding saamgestel word, wat gekataliseer word deur omliggende molekules, is dus die oorsaak van die groot faseafhanklike veranderinge.

Acknowledgements

My sincere gratitude to the following:

- My promoter, without whom not a single word would have been written.
- My parents, who always support me and never fail to produce a few words of encouragement.
- My colleagues in the chemistry department, for always being willing to give an opinion and providing an ear for a few thoughts.
- My friends, for their support and words of encouragement when my mood was perhaps not the best.
- Our computer-cluster administrator, who made the process of submitting a calculation a simple task.
- The National Research Foundation (NRF) and the University of Stellenbosch for their financial support
- The financial assistance of the Department of Labour (DoL) towards this research is hereby acknowledged. Opinions expressed and conclusions arrived at, are those of the author and are not necessarily to be attributed to the DoL.

Publications and Presentations

- A poster was presented at the 7th Congress of the World Association of Theoretically Oriented Chemists (WATOC) held from 16 to 21 January 2005 in Cape Town, South Africa. The poster was entitled *Effects of the Crystalline State on the Dative Bond.*
- A presentation was made at Indaba IV, Patterns in Nature, held from 17 to 22 August 2003 in Skukuza in the Kruger National Park, South Africa. The presentation was entitled *The Effect of the Solid State on the Nature of the Dative Bond*.
- Portions of the work from Chapter five were published as *Crystalline Effects on the Properties of the Dative Bond: A Computational Study of HCN–BF_3. J. Phys. Chem. A.*, **2004**, *108(40)*, 8378-8384.
- Another publication is being prepared containing portions of the work from Chapter six.

Contents

Chapter 1

Introduction

In the early 1990's, and mainly due to the work of Kenneth Leopold and his research group, gas phase structures became available which cast new light on our perception of the ability of the surroundings to stabilise structures in the condensed phase, in particular those with dative bonds. The idea of structural changes taking place upon phase change is in no way revolutionary. The changes observed under standard conditions however, are in the order of thousands of ångstroms and normally attributed to *crystal packing*.[1] The two most drastic examples of phase-dependent structural changes can be found in complexes with boron-nitrogen bonds, $HCN–BF_3$ and the related $CH_3CN–BF_3$. On going from the gas phase to the condensed phase, the former exhibits a 0.84 Å change in the B–N bond length, the latter a 0.38 Å change! The N–B–F angles also change considerably, by 14° and 10°, respectively. Large changes are also seen in other boron-nitrogen and sulphur-nitrogen adducts, but the bulk of this work revolves around $HCN–BF_3$ and $CH_3CN–BF_3$.

The initial aim of the study was to determine which specific effects in the crystalline state are responsible for the changes observed through experimental structure determination. The changes have predominantly been attributed to dipole-dipole interactions, mostly interacting over short distances. We wanted to investigate whether this was truly *the only* relevant effect. The study then proceeded to an investigation of the properties of the dative bond and how external effects, present in the crystalline state, lead to alterations in the way the bond is formed.

In the second chapter we give a brief summary of the literature on the subject of large changes between gas phase and condensed phase structures of the same compound. The changes revolve around the formation of so-called partially formed bonds in the gas phase and the majority of literature consists of studies on the partially formed bond and its significance.

The third chapter explains the nomenclature surrounding Lewis acids

and bases and contains some qualitative information on the relative strength of the donors and acceptors studied in this work.

Chapter four gives an introduction to computational chemistry. Much attention is given to the principles and theory behind the process of finding solutions to the time-independent Schrödinger equation within the restricted Hartree-Fock formalism by using single Slater determinants. Since this work utilises density functional theory (DFT), details of advanced techniques for the inclusion of electron correlation are skipped in favour of a discussion of DFT and its treatment of exchange and correlation energy. Basis sets and the associated nomenclature are briefly discussed. The final part of this chapter contains information on orbital-based analysis techniques of the wave function, atoms in molecules (AIM), natural population analysis (NPA) and atomic partial charges (an introduction in terms of Mulliken population analysis and information on deriving charges from the electrostatic potential).

The next two chapters contain the description and explanation of the studies done by us on the partially formed bond and related subjects. Chapter five explains our attempts to simulate the crystalline environment by explicitly including surrounding molecules. The chapter is started off by explaining some introductory tests done to probe the quality of the DFT exchange-correlational functional used in this work, the basis set, as well as the effect of the basis set superposition error (BSSE). Next, we thoroughly investigate the question of how many molecules are needed to catalyse the structural changes in $HCN–BF_3$ and $CH_3CN–BF_3$. The relationship between the changes in B–N bond length and the classical dipole-dipole interaction is determined for both $(HCN–BF_3)_n$ and $(CH_3CN–BF_3)_n$ as well as a complex that has been given a slightly similar treatment in published work, $(H_3N–BH_3)_n$. This is followed by an investigation of the effect of a single antiparallel molecule on the structure of $(HCN–BF_3)_2$. Finally, we give an explanation for the extreme basis set sensitivity of these systems.

The topic of chapter six is the effect of an external electric field on the dative bond in a series of representative complexes. An in-depth analysis is done on the bonding and resultant bonding changes in the complexes based primarily on AIM analysis and a study of the constitution and properties of the molecular orbitals (Kohn-Sham orbitals). A decomposition of the bonding energy of the isolated complexes into electrostatic, Pauli repulsion and orbital interaction is also done.

The final chapter contains a summary of the conclusions as well as suggestions for some future projects and questions that still need attention.

Chapter 2

Partially Formed Dative Bonds

2.1 Introduction

Every structural chemist is aware of the difference between bonded and nonbonded interactions. Chemical bond interactions arise from a sharing of electron pair density, resulting in covalent bonds, or because of strong electrostatics between fragments or atoms, resulting in ionic bonds. Nonbonded interactions occur between species or fragments that remain chemically distinct and occur over a much wider range of interaction distances. Using the sum of covalent bond radii of two atoms as well as the sum of the van der Waals radii, it seems a simple task to distinguish between these two interactions.

However, there exists still another type of bond, the dative bond. The simplest definition of the difference between covalent and dative bonds lies in their minimum energy rupture paths. Haaland[2] uses the example of H_3N–BH_3 and H_3C–CH_3. The covalent bond ruptures homolytically resulting in species with either net spin ($2H_3C\cdot$) or species with net charge ($H_3C:^{\ominus}$ and $CH_3^{\oplus}$). The dative bond ruptures heterolytically yielding either two species without net charge or spin ($H_3N:$ and BH_3), or two species with both net charge and net spin ($H_3N\cdot^{\oplus}$ and $BH_3\cdot^{\ominus}$).

Classification of bonds should not be taken as a trivial task as such. Just because the different classes have very distinct criteria, it does not exclude the possibility of bonds that lie in the intermediate range between bonded and nonbonded interaction. Examples of partially formed bonds existing in the condensed phase have been known in the crystallographic literature for some time.[3] However, species in the gas phase with partially formed bonds lying in this intermediate region have very low interaction energies, so low in fact, that they become influenced by the lattice energy when crystallising. Phase-dependent structural changes should thus occur in principle. This phenomenon was observed in perhaps its most drastic example when the microwave spectrum of HCN–BF_3 was determined in 1993[4] and com-

Table 2.1: Experimental structural data for selected boron-nitrogen and sulphur-nitrogen complexes.[a]

	Gas Phase			Solid State		
	r(B–N)	∠(NBX)	ref.[b]	r(B–N)	∠(NBX)	ref.[b]
$H_3N–BH_3$	1.658	104.7	8	1.564	113.3	9
$H_3N–BF_3$	1.673	[c]	10	1.60	107	11
$HCN–BF_3$	2.473	91.5	4	1.638	105.6	5
$CH_3CN–BF_3$	2.011	95.6	12	1.630	105.6	13
	Gas Phase			Solid State		
	r(S–N)	∠(NSO)	ref.[b]	r(S–N)	∠(NSO)	ref.[b]
$H_3N–SO_3$	1.957	97.6	14	1.771	102.5	15
$HCN–SO_3$	2.577	91.8	16	-	-	-[d]
$CH_3CN–SO_3$	2.466	92.0	16	-	-	-[d]

[a] Bond lengths in Ångstrom. Angles in degrees.
[b] Reference for experimental structure. [c] Not determined in experiment.
[d] Structures have not been obtained yet.

pared with the crystal structure.[5] This and other boron-nitrogen complexes will be discussed in the next section.

2.2 Large Gas-Solid Structure Differences

Table 2.1 lists a few complexes that show large structural changes upon phase change. The dative bond distance is shown, as well as the angle between this bond and the substituents on the acceptor atom. These are the two variables that change most in these complexes. Very good overviews and discussions of molecules that are only partially bound in the gas phase have been given by K. R. Leopold and coworkers.[6,7]

2.2.1 Boron-Nitrogen Adducts

The covalent bond radius of boron (0.70 Å) added to that of nitrogen (0.88 Å) is 1.58 Å.[17] Fully formed covalent bonds are thus expected to have a bond length in this region. The sum of van der Waals radii for boron and nitrogen is estimated as 2.91 Å by Leopold,[6] which is very close to the bond distance in the van der Waals complex $N_2–BF_3$ of 2.875 Å.[18] The two most striking examples of large structural changes are between two nitrogen-boron bonded species, $HCN–BF_3$ and $CH_3CN–BF_3$. In the former case the bond length decreases by 0.84 Å and in the latter the change is 0.38 Å! This is a remarkably large change and to date they remain the only two complexes showing a

phase-dependent change of this magnitude. The bond lengths of these complexes are 2.473 Å and 2.011 Å in the gas phase, which is clearly intermediate considering the lower bound of complete covalent interaction of 1.58 Å and the upper bound of van der Waals interaction of 2.875 Å.

The amine complex with BF_3, H_3N–BF_3, shows a comparatively small change. This bond is already very close to being fully formed in the gas phase, based on a comparison with the sum of covalent bond radii of boron and nitrogen. This complex has not been without its share of controversy, albeit due to experimental error. The crystal structure was determined in 1951, with a r(B–N) value of 1.60 Å.[11] The gas phase structure was determined in 1991 and a r(B–N) of 1.59 Å was established.[19] In 1994 Jonas and Frenking[20] did *ab initio* calculations on the molecule and found a boron-nitrogen distance of 1.68 $\pm$0.02 Å (the variation is due to different basis sets and correlation methods employed), which is considerably longer than the gas phase determination. Their calculations, together with the fact that the first determination was shorter than the crystal structure value, which would be a very unusual occurrence, prompted Fujiang *et al.*[10] to do a redetermination of the microwave structure. They found the gas phase bond to be 1.673 Å and the discrepancy from the first determination due to an underestimation of the experimental principal axis coordinate, z_B.

The borane acceptor equivalent complex, H_3N–BH_3, has a longer bond length than H_3N–BF_3 in the gas phase. This is not surprising since it is well established that BF_3 is a hard acid whereas BH_3 should be considered a soft acid.[21] In conjunction with the hard base NH_3 we thus expect a better and shorter interaction in H_3N–BF_3. In the solid state, the bond length changes by 0.094 Å in H_3N–BH_3 compared to 0.037 Å in H_3N–BF_3. This leads to a shorter condensed phase bond for the hard-soft interaction, compared to the hard-hard interaction. Once again, there was some controversy regarding the experimental structure determination, in this case, the crystal structure of H_3N–BH_3. It seems that in the first determination of the structure the assignment of the boron and nitrogen atoms was reversed. This was corrected in a neutron diffraction study by Klooster *et al.*[9]

Along with the change in dative bond length the hybridisation angle of the accepting moiety also changes significantly. The N–B–F angle in HCN–BF_3 and CH_3CN–BF_3 changes by 14° and 10°, respectively. Changes of similar order are witnessed for the other complexes (cf. Table 2.1). Upon some deeper thought, a change in these angles is not particularly surprising; simple chemical intuition and steric arguments suggest that the fluorine atoms should move away as the donor approaches. The magnitude of the change is the surprising effect. However, after some more consideration it should not really be. In the free adduct the hybridisation at the boron atom is sp^2, corresponding to a trigonal planar structure. Accompanying bond formation is a change to tetrahedral sp^3 hybridisation. It is thus foreseeable that

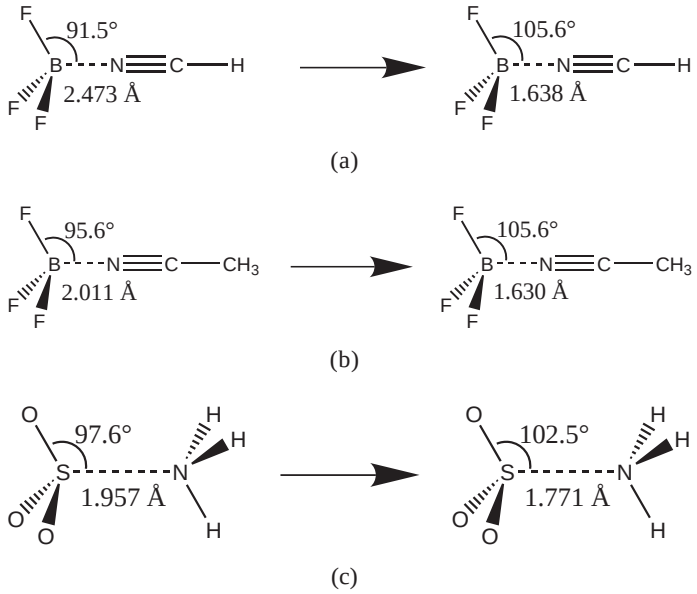

Figure 2.1: The structure of $HCN–BF_3$ (a, top), $CH_3CN–BF_3$ (b, middle) and $H_3N–SO_3$ as it progresses from the gas phase (left) to the crystal phase (right).

as the molecule progresses from the van der Waals limit to the covalent limit the hybridisation angle should also change considerably.

The structures of the borane complexes with acetonitrile and hydrogen cyanide have not been published to our knowledge in neither gas nor solid state, but several theoretical studies regarding their molecular structure have been published.[22–25]

2.2.2 Sulphur-Nitrogen Adducts

The S–N bond length in the amine complex with SO_3, $H_3N–SO_3$, shortens by 0.186 Å upon crystallisation. Although reference is made to $H_3N–SO_3$ as an amine-sulphurtrioxide complex it is in fact the zwitterionic form ($^+H_3N–SO_3^-$) of sulphamic acid ($H_2N–HSO_3$). Wong *et al.*[26] have shown that the zwitterionic form is 0.5 kcal.mol^{-1} less stable in the gas phase; however in the solid state the species crystallises as $^+H_3N–SO_3^-$. The N–S–O angle also changes by 4.9°.

The microwave structures of $HCN–SO_3$ and $CH_3CN–SO_3$ have been determined.[16] The hydrogen cyanide complex has the longer bond in the gas phase of the two, although the difference of 0.111 Å is much smaller than between the BF_3 acceptors with similar donors. Unfortunately, isolating the sulphurtrioxide complexes with nitriles proves extremely difficult and no experimental structures are available.

Finally, just a word on the sum of covalent and van der Waals radii of ni-

trogen and sulphur. The sum of covalent bond radii of sulphur and nitrogen is 1.74 Å, which is very close to the 1.771 Å S–N bond length in solid H_3N–SO_3.[15] The van der Waals radius of sulphur depends on its oxidation state, but using the Ar–S distance in Ar–SO_3 as 3.350 Å together with the standard van der Waals radii of argon (1.92 Å) and nitrogen (1.5 Å) one estimates a S–N van der Waals distance of 2.93 Å. These then provide the lower and upper bounds of interaction.

2.3 Computational Simulation of Crystalline Effects

Regarding the molecules in this study, two approaches have been identified in the literature for the simulation of crystalline effects: firstly, the molecule is optimised in the presence of a properly chosen solvent / medium, secondly, and to a much lesser extent, the surroundings are taken into account by explicitly adding the surrounding molecules. The first approach centres around the self-consistent reaction field (SCRF) method, which will be described in this section. The second approach is of course computationally much more intensive and is only feasible for smaller systems. It also has the advantage (disadvantage?) that it does not simulate one specific property of the crystal field, but rather imposes a total effect. Once the finer details of the exact nature of the bond changes have been established, it is possible to construct additional models which explicitly simulate the required effect.

2.3.1 Continuum Models

The effects of solvents on the energies of organic compounds can be related to the dielectric constant of the solvent, as long as specific solvent effects such as hydrogen bonding and donor-acceptor interactions (between solute and solvent) are not present. The Onsager reaction field model[27] is appropriate for such studies and has been incorporated into molecular orbital theory by Tapia and Goscinski.[28] In MO theory, the electrostatic solvent effect may be taken as an additional term, H_1, in the Hamiltonian of the isolated molecule, H_0,

$$H_{\mathrm{rf}} = H_0 + H_1$$

The perturbation term describes the coupling between the molecular dipole operator ($\hat{\mu}$) and the reaction field, $\mathbf{R}$,

$$H_1 = -\hat{\mu} \cdot \mathbf{R}$$

The reaction field (electric field) then is proportional to the molecular dipole moment. The implementation of this method is described by Wong *et al.*[29] In the self-consistent reaction field (SCRF) model the solvent is represented by a continuous dielectric, characterised by a given dielectric constant, ε. The solute is assumed to be embedded in a spherical cavity, with radius a_0, in

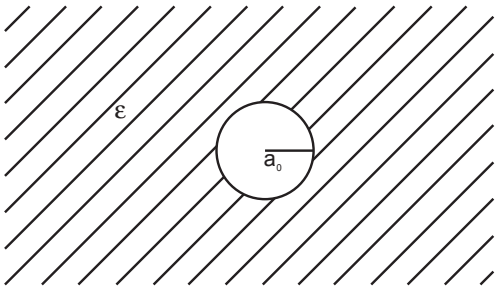

Figure 2.2: Onsager reaction field model. The solute is placed in a spherical cavity, with radius a_0, surrounded by a continuous medium of dielectric constant ε. *(Reproduced from Ref. 29. Copyright 1991 American Chemical Society)*

the medium. The permanent dipole of the solute will induce a dipole in the medium, which in turn will interact with the molecular dipole of the solute again, to lead to stabilisation (see Figure 2.2).

As mentioned previously, it is known through experiment that sulphamic acid ($H_2N–HSO_3$) prefers the zwitterionic form ($^+H_3N–SO_3^-$) in the solid state. After Hickling and Woolley[30] calculated a best S–N distance of 1.95 Å, which is still considerably longer than the experimental value (1.771 Å), the question arose whether the large difference is a basis set effect, due to inadequate electron correlation or a genuine medium effect. Wong *et al.*[26] investigated the effect of solvent on the stability of the neutral and the zwitterionic form using SCRF. Their first observation was the significant change occurring on going from 6-31G(d) to 6-31+G(d), i.e. inclusion of diffuse functions, and from 6-31G(d) to 6-31G(2d), i.e. adding an additional set of d-type polarisation functions. In both cases the S–N bond length reduces considerably. Electron correlation does not prove to be of similar significant importance. However, it was when the medium was introduced in calculations that they concluded this to be the major cause of the bond shortening. The calculated bond length is shortened by between 0.06 and 0.11 Å from the gas phase to condensed medium.

After the determination of the gas phase structures of $HCN–BF_3$ and the related $CH_3CN–BF_3$, Jiao and von Ragué Schleyer[31] did SCRF calculations on these systems. They obtained a separation of 2.63 Å in a nonpolar medium which shortens to 1.707 Å in a simulated $\varepsilon = 15$ medium. From $\varepsilon = 20 – 115$ neither the B–N separation nor the dipole moment changes significantly (see Figure 2.3). They thus attributed the bond shortening to the dipolar crystal field. Based on similar calculations on $N_2–BF_3$ they also concluded that the medium effects are dependent on the permanent dipole of the donor.

Theoretical calculations on the geometry of $H_3N–BH_3$ within the electric field of a surrounding solvent using the SCRF model predicts a B–N bond shortening from 1.66 Å for the isolated species to 1.62 Å in the presence of hexane and 1.57 Å in the presence of water.[32]

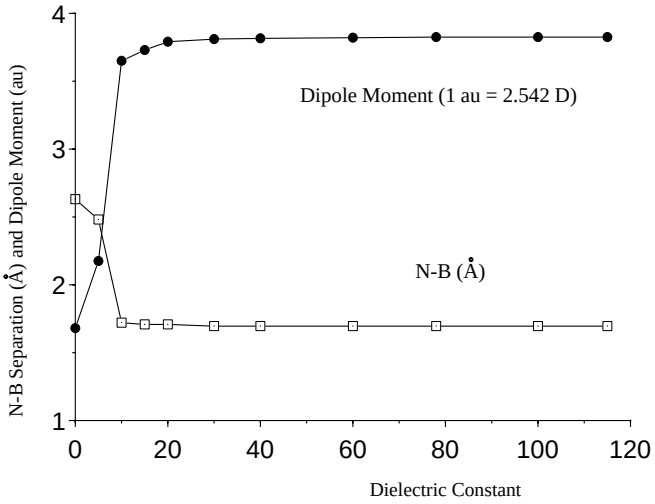

Figure 2.3: The B–N bond distance and dipole moment of HCN–BF_3 calculated as a function of the dielectric constant of the environment using SCRF theory. *(Reproduced from Ref. 31. Copyright 1994 American Chemical Society.)*

Despite the fundamental differences between the fixed and discrete lattice of a crystal and the variable changes of the solution phase, based on the success of the SCRF method, the continuum model seems to be a suitable representation of environmental effects in the crystal phase.

2.3.2 Explicit Molecular Models

One can also go about by explicitly adding the surrounding molecules. Jonas *et al.*[33] optimised a dimer and tetramer of H_3N–BH_3 and found that short range dipole-dipole interactions in the tetramer accounts for 60% of the shortening. Their monomer, dimer and tetramer bond lengths are 1.662 Å, 1.637 Å and 1.604 Å, respectively. A similar optimisation of dimeric H_3N–BF_3 shows a bond length decrease of 0.05 Å. It is worthwhile to note that they used structures that are stationary points on the isolated dimer and tetramer potential energy surfaces only (with symmetry restrictions) and their models do not necessarily reflect coordinates and molecular alignment in the crystal structure.

Dillen and Verhoeven[34] used large models consisting of 8, 10, 18, 20 and 30 molecules surrounding a H_3N–BH_3 molecule. The central molecule was optimised while the surrounding molecules, whose coordinates were taken from the crystal structure, were kept frozen. Whereas the clusters used by Jonas *et al.* were aligned specifically to maximize dipole-dipole interactions, in this work the molecular arrangement simulates the true crystal environment. Although the B–N bond shows a progressive decrease as the crystal model is

increased in size, the orientation of the surrounding molecules proves to be of critical importance. A clear relationship was found between the stabilising or destabilising nature of the dipole-dipole interactions and the B–N bond length. This was observed in the largest of the models, where the addition of 12 molecules to the 18 of a previous model, but not with a similar orientation, did not result in a shortening of the bond length. Calculations on artificially aligned molecular aggregates confirm this result. The authors concluded that short range dipole-dipole interactions are indeed of importance, but that the effect of long range interactions should not be underestimated.

Alongside each $HCN–BF_3$ molecule in the crystal structure lays an anti-parallel partner 3.8 Å away. This is an ideal orientation to maximize dipole-dipole interactions and this observation led to the attempt of Iglesias *et al.*[35] to determine whether only a single partner could account for the changes. Their MP2/6-31G** calculations produced a C_{2h} dimeric B–N bond length of 2.292 Å and seemed to suggest that a cooperative mechanism plays an important, yet not decisive, role. Another attempt at this was made by Cabaleiro-Lago and Ríos[36] two years later in 1998, using several different levels of theory. They calculated a minimum with MP2/6-31++G** which has a short B–N bond distance of 1.731 Å. Reoptimising this minimum at MP2/6-31G** resulted in a secondary, higher lying, minimum than the one reported by Iglesias, albeit with a shorter B–N bond of 1.82 Å. Severe basis set dependence is thus a property of this system. They concluded that most of the structural changes are due to a single nearest unit.

2.4 Mechanisms for Phase-Dependent Changes

A molecule distorts from its gas phase geometry if the interaction energy with its local environment in the condensed phase is sufficient to offset the energetic cost of the changes. The largest changes are thus expected in cases where the gas phase bond energy is the lowest. Indeed, Jonas *et al.*[33] determined a strong correlation between binding energies of donor-acceptor complexes and the difference between the *ab initio* gas phase bond lengths and and experimental crystal structure values. The most probable mechanism is related to an increase in molecular dipole moment of the adduct, which increases the interaction in a polar/polarisable medium and thus lowers the total energy.

Oh *et al.*[37] have obtained evidence for a dipolar enhancement mechanism in $(CH_3)_3N–SO_2$. They used the known crystal structure and *ab initio* calculations to show that the combination of a flat potential surface and a sharply rising dipole moment function could allow the dipole-dipole interaction energy in the solid to provide the energetic cost of contracting the S–N bond.

For $HCN–BF_3$ and $CH_3CN–BF_3$ a considerable increase in the molecular dipole is expected as the acceptor distorts from its initially planar geometry

to the tetrahedral structure in the adduct. Using the calculated dipole moment of HCN–BF_3 at the B–N separation distance in the crystal phase, 8.2 D, the interaction energy between two antiparallel molecules in the crystal is roughly 8.5 kcal.mol^{-1}.[38] The molar lattice energy, determined from a thermodynamic cycle and vapor pressure measurements of the crystal, is 23.7 kcal.mol^{-1}. This means that the dipole-dipole interaction energy between just two molecules in the crystal is more than one-third of the total molar lattice energy. This shows the dominance of nearest neighbours and raises the question: how many molecules are needed to simulate the total changes in the crystal phase?[6] The results of Jonas *et al.*[33] (for H_3N–BH_3 and H_3N–BF_3), Dillen and Verhoeven[34] (for H_3N–BH_3) and Cabaleiro-Lago and Ríos[36] (for HCN–BF_3) are pertinent to this question. Also, in this regard, the microwave spectrum of HCN$\cdots$HCN–BF_3 has been determined and shows that a single nearest neighbour causes a 0.174 Å contraction of the B–N bond.[39] Earlier, a similar determination of the microwave spectrum of HCN$\cdots$HCN–SO_3 showed a 0.107 Å decrease in the S–N bond, compared to isolated gas phase HCN–SO_3.[40]

2.5 Structure Correlation

Variations in structure among closely related compounds is not uncommon in the solid state.[3] Bürgi and Dunitz[41] performed a classic study by interpreting each structure within a range of similar compounds as providing a view of a particular bond type at a different stage of formation to map the transformations which take place during related chemical reactions.

It is possible to use the gas phase structures of related BF_3 and BH_3 acceptors in a similar approach as snapshots along the reaction path for the formation of B–N bonds in general. Dvorak *et al.*[12] was the first to do this by correlating r(B–N) with $\angle$(NBF) in a series of related compounds to obtain a measure of the response of the planar BX_3 donor to the approaching nitrogen donor (see Figure 2.4).

Hankinson *et al.*[38] have calculated the reaction paths for the formation of HCN–BF_3 and H_3N–BF_3. They compared the N–B–F angle as a function of the B–N distance with experimental data and found a reasonable agreement between the calculations and the experimental data. Both r(B–N) fixed and $\angle$(NBF) fixed optimisations were done. Following the approach of Eisenstein and Dunitz[42] and using parameters derived by Murray-Rust *et al.*[43,44] they showed that the correlation between r(B–N) and $\angle$(NBF) can be described by substituting the relationship between the N–B–F angle, α, and the B–N bond order, n,

$$n = 9\cos^2\alpha$$

into the empirical equation derived by Pauling[45] relating bond length and

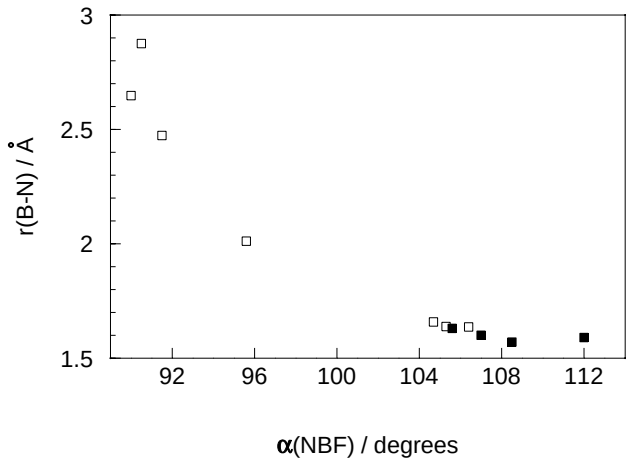

Figure 2.4: A plot of the B–N bond length vs the N–B–F (or N–B–H) angle for some addition complexes of BF_3 and BH_3 with nitrogen donors. Open squares represent gas phase data and solid squares correspond to crystallographic data. *(Reproduced from Ref. 12. Copyright 1992 Americal Chemical Society.)*

bond order,

$$r_n - r_1 = -c \log n$$

where r_n is the bond length of a bond with order n, r_1 is the bond length of a bond with order 1 and c is a constant to be determined for each system.

Burns *et al.*[16] extended this structure correlation to also include SO_3 acceptors and determined the constants in the equation for the bond length between donor, D= boron / sulphur, and nitrogen,

$$r(DN) = r_1(DN) + c_{DN} \log(9 \cos^2 \alpha)$$

For B–N bonds, $r_1(BN)$ = 1.580 Å and c_{BN} = -0.441 Å. For S–N bonds, $r_1(SN)$ = 1.621 Å and c_{SN} = -0.449 Å. A few specific remarks made by them regarding the difference between BF_3 and SO_3 acceptors are worth mentioning. For a given donor, the angular distortion of BF_3 exceeds that of the equivalent SO_3 complex. Considering that the bond distances in Ar–SO_3[46] and Ar–BF_3[47] are 3.350 Å and 3.325 Å and using the van der Waals radius of argon as 1.92 Å, the van der Waals radii of BF_3 and SO_3 are 1.4 Å, which is about equal to the nonbonded radii of fluorine and oxygen. They suggest that this means that in forming weak bonds it is the crown formed by the oxygens or fluorines that sets the contact distance. Finally, bond formation to SO_3 seems to lag behind that to BF_3, based on the location of similar donors on the correlation curves.

2.6 The Nature of Boron-Nitrogen and Sulphur-Nitrogen Interactions

The strength of computational chemistry lies in its ability to determine the nature of bonds and contributions from physically meaningful terms to the bonding.

The question of whether the changes to the structure are due to different minima on the potential energy surface (PES) has been investigated specifically for $HCN–BF_3$ by Hankinson *et al.*[38] and for $CH_3CN–BF_3$ by Giesen and Phillips.[48] These authors calculated potential energy curves for the r(B–N) coordinate. The $HCN–BF_3$ molecule shows a single minimum, whereas $CH_3CN–BF_3$ does indeed show two minima at 1.8 Å to 1.9 Å and at 2.2 Å to 2.3 Å, depending on the levels of theory and basis sets used. In all cases though, the PES is remarkably flat. Giesen and Phillips[48] also found that the longer minimum in $CH_3CN–BF_3$ is primarily an electrostatic interaction whereas the shorter minimum is a partial covalent bond.

In their study of 18 Lewis acid-base complexes Jonas *et al.*[33] concluded that, based on topological analysis of the electron density, the strongly bound complexes have significant covalent contributions to their dative bonds, whereas electrostatic contributions are responsible for the weakly bound complexes. They also concluded that there exists no correlation between the degree of charge transfer and strength of bond between complexes with different donors and acceptors and that a large covalent contribution to the bond does not necessarily constitute a strong bond! Wong *et al.*[49] found the sulphur-nitrogen bonds of SO_2 and SO_3 acceptors to be strongly ionic with significant charge transfer and little electron pair sharing. Jonas *et al.*[33] deduced similar results. In contrast to that of the other SO_3 acceptors studied in the literature, $H_3N–SO_3$ also has a considerably covalent bond, but electron pair sharing also plays a role.[26]

Mo and Gao[50] used an energy decomposition scheme developed by them which partitions Hartree-Fock interaction energy into geometry distortion, electrostatic, exchange repulsion, polarisation and charge transfer contributions.[51–53] They performed an extensive analysis on Lewis acid-base complexes of various nitrogen donors and sulphur and boron acceptors and found two main classes of compounds:

- Weakly bonded complexes, with interaction energies between 3 and 9 kcal.mol^{-1} and separations between 2.5 Å and 3.1 Å. Their binding character is primarily due to electrostatic interactions.

- Strongly interacting complexes, with interacting energies more than 20 kcal.mol^{-1} with shorter bond distances. Their binding character is mainly due to charge transfer and polarisation.

Chapter 3

Lewis Acids and Bases

3.1 Introduction

The nomenclature introduced by G. N. Lewis has become synonymous with donor-acceptor complexes. Also, some principles and previous work explaining dative bond strength may prove insightful to the reader before the results of this work is presented. Therefore, we will briefly state some Lewis acid-base definitions and take a look into general considerations of bond strength between donating and accepting species.

A discussion of hard and soft Lewis acids and bases (HSAB) will not be attempted. Many of the insights given by HSAB are based on frontier molecular orbitals (FMOs) consisting of the highest occupied molecular orbital (HOMO) of the donor and lowest unoccupied molecular orbital (LUMO) of the acceptor. However, in some cases HOMO-LUMO interactions do not provide a complete picture of the important factors in bonding. It is a very useful theory but we have opted to base our investigation on full molecular orbital calculations applied through density functional theory in conjunction with quantitative techniques of analysis. For our purposes merely stating the difference between hard and soft acids and bases and clearly distinguishing between them is appropriate. This is done in Tables 3.1 and 3.2. A very good discussion incorporating the method of choice in this work, density functional theory, was done by R. G. Pearson.[54]

3.2 Lewis Acids and Bases

3.2.1 Nomenclature

Lewis acid-base definitions provide a convenient terminology for the description of compounds containing a dative bond. Lewis first proposed the theory (it is more accurate to describe it as a set of terms with which to classify and define interacting species rather than a theory) by generalising the defin-

Table 3.1: Classification of hard and soft Lewis acids

Class I / Hard	Class II / Soft
H^+,Li^+,Na^+,K^+	Cu^+,Ag^+,Au^+,Hg^+,Hg^{2+}
Be^{2+},Mg^{2+},Ca^{2+},Sr^{2+}	Cd^{2+},Ag^+,Pt^{2+},Pt^{4+}
Sc^{3+},La^{3+},U^{4+},Pu^{4+}	
Ti^{4+},Zr^{4+},Hf^{4+},Mn^{2+},Fe^{3+}	
BF_3,BCl_3,$Al(CH_3)_3$,$AlCl_3$,AlH_3,Ga^{3+}	BH_3,$Ga(CH_3)_3$,$GaCl_3$
CO_2,SO_3	HO^+,RO^+,RS^+,Br_2,I_2
Borderline Acids	
Fe^{2+},Ni^{2+},Cu^{2+},Zn^{2+}	
Rh^{3+},Ir^{3+},Ru^{3+},Os^{2+}	
SO_2,$B(CH_3)_3$,GaH_3	

Table 3.2: Classification of hard and soft Lewis bases.

Class I / Hard	Class II / Soft
H_2O,OH^-,O^{2-},F^-	H^-
CO_3^{2-},NO_3^-,SO_4^{2-}	CN^-,RNC,CO
NH_3,RNH_2,N_2H_4	R_2S,RSH,RS^-
Borderline Bases	
N_3^-,N_2,SO_3^{2-}	

ition of acids and bases in 1923[55] and it was more formally stated in 1928 by Cady and Elsey.[56] The theory is used for the description of the interaction between electron rich and electron poor species given by the generalised equation

$$A + :B \longrightarrow A{-}B \tag{3.1}$$

In Equation 3.1 A is a Lewis acid or electron acceptor and B a Lewis base or electron donor. From a molecular orbital (MO) standpoint the donor orbital is usually the highest unoccupied molecular orbital (HOMO). The interacting orbital on the acceptor then is the lowest occupied molecular orbital (LUMO). The classical example of these species is H_3N–BH_3, which was synthesised by Gay-Lussac[57] as early as 1809. Jensen[21] has given a thorough report on the definitions of Lewis acids and bases.

3.2.2 General Lewis Acid-Base Strength

Comparison of the absolute strengths of Brønsted acids and bases is possible in principle since universal standards, H^+ and OH^-, exist. However, Lewis acids and bases do not share that convenience and in spite of the popularity of the theory the evaluation of strengths remains difficult. At best it is possible to compare the relative strengths within a group of acids / bases with *equivalent* donors / acceptors. For this reason only the acids and bases touched on in this work will be mentioned. The acids are BH_3, BX_3 (X = F, Cl, Br) and SO_3. The bases are NH_3, HCN and CH_3CN. This is not meant to be a complete overview of the topic of relative Lewis strengths but should serve to give the reader an idea of what to expect when complexes of these combinations of donors and acceptors are compared. The importance of specifying the reaction phase when comparing these species is evident from the topic of this work. It is essentially to keep this in mind and to not simply compare values from the literature blindly.

3.2.3 BX_3 (X = F, Cl, Br)

It is well known that the order of acidity of the boron trihalides is[58]

$$BBr_3 > BCl_3 \geq BF_3$$

which is the opposite of what is expected on the grounds of electronegativity and steric effects. More electronegative substituents withdraw more charge from the boron atom and this should lead to a more favourable interaction with a donor. Calculations of the partial atomic charge on the boron for the trihalides (BX_3) do indeed give larger positive values when X becomes more electronegative and thus illustrates that an intuitive explanation on the basis of electron deficiency fails to explain the trend.[33,59,60] On the basis of steric grounds, BF_3 would be expected to be the best acceptor since larger, more diffuse atoms should destabilise interaction with a donor to a higher degree.

It has been suggested that pπ bonding between the halogen and boron stemming from donation of the halogen lone pairs into the empty boron 2p orbital is partly responsible for the relative strengths.[58] Since the lone pairs on fluorine are formally located in 2p orbitals and those on chlorine and bromine in 3p and 4p respectively, the overlap is expected to decrease in the order F > Cl > Br. Brinck *et al.*[59] have shown that the overlap for Cl is indeed larger than for F and Frenking *et al.*[60] have shown that the order is *always* F < Cl < Br < I.

Recently though, the higher Lewis acid strength of BCl_3 compared to BF_3 in the complex H_3N–BX_3 was attributed to an intrinsic property of the specific molecule.[61] Covalent interactions between the HOMO of the donor and the LUMO of the acceptor are stronger for BCl_3 since it has a lower lying LUMO. This once again echoes the inability to compare Lewis acid-base strengths absolutely.

3.2.4 The Acids BH_3, BF_3 and SO_3

The acceptor orbital in both BH_3 and BF_3 is the 2p orbital of the boron. The difference between these two species lies in the interaction of the hydrogen atoms and fluorine atoms with both the accepting orbital on the boron and the donating orbital or orbitals of the donor. Jonas *et al.*[33] have concluded that BH_3 is the stronger Lewis acid of the two, based on its interaction energy with NH_3. They also showed that the B–F bond length is a sensitive probe for the strength of the interaction. This is because BF_3 is stabilised by strong π-donation of fluorine lone pairs into the formally empty 2p orbital of the boron.

Deakyne and Liebman[62] have done a detailed comparison between the bonding in BF_3 and SO_3 and concluded that SO_3 is the stronger Lewis acid. Their conclusion was based on the charge transfer and B–F and S–O bond length changes upon complexation and most importantly on the enthalpy of the exchange reaction

$$\Lambda b \cdot BF_3 + SO_3 \longrightarrow \Lambda b \cdot SO_3 + BF_3$$

where Λb is any one of the following anionic bases F^-, OH^-, NH_2^-, CH_3^- or CF_3^-. At first glance this may seem contradictory to what is suggested by the crystal structures of H_3N–BF_3 and H_3N–SO_3 in which the former complex has a boron-nitrogen bond length of 1.60 Å[11] and the latter 1.771 Å.[15] This only serves to highlight a very important observation: *bond lengths and bond energies share no correlation* for donor-acceptor complexes.[63,64]

3.2.5 The Bases NH_3, HCN and CH_3CN

Jonas *et al.*[33] have calculated the order of decreasing donor strength as $NH_3 >> CH_3CN > HCN$. Comparing only the nitrile components, the CH_3 group has a larger inductive (+I) effect making it a stronger electron donor.[65] This stabilises the nitrogen atom by replacing the charge transferred upon complexation, an effect which has been dubbed the *pileup effect* by Gutmann.[66]

Chapter 4

Introduction to Computational Chemistry

4.1 Introduction

This chapter will deal with computational chemistry methods. Since *ab initio* theory originates from the Schrödinger equation we will start our discussion there. The comprehension of several concepts within computational chemistry relies on an understanding of the Hartree-Fock equations. Many of the conclusions resulting from deriving a basic method of approximating solutions to the Schrödinger equation play fundamental roles in various facets of the field. Hence they will be discussed in detail in order to show the origins of these concepts. Perturbations on the basic single determinant electronic Hamiltonian are also discussed and brief mention is made of additional methods to include electron correlation.

Most of the calculations in this work were carried out using density functional theory (DFT). Therefore little time is spent on other "advanced" methods in favour of a detailed discussion of DFT.

The "building blocks" of computational methods, basis sets, will also be discussed.

Population analysis and attribution of atomic partial charge play an important role in understanding molecular bonding. We leave this discussion at the basic introductory methods of analysis. Other advanced procedures of population analysis will be elaborated on when they are introduced in the text.

Due to the generality of the concepts in this chapter individual referencing will be dropped. Instead the reader is referred to the following excellent textbooks from which this summary was compiled: *Quantum Chemistry* by Levine,[67] *Modern Quantum Chemistry: Introduction to Advanced Electronic Structure Theory* by Szabo and Ostlund,[68] *Introduction to Computational Chemistry* by Jensen[69] and *Essentials of Computational Chemistry* by Cramer.[70] In

cases where books dealing with specific subjects were used they will be referenced as applied.

4.2 Formulating the Electronic Problem

In this section a fundamentally important notation and computational principles are discussed. The Schrödinger equation, which is our main concern in computational chemistry, is stated and some approximations and simplifications needed to solve the equation are introduced.

4.2.1 Bra-ket Notation

The very powerful notation introduced by Dirac will be used extensively in this chapter. Therefore, before commencing any discussion an explanation of this notation will be given. A vector $\vec{a}$ in N dimensions with N basis vectors, $\{i_N\}$ is written in this notation as the *ket* vector

$$|a\rangle = \sum_{i=1}^{N} i_N a_i$$

The matrix notation of this vector, in the basis $\{i_N\}$, is

$$\mathbf{a} = \begin{pmatrix} a_1 \\ a_2 \\ \vdots \\ a_N \end{pmatrix}$$

Similarly, the *bra* vector in its basis $\{i_N\}$ is given by

$$\langle a| = \sum_{i=1}^{N} a_i^* i_N$$

and in matrix notation as the adjoint (the transpose of the matrix containing the complex conjugates)

$$\mathbf{a}^\dagger = \begin{pmatrix} a_1^* & a_2^* & \cdots & a_N^* \end{pmatrix}$$

The scalar product between a bra $\langle a|$ and a ket $|b\rangle$ is defined as

$$\langle a||b\rangle \equiv \langle a|b\rangle = \mathbf{a}^\dagger\mathbf{b} = \begin{pmatrix} a_1^* & a_2^* & \cdots & a_N^* \end{pmatrix} \begin{pmatrix} b_1 \\ b_2 \\ \vdots \\ b_N \end{pmatrix} = \sum_{i=1}^{N} a_i^* b_i$$

A further use of this notation is the extension to functions. To make the analogy it is convenient to introduce the notation

$$a(x) \equiv |a\rangle \qquad a^*(x) \equiv \langle a|$$

or more specifically for our interests

$$\psi_i(x) \equiv |i\rangle \qquad \psi_i^*(x) \equiv \langle i|$$

The product of two functions (comparable with the scalar product between two vectors) is then written as

$$\langle a|b\rangle = \int a^*(x)b(x)\,dx$$

Finally, an operator $\hat{\mathcal{O}}$ is defined as an entity acting on a function $a(x)$ to yield the function $f(x)$,

$$\hat{\mathcal{O}}a(x) = f(x)$$

which can be written as

$$\hat{\mathcal{O}}|a\rangle = |f\rangle$$

Applying the notation conventions introduced above we find that

$$\langle a|\hat{\mathcal{O}}|b\rangle = \int a^*(x)\hat{\mathcal{O}}b(x)\,dx = \int a^*(x)f(x)\,dx$$

It will become very convenient to interpret $\langle a|\hat{\mathcal{O}}|b\rangle$ in terms of a general matrix element,

$$\langle a|\hat{\mathcal{O}}|b\rangle = O_{ab}$$

where O_{ab} is an element of the $a \times b$ matrix $\mathbf{O}$, which is the matrix representation of the $\hat{\mathcal{O}}$ operator.

4.2.2 The Variational Principle

Given a normalised wave function $|\Phi\rangle$, the expectation value of the operator $\hat{\mathcal{H}}$ is given by

$$\langle\Phi|\hat{\mathcal{H}}|\Phi\rangle$$

We now assume that the $\hat{\mathcal{H}}$ operator will generate the exact ground state energy, $\mathcal{E}_0$, given the ground state wave function, $|\Phi_0\rangle$. The *variational principle* states that given any trial wave function $|\tilde{\Phi}\rangle$, the expectation value of the $\hat{\mathcal{H}}$ operator with this trial wave function will be an upper bound to the exact energy,

$$\langle\tilde{\Phi}|\hat{\mathcal{H}}|\tilde{\Phi}\rangle \geq \mathcal{E}_0$$

4.2.3 The Schrödinger Equation

Most of computational chemistry revolves around finding approximate solutions to the time-independent non-relativistic Schrödinger equation

$$\hat{\mathcal{H}}|\Phi\rangle = \mathcal{E}|\Phi\rangle \tag{4.1}$$

where $\hat{\mathcal{H}}$ is the Hamiltonian operator for a system of nuclei and electrons. The Hamiltonian for N electrons and M nuclei, in atomic units, is

$$\begin{aligned}\hat{\mathcal{H}} = &-\sum_{i=1}^{N}\frac{1}{2}\nabla_i^2 - \sum_{A=1}^{M}\frac{1}{2M_A}\nabla_A^2 - \sum_{i=1}^{N}\sum_{A=1}^{M}\frac{Z_A}{r_{iA}} \\ &\sum_{i=1}^{N}\sum_{j>i}^{N}\frac{1}{r_{ij}} + \sum_{A=1}^{M}\sum_{B>A}^{M}\frac{Z_A Z_B}{R_{AB}}\end{aligned} \tag{4.2}$$

where M_A is the ratio of the mass of the nucleus A to the mass of an electron, Z_A is the atomic number of nucleus A, r_{iA} is the distance from the ith electron to the Ath nucleus, r_{ij} is the distance between the ith electron and the jth electron, r_{AB} is the distance between the Ath nucleus and the Bth nucleus and the Laplacian operators ∇_i^2 and ∇_A^2 denote differentiation with respect to the coordinates of the ith electron and the Ath nucleus. The different terms are:

- $-\sum_{i=1}^{N}\frac{1}{2}\nabla_i^2$: kinetic energy of the electrons
- $-\sum_{A=1}^{M}\frac{1}{2M_A}\nabla_A^2$: kinetic energy of the nuclei
- $-\sum_{i=1}^{N}\sum_{A=1}^{M}\frac{Z_A}{r_{iA}}$: coulomb attraction between electrons and nuclei
- $\sum_{i=1}^{N}\sum_{j>i}^{N}\frac{1}{r_{ij}}$: repulsion between the electrons
- $\sum_{A=1}^{M}\sum_{B>A}^{M}\frac{Z_A Z_B}{R_{AB}}$: repulsion between the nuclei

The specification of the Hamiltonian is greatly simplified if it is done as above in atomic units. The derivation of these units will be explained in the next section.

4.2.4 Atomic Units

To see how atomic units arise, we consider only the part of the Schrödinger equation for a hydrogen atom dealing with the electrons, in SI units,

$$\left[-\frac{\hbar^2}{2m_e}\nabla^2 - \frac{e^2}{4\pi\epsilon_0 r}\right]\Phi = \mathcal{E}\Phi \tag{4.3}$$

where $\hbar$ is Planck's constant divided by 2π, m_e is the mass of the electron and $-e$ is the charge on the electron. We now transform the Cartesian coordinates

Table 4.1: Some atomic units and the conversion factors to SI units.

Physical Quantity	Conversion factor	in SI units
Length	a_0	5.2918×10^{-11} m
Mass	m_e	9.1095×10^{-31} kg
Charge	e	1.6022×10^{-19} C
Energy	$\mathcal{E}_a$	4.3598×10^{-18} J
Angular Momentum	$\hbar$	1.0546×10^{-34} J.s
Electric Dipole Moment	ea_0	8.4784×10^{-30} C.m
Electric Field	$\mathcal{E}_a e^{-1} a_0^{-1}$	5.1423×10^{11} V.m^{-1}

into a different set of coordinates, $x, y, z \rightarrow \lambda x', \lambda y', \lambda z'$ where λ is the relation factor. Equation 4.3 then becomes

$$\left[-\frac{\hbar^2}{2m_e\lambda^2}\nabla'^2 - \frac{e^2}{4\pi\epsilon_0\lambda r'} \right] \Phi' = \mathcal{E}\Phi'$$

The constants in front of the two terms can now be factored out

$$\mathcal{E}_a \left[-\frac{1}{2}\nabla'^2 - \frac{1}{r'} \right] \Phi' = \mathcal{E}\Phi' \tag{4.4}$$

provided we choose

$$\frac{\hbar^2}{m_e\lambda^2} = \frac{e^2}{4\pi\epsilon_0\lambda} = \mathcal{E}_a \tag{4.5}$$

The atomic unit of energy has now been defined as $\mathcal{E}_a$ and is called the Hartree. The atomic unit of length, a_0, called the Bohr, can now be determined by solving the value of λ from Equation 4.5,

$$\lambda = \frac{4\pi\epsilon_0\hbar^2}{m_e e^2} = a_0$$

If we now let $\mathcal{E}' = \mathcal{E} / \mathcal{E}_a$, the dimensionless form of the Schrödinger equation follows from Equation 4.4,

$$\left(-\frac{1}{2}\nabla'^2 - \frac{1}{r'} \right) \Phi' = \mathcal{E}'\Phi'$$

Table 4.1 lists some common atomic units and shows the conversion factors to SI units.

4.2.5 The Born-Oppenheimer Approximation

In Section 4.2.3 we gave the Hamiltonian describing both the electrons and nuclei. Nuclei, however, are much heavier than electrons, and one can consider the electrons in a molecule as moving in a potential generated by a set of

fixed nuclei. Under these conditions, the second term in Equation 4.2 (kinetic energy of nuclei) becomes zero and the last term (repulsion between nuclei) becomes a constant. The electronic Hamiltonian then is

$$\hat{\mathcal{H}}_{elec} = -\sum_{i=1}^{N} \frac{1}{2}\nabla_i^2 - \sum_{i=1}^{N}\sum_{A=1}^{M} \frac{Z_A}{r_{iA}} + \sum_{i=1}^{N}\sum_{j>i}^{N} \frac{1}{r_{ij}} \tag{4.6}$$

The Schrödinger equation involving just the electronic Hamiltonian thus is

$$\hat{\mathcal{H}}_{elec}\Phi_{elec} = \mathcal{E}_{elec}\Phi_{elec} \tag{4.7}$$

where Φ_{elec} is the electronic wave function depending explicitly on the coordinates of the electrons and parametrically on the coordinates of the nuclei,

$$\Phi_{elec} = \Phi_{elec}(\{\mathbf{r}_i\};\{\mathbf{R}_A\})$$

The total energy for a system with fixed nuclei is then given by

$$\mathcal{E}_{tot} = \mathcal{E}_{elec} + \sum_{A=1}^{M}\sum_{B>A}^{M} \frac{Z_A Z_B}{R_{AB}}$$

Since the electrons move so much faster than the nuclei once the electronic problem is solved, their coordinates in the Hamiltonian (Equation 4.2) can be replaced by averaged values over the electronic wave function. This then generates a nuclear Hamiltonian, which when solved provides a potential for nuclear motion and a subsequent potential energy surface.

We are mainly interested in the solution of the electronic problem. Henceforth, unless explicitly specified otherwise, the subscript "elec" will be dropped and the electronic Hamiltonian will be given by $\mathcal{H}$ only.

4.2.6 Spatial and Spin Orbitals

In the quantum mechanical formulation an *orbital* (often explicitly referred to as an one-electron orbital or function) is defined as a wave function for a single electron. A *spatial orbital*, $\psi_i(\mathbf{r})$, is a function of only the position ($\mathbf{r}$) of the particle. The probability of finding an electron in a volume element $d\mathbf{r}$ is given by $|\psi(\mathbf{r})|^2\, d\mathbf{r}$. Spatial orbitals will usually be defined as being orthonormal and thus adhere to the following condition,

$$\int \psi_i^*(\mathbf{r})\psi_j(\mathbf{r})\, d\mathbf{r} = \delta_{ij}$$

where δ_{ij} is the Kronecker delta,

$$\delta_{ij} = \begin{cases} 1 \text{ if } i = j \\ 0 \text{ otherwise} \end{cases}$$

A complete description of an electron is only possible if we consider the spin as well. What is often referred to as "spin up" and "spin down" can be manifested by two *orthonormal* functions, $\alpha(\omega)$ and $\beta(\omega)$. Both are functions of the spin coordinate ω. An electron can be described completely by a set of four coordinates,

$$\mathbf{x} = \{\mathbf{r}, \omega\}$$

Combining the spatial orbitals with the spin functions gives *spin orbitals*,

$$\chi(\mathbf{x}) = \begin{cases} \psi(\mathbf{r})\alpha(\omega) \\ \text{or} \\ \psi(\mathbf{r})\beta(\omega) \end{cases}$$

4.2.7 Antisymmetry of Wave Functions

A very general statement of the Pauli exclusion principle is found in one of the quantum mechanical postulates and states that many electron wave functions should be antisymmetric with respect to interchange of any two electrons,

$$\Phi(\mathbf{x}_1, \ldots, \mathbf{x}_k, \ldots, \mathbf{x}_l, \ldots, \mathbf{x}_N) = -\Phi(\mathbf{x}_1, \ldots, \mathbf{x}_l, \ldots, \mathbf{x}_k, \ldots, \mathbf{x}_N) \tag{4.8}$$

4.2.8 Slater Determinants

A system of noninteracting electrons is described by a Hamiltonian of the form

$$\hat{\mathcal{H}}_{nonint} = \sum_{i=1}^{N} \hat{h}(i) \tag{4.9}$$

where the operator describing (only) the kinetic and potential energy of the ith electron is given by $\hat{h}(i)$. Since $\hat{\mathcal{H}}_{nonint}$ is a sum of one-electron Hamiltonians a wave function which is a product of one-electron spin orbitals for each electron (also referred to as a *Hartree product*) will satisfy the equation

$$\hat{\mathcal{H}}_{nonint} \left[\chi_i(\mathbf{x}_1)\chi_j(\mathbf{x}_2)\cdots\chi_k(\mathbf{x}_N)\right] = E\left[\chi_i(\mathbf{x}_1)\chi_j(\mathbf{x}_2)\cdots\chi_k(\mathbf{x}_N)\right]$$

where the eigenvalue E is simply the sum of the spin orbital energies,

$$E = \varepsilon_i + \varepsilon_j + \cdots + \varepsilon_k$$

Hartree products do not satisfy the antisymmetry principle (cf. Equation 4.8). Fortunately, antisymmetry can be achieved by creating a wave function from a so-called *Slater determinant*,

$$\Psi(\mathbf{x}_1, \mathbf{x}_2, \ldots, \mathbf{x}_N) = \frac{1}{\sqrt{N!}} \begin{vmatrix} \chi_i(\mathbf{x}_1) & \chi_j(\mathbf{x}_1) & \cdots & \chi_k(\mathbf{x}_1) \\ \chi_i(\mathbf{x}_2) & \chi_j(\mathbf{x}_2) & \cdots & \chi_k(\mathbf{x}_2) \\ \vdots & \vdots & & \vdots \\ \chi_i(\mathbf{x}_N) & \chi_j(\mathbf{x}_N) & \cdots & \chi_k(\mathbf{x}_N) \end{vmatrix} \tag{4.10}$$

The factor $\frac{1}{\sqrt{N!}}$ is a normalisation constant. The Slater determinant specifies a wave function of N electrons in N spin orbitals without explicitly specifying which electron is in which orbital. Interchange of any two rows in the Slater determinant changes the sign of the determinant, hereby satisfying the antisymmetry condition. The Pauli exclusion principle is implied by the property of a determinant that it becomes zero when two columns are equal (this will occur when two electrons occupy the same spin orbital in the determinant). Using the principles of calculating determinants the definition of a Slater determinant is

$$|\chi_i(\mathbf{x}_1)\chi_j(\mathbf{x}_2)\cdots\chi_k(\mathbf{x}_N)\rangle = \frac{1}{\sqrt{N!}}\sum_{n=1}^{N!}(-1)^{p_n}\hat{\mathcal{P}}_n\{\chi_i(1)\chi_j(2)\cdots\chi_k(N)\} \tag{4.11}$$

where, to introduce a popular shortened way of writing, $\chi_i(\mathbf{x}_l) \equiv \chi_i(l)$. $\hat{\mathcal{P}}_n$ is an operator that generates the nth permutation of the electron labels $1, 2, \ldots, N$ and p_n is the number of transpositions or interchanges required to obtain the permutation.

A short-hand notation for a normalised Slater determinant, which includes the normalisation factor, is to show only the diagonal elements,

$$\Psi(\mathbf{x}_1, \mathbf{x}_2, \ldots, \mathbf{x}_N) = |\chi_i(\mathbf{x}_1)\chi_j(\mathbf{x}_2)\cdots\chi_k(\mathbf{x}_N)\rangle$$

4.3 Operators of the Hamiltonian

In this section the application of the Hamiltonian operator on a single determinant wave function is explained. The operation of the Hamiltonian can be divided into operators involving only one as well as two electrons. Consequences of the operation is thus seen in terms of these individual operators. This leads to the formulation of the one-electron and two-electron integrals and the coinciding operators, which play a crucial role within computational chemistry.

4.3.1 One-Electron and Two-Electron Operators

Let us consider an antisymmetric wave function

$$|\Psi_0\rangle = |\chi_1\chi_2\cdots\chi_a\chi_b\cdots\chi_N\rangle$$

where the subscript 0 of the wave function indicates the ground state. The electrons are always written in the order $\mathbf{x}_1, \mathbf{x}_2, \ldots, \mathbf{x}_N$, hence the notation has been simplified by dropping the electronic coordinates. The variation principle now stipulates that the best wave function is that which minimises the energy,

$$E_0 = \langle\Psi_0|\hat{\mathcal{H}}|\Psi_0\rangle \tag{4.12}$$

The operation of the Hamiltonian (Equation 4.6) can be separated into two parts:

- The kinetic and attractive potential energy of every electron in a system of N electrons, given by

$$\hat{\mathcal{O}}_1 = \sum_{i=1}^{N} h(i) = \sum_{i=1}^{N} -\frac{1}{2}\nabla_i^2 - \sum_{A}^{M} \frac{Z_A}{r_{iA}} \tag{4.13}$$

  This operator depends only on the position of the electron in question and hence it is referred to as an *one-electron operator*

- The electron-electron interaction between every pair of electrons, given by

$$\hat{\mathcal{O}}_2 = \sum_{i=1}^{N} \sum_{j>i}^{N} \frac{1}{r_{ij}} \tag{4.14}$$

  This operator depends on the position of both the ith and jth electron and is called a *two-electron operator*

4.3.2 The General One-Electron Term

We now look at the effect of the first operator $\hat{\mathcal{O}}_1$ (Equation 4.13) on the energy of the wave function (Equation 4.12) in terms of the general matrix element,

$$\langle \Psi_0 | \hat{\mathcal{O}}_1 | \Psi_0 \rangle = \langle \Psi_0 | \hat{h}(1) + \hat{h}(2) + \cdots + \hat{h}(N) | \Psi_0 \rangle$$

Because the electrons are indistinguishable the result of $\langle \Psi_0 | \hat{h}(1) | \Psi_0 \rangle$ will be similar to that of $\langle \Psi_0 | \hat{h}(2) | \Psi_0 \rangle$, etc. and we can just write

$$\langle \Psi_0 | \hat{\mathcal{O}}_1 | \Psi_0 \rangle = N \langle \Psi_0 | \hat{h}(1) | \Psi_0 \rangle$$

Using the definition of a Slater determinant (Equation 4.11), it can be shown that this simplifies to

$$\langle \Psi_0 | \hat{\mathcal{O}}_1 | \Psi_0 \rangle = \sum_{a}^{N} \langle a | \hat{h} | a \rangle$$

The term $\langle a | \hat{h} | a \rangle$ can be given the shorthand notation, h_{aa}.

4.3.3 The General Two-Electron Term

Similarly we can look at the effect of the second operator $\mathcal{O}_2$ (Equation 4.14) on the energy of the wave function. The general matrix element in this case is

$$\langle \Psi_0 | \hat{\mathcal{O}}_2 | \Psi_0 \rangle = \langle \Psi_0 | \frac{1}{r_{12}} + \frac{1}{r_{13}} + \cdots + \frac{1}{r_{23}} + \cdots + \frac{1}{r_{N-1,N}} | \Psi_0 \rangle$$

Each of the $\frac{1}{r_{mn}}$ operators will give the same result since we do not distinguish between identical electrons. Their combined effect can be given by one operator multiplied by the number of total electron pairs,

$$\langle \Psi_0 | \hat{\mathcal{O}}_2 | \Psi_0 \rangle = \frac{N(N-1)}{2} \langle \Psi_0 | \frac{1}{r_{12}} | \Psi_0 \rangle$$

The definition of a Slater determinant can be applied to this general matrix element, resulting in

$$\langle \Psi_0 | \hat{\mathcal{O}}_2 | \Psi_0 \rangle = \frac{1}{2} \sum_a^N \sum_b^N \langle ab|ab\rangle - \langle ab|ba\rangle$$

Here we have introduced the *physicist's notation*, used to simplify the writing of specific two-electron integrals

$$\int \chi_a^*(1)\chi_b^*(2) \frac{1}{r_{12}} \chi_a(1)\chi_b(2)\, d\mathbf{x}_1 d\mathbf{x}_2 = \langle \chi_a(1)\chi_b(2) | \chi_a(1)\chi_b(2)\rangle = \langle ab|ab\rangle$$

4.3.4 Coulomb and Exchange Operators

The derivation of the general two-electron term introduces the *Coulomb* and *exchange* integrals, given by $\langle ab|ab\rangle$ and $\langle ab|ba\rangle$, respectively.

Full notation for the Coulomb integral term is

$$\int \chi_a^*(1)\chi_b^*(2) \frac{1}{r_{12}} \chi_a(1)\chi_b(2)\, d\mathbf{x}_1 d\mathbf{x}_2 = \langle ab|ab\rangle = J_{ab} \tag{4.15}$$

The integral can be rearranged,

$$\int \chi_a^*(1)\chi_b^*(2) \frac{1}{r_{12}} \chi_a(1)\chi_b(2)\, d\mathbf{x}_1 d\mathbf{x}_2 = \int |\chi_a(1)|^2 \frac{1}{r_{12}} |\chi_b(2)|^2\, d\mathbf{x}_1 d\mathbf{x}_2 \tag{4.16}$$

which shows that this is the classic Coulomb repulsion between the charge distributions of electron 1 in orbital χ_a and electron 2 in χ_b.

For the exchange integral term the full notation is

$$\int \chi_a^*(1)\chi_b^*(2) \frac{1}{r_{12}} \chi_b(1)\chi_a(2)\, d\mathbf{x}_1 d\mathbf{x}_2 = \langle ab|ba\rangle = K_{ab} \tag{4.17}$$

Since the same electron is in different orbitals on the left and right of the operator, a similar rearrangement cannot be done. Therefore, this integral cannot be given a classical interpretation. It results from *exchange correlation*, meaning that the motion of electrons with parallel spin is correlated within the Slater determinant.

The operators which are used to generate the Coulomb and exchange integrals will be shown in terms of their effect on the spin orbital, $\chi_a(1)$. The

Coulomb operator, $\hat{\mathcal{J}}_b$, whose expectation value is simply the Coulomb integral, is given by

$$\hat{\mathcal{J}}_b(1)\chi_a(1) = \left[\int \chi_b^*(2)\frac{1}{r_{12}}\chi_b(2)\,d\mathbf{x}_2\right]\chi_a(1) \tag{4.18}$$

The exchange operator, $\hat{\mathcal{K}}_b$, whose expectation value is the exchange integral, is

$$\hat{\mathcal{K}}_b(1)\chi_a(1) = \left[\int \chi_b^*(2)\frac{1}{r_{12}}\chi_a(2)\,d\mathbf{x}_2\right]\chi_b(1) \tag{4.19}$$

4.4 The Hartree-Fock Approximation

In this section we show how the derivations of the previous sections can be applied to approximate solutions to the Schrödinger equation. We show how the minimum energy wave function can be determined, convert the spin orbitals to spatial orbitals and introduce basis sets to the mix. This in turn results in the Roothaan-Hall equations, used to solve the spin-restricted Hartree-Fock equations. Little attention is given to the spin-unrestricted case, but appropriate references to this problem are given where applicable.

4.4.1 The Energy of a Slater Determinant

We are interested in the energy, $E_0 = \langle\Psi_0|\hat{\mathcal{H}}|\Psi_0\rangle$ of a single Slater determinant $|\Psi_0\rangle = |\chi_1\chi_2\cdots\chi_a\chi_b\cdots\chi_N\rangle$ of an N electron system. The energy is given by combining the results from Section 4.3.2 and Section 4.3.3,

$$E_0 = \sum_{a=1}^{N}\langle a|\hat{h}|a\rangle + \frac{1}{2}\sum_{a=1}^{N}\sum_{b=1}^{N}(\langle ab|ab\rangle - \langle ab|ba\rangle) \tag{4.20}$$

4.4.2 Minimising the Hartree-Fock Energy

The minimum energy can be obtained by minimising with respect to the spin orbitals $\{\chi_a\}$ subject to the constraint that they remain orthonormal,

$$\int \chi_a^*(1)\chi_b(1)\,d\mathbf{x}_1 = \langle a|b\rangle = \delta_{ab}$$

Minimisation with constraints can be done with the technique of Lagrange multipliers. Therefore, we need to consider the Lagrange functional

$$\mathcal{L} = E_0 - \sum_{a=1}^{N}\sum_{b=1}^{N}\lambda_{ab}(\langle a|b\rangle - \delta_{ab}) \tag{4.21}$$

where $\{\lambda_{ab}\}$ is the set of Lagrange multipliers. Minimisation of the energy is thus obtained by varying the spin orbitals and setting $\delta\mathcal{L}$ equal to zero,

$$\delta\mathcal{L} = \delta E_0 - \sum_{a=1}^{N}\sum_{b=1}^{N}\lambda_{ab}(\langle\delta a|b\rangle + \langle a|\delta b\rangle) = 0 \tag{4.22}$$

where we have made use of the fact that $\delta\langle a|b\rangle = \langle\delta a|b\rangle + \langle a|\delta b\rangle$. The δE_0 term is given by

$$\begin{aligned}\delta E_0 = &\sum_{a=1}^{N}(\langle\delta a|\hat{h}|a\rangle + \langle a|\hat{h}|\delta a\rangle)\\ &+\frac{1}{2}\sum_{a=1}^{N}\sum_{b=1}^{N}(\langle\delta ab|ab\rangle + \langle a\delta b|ab\rangle + \langle ab|\delta ab\rangle + \langle ab|a\delta b\rangle)\\ &-\frac{1}{2}\sum_{a=1}^{N}\sum_{b=1}^{N}(\langle\delta ab|ba\rangle + \langle a\delta b|ba\rangle + \langle ab|\delta ba\rangle + \langle ab|b\delta a\rangle)\end{aligned}$$

Since the double summation runs over *all* spin orbitals and in general, $\langle ij|kl\rangle = \langle ji|lk\rangle$, the first and second terms are identical, as well as the third and last terms. In both double summations they can thus be collected to cancel the $\frac{1}{2}$ factor. Also, making use of the fact that $\langle ij|kl\rangle = \langle kl|ij\rangle^*$ and $\langle i|\hat{h}|j\rangle = \langle j|\hat{h}|i\rangle^*$ the above then simplifies to

$$\begin{aligned}\delta E_0 = &\sum_{a=1}^{N}\langle\delta a|\hat{h}|a\rangle + \sum_{a=1}^{N}\sum_{b=1}^{N}(\langle\delta ab|ab\rangle - \langle\delta ab|ba\rangle)\\ &+\sum_{a=1}^{N}\langle\delta a|\hat{h}|a\rangle^* + \sum_{a=1}^{N}\sum_{b=1}^{N}(\langle\delta ab|ab\rangle^* - \langle\delta ab|ba\rangle^*)\end{aligned} \tag{4.23}$$

The second part of $\delta\mathcal{L}$, relating to the orthogonality constraint, is

$$\begin{aligned}\sum_{a=1}^{N}\sum_{b=1}^{N}\lambda_{ab}(\langle\delta a|b\rangle + \langle a|\delta b\rangle) &= \sum_{ab}\lambda_{ab}\langle\delta a|b\rangle + \sum_{ab}\lambda_{ab}\langle a|\delta b\rangle\\ &= \sum_{ab}\lambda_{ab}\langle\delta a|b\rangle + \sum_{ab}\lambda_{ab}^*\langle\delta a|b\rangle^*\end{aligned} \tag{4.24}$$

These equations can be written in a much simpler form by introducing an operator, the *Fock operator*, which generates the required one-electron and two-electron terms using the one-electron Hamiltonian operator and the Coulomb and exchange operators,

$$\hat{\mathcal{F}}(1) = \hat{h}(1) + \sum_{b=1}^{N}\left[\hat{\mathcal{J}}_b(1) - \hat{\mathcal{K}}_b(1)\right] \tag{4.25}$$

The Fock operator is thus the sum of a *core-Hamiltonian operator*, $\hat{h}(1)$ and an *effective* one-electron potential operator, called the *Hartree-Fock potential*, $v^{HF}(1)$,

$$v^{HF}(1) = \sum_{b=1}^{N}\left[\hat{\mathcal{J}}_b(1) - \hat{\mathcal{K}}_b(1)\right]$$

Equations 4.23 and 4.24 can now be substituted into the equation for $\delta\mathcal{L}$ (Equation 4.22), the complex conjugate terms grouped and the Fock operator incorporated. The expression is rewritten in order to accommodate the notation in which the operators were defined in Equations 4.18 and 4.19,

$$\begin{aligned}\delta\mathcal{L} &= \sum_{a=1}^{N}\int \delta\chi_a^*(1)\left[h(1)\chi_a(1) + \sum_{b=1}^{N}(\hat{\mathcal{J}}_b(1) - \hat{\mathcal{K}}_b(1))\chi_a(1) - \sum_{b=1}^{N}\lambda_{ab}\chi_b(1)\right] d\mathbf{x}_1 \\ &\quad + \text{complex conjugate} \\ &= \sum_{a=1}^{N}\int \delta\chi_a^*(1)\left[\hat{\mathcal{F}}(1)\chi_a(1) - \sum_{b=1}^{N}\lambda_{ab}\chi_b(1)\right] d\mathbf{x}_1 + \text{ complex conjugate} \\ &= 0\end{aligned}$$

Since $\delta\chi_a^*(1)$ is arbitrary, and the result must hold for both $|\chi_a\rangle$ and $\langle\chi_a|$, the quantity in square brackets must be zero for all $\{\chi_a\}$,

$$\hat{\mathcal{F}}(1)\chi_a(1) = \sum_{b=1}^{N}\lambda_{ab}\chi_b(1) \qquad a = 1, 2, \ldots, N \tag{4.26}$$

Note that the Fock operator is associated with the *variation* of the energy and that it is not simply a sum of Hamiltonian operators. This can be seen by comparing the effect of the Hamiltonian (thus the electronic energy of the system, Equation 4.20) with the Fock operator (Equation 4.25); both are rewritten in terms of one-electron integrals and Coulomb and exchange integrals,

$$E = \sum_{a}^{N} h_{aa} + \frac{1}{2}\sum_{ab}^{N}(J_{ab} - K_{ab})$$

$$\hat{\mathcal{F}} = h_{aa} + \sum_{b}^{N}(J_{ab} - K_{ab})$$

A sum of Fock operators will thus count the Coulomb and exchange contributions twice.

4.4.3 The Canonical Hartree-Fock Equations

The final step is simplifying The Hartree-Fock equations by introducing an unitary transformation. This transformation preserves orthonormality and produces a set of alternative spin orbitals which makes the matrix of Lagrange multipliers diagonal. These alternative spin orbitals are called *canonical spin orbitals* and they transform Equation 4.26 into

$$\hat{\mathcal{F}}|\chi_a\rangle = \varepsilon_a|\chi_a\rangle \tag{4.27}$$

The ε_a eigenvalues are explained in the next section.

4.4.4 Orbital Energies

The Lagrange multipliers in Equation 4.27 are the expectation values of the Fock operator in the canonical spin orbital basis and can thus be interpreted as the orbital energies,

$$\varepsilon_a = \langle a|\hat{\mathcal{F}}|a\rangle$$

The total energy, however, is not just the sum of orbital energies. The orbital energy includes interaction terms with all other electrons, meaning that in the double summation over all orbitals the interaction between any two electrons is counted twice. The correct ground state electronic energy in terms of the orbital energies is thus obtained by subtracting the double count,

$$E_0 = \sum_{a=1}^{N} \varepsilon_a - \frac{1}{2}\sum_{a=1}^{N}\sum_{b=1}^{N}(\langle ab|ab\rangle - \langle ab|ba\rangle) \tag{4.28}$$

4.4.5 Conversion of Spin Orbitals to Spatial Orbitals

Up till now all equations have been derived in terms of spin orbitals. To facilitate further discussion, these equations can be converted to equations in terms of spatial orbitals.

Closed-shell systems can be restricted to doubly occupied molecular orbitals with identical spatial functions for both spins (see Section 4.2.6). This is called *restricted Hartree-Fock* (RHF) theory. Open-shell systems can have singly occupied molecular orbitals with different spatial functions for the α and β spin. This is called *unrestricted Hartree-Fock* (UHF) theory. The doubly occupied part of an open shell system can be computed as restricted with the singly occupied part unrestricted, leading to *restricted open-shell Hartree-Fock* (ROHF) theory.

For a set of spin orbitals $\{\chi_a|a = 1, 2, \ldots, N\}$ where N is an even number, the Hartree-Fock energy is given by Equation 4.20. Since the wave function contains $N/2$ spin orbitals with α spin and $N/2$ spin orbitals with β spin, the sum over N spin orbitals can be written as

$$\sum_{a}^{N}\chi_a = \sum_{a}^{N/2}\psi_a\omega(\alpha) + \sum_{a}^{N/2}\psi_a\omega(\beta)$$

The above equation can be used to rewrite the summations in Equation 4.20 in terms of spatial orbitals and spin functions. Integrating over both the spatial coordinates and spin and using the orthonormality of spin functions ($\langle\alpha|\beta\rangle = \langle\beta|\alpha\rangle = 0$ and $\langle\alpha|\alpha\rangle = \langle\beta|\beta\rangle = 1$) results in the cancelation and grouping of some terms, giving the Hartree-Fock energy for a closed-shell system as

$$E_0 = 2\sum_{a}^{N/2}\langle a|\hat{h}|a\rangle + \sum_{ab}^{N/2}(2\langle ab|ab\rangle - \langle ab|ba\rangle) \tag{4.29}$$

Similarly, the Fock operator for a closed-shell is evaluated as

$$\hat{\mathcal{F}}(1) = \hat{h}(1) + \sum_{b=1}^{N/2}(2\hat{\mathcal{J}}_b(1) - \hat{\mathcal{K}}_b(1)) \tag{4.30}$$

and the Hartree-Fock equations become

$$\hat{\mathcal{F}}|\psi_i\rangle = \varepsilon_i|\psi_i\rangle \tag{4.31}$$

The most frequently encountered systems in chemistry are closed-shell, including all the systems discussed in this work. For discussions on UHF and ROHF wave functions see Szabo and Ostlund[68] and Hurley,[71] respectively.

4.4.6 The Roothan-Hall Equations

The problem of determining the optimal molecular orbitals can be simplified by writing each molecular orbital in terms of a set of K known spatial basis functions,

$$\psi_i = \sum_{\mu=1}^{K} c_{\mu i}\varphi_\mu$$

Introducing the above expression into the Hartree-Fock equations (Equation 4.31), multiplying from the left by a specific basis funtions $\phi_\nu^*(1)$ and integrating gives the Roothan-Hall equations,

$$\sum_{\mu=1}^{K} c_{\mu i}\int \varphi_\nu^*(1)\mathcal{F}(1)\varphi_\mu(1)\,d\mathbf{r}_1 = \varepsilon_i \sum_{\mu=1}^{K} c_{\mu i}\int \varphi_\nu^*(1)\varphi_\mu(1)\,d\mathbf{r}_1$$

which can be written as a single *matrix equation* as

$$\hat{\mathbf{F}}\mathbf{C} = \mathbf{S}\mathbf{C}\boldsymbol{\varepsilon} \tag{4.32}$$

where $\mathbf{C}$ is the matrix of coefficients, given individually by $c_{\mu i}$, $\boldsymbol{\varepsilon}$ is the diagonal matrix of orbital energies, $\mathbf{S}$ is the *overlap matrix* with elements $\langle\mu|\nu\rangle$ and $\mathbf{F}$ is the Fock matrix with elements $\langle\mu|\mathcal{F}|\nu\rangle$. The coefficients matrix is also sometimes referred to as a *density matrix*. For RHF systems it is given by

$$P_{\mu\nu} = 2\sum_{i=1}^{N/2} c_{\mu i}c_{\nu i}^* \tag{4.33}$$

4.4.7 The SCF-Procedure

The procedure for solving the Hartree-Fock equations (for closed-shell systems the Roothaan-Hall equations) is also called the *self-consistent field* (SCF) method and proceeds as follows:

- Specify a set of nuclear coordinates, a number of electrons, a basis set and guess an initial density matrix.
- Calculate the required one-electron and two-electron integrals.
- Form the Fock matrix.
- Diagonalise the Fock matrix and determine the molecular orbitals
- Form the new density matrix.
- If the density matrix is sufficiently close to the previous one, the procedure is complete, otherwise, use the new density matrix and proceed from the second step.

4.5 Post Hartree-Fock Methods

Up till now we have dealt only with single determinant wave functions which introduces some inherent inaccuracy. We explain the concept of electron correlation and introduce some methods to obtain a more accurate wave function.

4.5.1 Electron Correlation

In the Hartree-Fock approximation the energy is determined through a Hamiltonian that is a sum of independently calculated one-electron operators and every electron is calculated in a static, averaged field generated by the other electrons. Correlation energy is defined as the difference between the single determinant energy and the lowest possible energy for the system. Physically this corresponds to the movement of the electrons being correlated. In terms of electron densities, the probability of finding an electron in the immediate vicinity of another electron is reduced. For electrons of opposite spin, this phenomenon is referred to as the *Coulomb hole*, for electrons of the same spin, it is called the *Fermi hole*.

The weakness of the HF approximation arises because it utilises a single Slater determinant as a trial wave function. In order to include correlation one must use a trial wave function consisting of more than one Slater determinant,

$$\Psi = c_0\Psi_{HF} + \sum_{i=1}^{K} c_i\Psi_i$$

where Ψ_{HF} is the reference determinant and Ψ_i are excited determinants. The different methods arise from the manner in which they calculate the coefficients c_i. The number of excited determinants, K, depends on the size of the basis set. Due to the popularity of Møller-Plesset perturbation theory it will be discussed in short. Other techniques for including correlation will just be mentioned briefly.

4.5.2 Møller-Plesset Perturbation Theory

The basic idea behind perturbation theory is that exact eigenfunctions and eigenvalues of a operator can be used to estimate the eigenfunctions and eigenvalues of a more complicated operator that is related to the simple operator through a known perturbation. We will not discuss the results from basic perturbation theory (see Section 6.1 in Szabo and Ostlund[68] for the derivation). In 1934 Møller and Plesset[72] proposed a perturbation treatment of molecules. Following their idea, the Hamiltonian operator can be given as

$$\hat{\mathcal{H}} = \hat{\mathcal{H}}_0 + \lambda\hat{\mathcal{H}}'$$

where $\hat{\mathcal{H}}_0$ is the unperturbed Hamiltonian and λ is a factor determining the strength of the perturbation. The perturbed Hamiltonian is given as the difference between the true molecular Hamiltonian (Equation 4.6) and the non-interacting Hamiltonian (a sum of Fock operators, Equation 4.25),

$$\begin{aligned}
\hat{\mathcal{H}}' &= \hat{\mathcal{H}} - \hat{\mathcal{H}}_0 \\
&= -\sum_{i=1}^{N}\frac{1}{2}\nabla_i^2 - \sum_{i=1}^{N}\sum_{A=1}^{M}\frac{Z_A}{r_{iA}} + \sum_{i=1}^{N}\sum_{j>i}^{N}\frac{1}{r_{ij}} \\
&\quad - \left[-\sum_{i=1}^{N}\frac{1}{2}\nabla_i^2 - \sum_{i=1}^{N}\sum_{A=1}^{M}\frac{Z_A}{r_{iA}} + \sum_{i=1}^{N}\sum_{j=1}^{N}(\hat{\mathcal{J}}_j(i) - \hat{\mathcal{K}}_j(i))\right] \\
&= \sum_{i=1}^{N}\sum_{j>i}^{N}\frac{1}{r_{ij}} - \sum_{i=1}^{N}\sum_{j=1}^{N}(\hat{\mathcal{J}}_j(i) - \hat{\mathcal{K}}_j(i))
\end{aligned}$$

The perturbation is thus the difference between the true electron-electron interactions and the averaged HF potential. The expectation values of both parts of the above operator have already been derived in Sections 4.3.3 and 4.3.4 and can be substituted into the expression for the first-order correction to the ground state energy,

$$\begin{aligned}
E_0^{(1)} &= \langle\Psi_0|\hat{\mathcal{H}}'|\Psi_0\rangle \\
&= \frac{1}{2}\sum_{i}^{N}\sum_{j}^{N}(\langle ij|ij\rangle - \langle ij|ji\rangle) - \sum_{i}^{N}\sum_{j}^{N}(\langle ij|ij\rangle - \langle ij|ji\rangle) \\
&= -\frac{1}{2}\sum_{i}^{N}\sum_{j}^{N}(\langle ij|ij\rangle - \langle ij|ji\rangle)
\end{aligned}$$

The zeroth-order energy is given by the expectation value of the unperturbed Hamiltonian, which is just the sum of the orbital energies, ε_i. The total energy including the first-order correction is exactly the Hartree-Fock energy (cf. Equation 4.28). The first correction due to electron correlation thus occurs in the second-order energy. The expression for the energy correction

is

$$\sum_{i<j}^{occ}\sum_{k<l}^{vir}\frac{|\langle\Psi_0|\hat{\mathcal{H}}'|\Psi_{ij}^{kl}\rangle|^2}{E_0 - E_{ij}^{kl}}$$

where the occupied orbitals are given indices i and j and the virtual/unoccupied orbitals k and l. The Slater determinant generated by exciting an electron in orbital i and one in orbital j to orbital k and l is given by Ψ_{ij}^{kl}. The summation is restricted so that every excitation is only counted once. The difference in energy between two Slater determinants is essentially the difference between orbitals energies, thus

$$E_0 - E_{ij}^{kl} = \varepsilon_i + \varepsilon_j - \varepsilon_k - \varepsilon_l$$

and the energy correction due to second-order Møller-Plesset perturbation theory (MP2) becomes

$$E_0^{(2)} = \sum_{i<j}^{occ}\sum_{k<l}^{vir}\frac{|\langle ij|kl\rangle - \langle ij|lk\rangle|^2}{\varepsilon_i + \varepsilon_j - \varepsilon_k - \varepsilon_l}$$

Derivation of higher order MPn corrections can be found in Szabo and Ostlund,[68] Section 6.5.

4.5.3 Configuration Interaction

The *configuration interaction* (CI) method writes the trial wave function as a linear combination of determinants with the expansion coefficients determined by requiring that the energy should be stationary. The molecular orbitals used for building the determinants are taken from the Hartree-Fock calculation,

$$\Psi_{CI} = c_0\Psi_{HF} + \sum_S c_s\Psi_s + \sum_D c_D\Psi_D + \ldots = \sum_{i=0} c_i\Psi_i$$

where the subscripts S and D denotes single and double excitations. The energy of the system can now be minimised subject to the constraint that the CI wave function is normalised. Including all possible excitations leads to the full CI wave function. Within the choice of basis set this is the best possible calculation that can be done and a full CI with an infinite basis set is an exact solution to the Schrödinger equation. In practice, however, the excitation levels are truncated at some predefined level. Since truncating at the singles level (CIS) does not provide any improvement over HF, the lowest level of improvement is obtained by including only double excitations (CID). A slight improvement over this is including both doubles and singles (CISD).

The *multi-configuration self-consistent field* (MCSCF) method not only optimises the coefficients but also the molecular orbitals used in the additional determinants. Additionally, *multi-reference configuration interaction* (MRCI) methods use not a HF wave function but a MCSCF wave function as excitation reference.

4.5.4 Coupled Cluster

The principle behind *coupled cluster* (CC) theory is that the full CI wave function can be described as

$$\Psi_{CC} = e^{\hat{T}}\Psi_{HF}$$

where $\hat{T}$ is the cluster operator defined as the sum of the individual operators for a system of N electrons that generate all possible determinants having $i = 1, 2, \ldots, N$ excitations. Operating with the full $\hat{T}$ operator on the HF determinant gives in essence the full CI solution. The difference between CI and CC can be seen in a Taylor expansion of the CC equation. We use double excitations as a representative example,

$$\Psi_{CCD} = e^{\hat{T}_2}\Psi_{HF} \qquad \hat{T}_2 = \sum_{i<j}^{occ}\sum_{k<l}^{vir} t_{ij}^{kl}\Psi_{ij}^{kl}$$
$$= \left(1 + \hat{T}_2 + \frac{\hat{T}_2^2}{2!} + \frac{\hat{T}_2^3}{3!} + \cdots\right)\Psi_{HF}$$

where $\hat{T}_2$ is the cluster operator incorporating all double excitations and t_{ij}^{kl} are called the amplitudes. Each application of $\hat{T}_2$ generates double excitations, so the product of two consecutive applications, $\hat{T}_2\hat{T}_2$, generates quadruple excitations and three applications generates hextuple excitations, etc. In practice once again, the number of terms needs to be limited. Including only $\hat{T}_1$ does not give any improvement over HF. Using $\hat{T}_2$ leads to coupled cluster doubles (CCD) and $\hat{T}_1 + \hat{T}_2$ leads to coupled cluster singles and doubles (CCSD). Including triples leads to CCSDT, but this is not very computationally effective and in practice the CCSD(T) method is rather used, which approximates the triple excitations through perturbation theory.

4.6 Density Functional Theory

In this section we introduce the main method of calculation applied throughout this work, *density functional theory* (DFT). The book by Koch and Holthausen[73] was used extensively in compiling this section. For further information, especially regarding the strengths and weaknesses of DFT, the reader is referred to this book. A wide array of exchange and correlation functionals exists and referring to each one is impossible. Instead, references to the specific functionals applied in this work will be given when the functionals are introduced in the discussion of the results and computational methods used.

4.6.1 Early Models

The earliest *a priori* attempt at evaluating the molecular energy based on only the electron density was that of Thomas and Fermi.[74,75] Their model

treats the kinetic energy with a quantum statistical model while the electron-electron and electron-nuclear contributions are treated classically,

$$E[\rho(\mathbf{r})] = \frac{3}{10}(3\pi^2)^{2/3}\int \rho^{5/3}(\mathbf{r})\,d\mathbf{r} - \sum_{A=1}^{M}\int \frac{Z_A}{R_{A1}}\rho(\mathbf{r})\,d\mathbf{r} + \frac{1}{2}\int\int \frac{\rho(\mathbf{r}_1)\rho(\mathbf{r}_2)}{r_{12}} \times d\mathbf{r}_1 d\mathbf{r}_2$$

At that time, however, it was assumed without proof that the correct electron density is that which minimises the energy subject to the constraint that $\int \rho(\mathbf{r}_1)\,d\mathbf{r}_1 = N$. In this sense then the model is only of historical importance. In 1951 J. C. Slater[76] proposed an expression for the exchange energy of a system based on the electron density,

$$E_x[\rho(\mathbf{r})] = -\frac{9\alpha}{8}\left(\frac{3}{\pi}\right)^{1/3}\int \rho^{4/3}(\mathbf{r})\,d\mathbf{r}$$

Earlier, Bloch and Dirac[77,78] derived a smiliar expression in which α had the value of $\frac{2}{3}$ and combined with the Thomas-Fermi expression gave the Thomas-Dirac-Fermi model.

4.6.2 The Hohenberg-Kohn Theorem

The above models were all based on the assumption (at that time unproved) that the ground state energy can be given by an exact functional of the electron density. This assumption was turned into a fundamental principle of DFT by Hohenberg and Kohn[79] in 1964. We briefly state these theorems.

The Existence Theorem

This theorem is quoted directly from the paper:

> *the external potential $V_{ext}(\mathbf{r})$ is (to within a constant) a unique functional of $\rho(\mathbf{r})$; since, in turn $V_{ext}(\mathbf{r})$ fixes $\hat{\mathcal{H}}$ we see that the full many particle ground state is a unique functional of $\rho(\mathbf{r})$.*

The Hohenberg-Kohn Variational Principle

Hohenberg and Kohn also showed that the variational theorem, as in molecular orbital theory, applies in the case of an electron density functional and that the energy of a trial electron density will always be an upper bound to the true ground state energy,

$$E[\tilde{\rho}(\mathbf{r})] \geq E_0[\rho_0(\mathbf{r})]$$

4.6.3 The Kohn-Sham Approach

The ground state density of an N electron system represented by the anti-symmetric wave function Ψ_0 is

$$\rho_0 = N \int |\Psi_0(\mathbf{x}_1, \mathbf{x}_2, \ldots, \mathbf{x}_N)|^2 \, d\omega_1 d\mathbf{x}_2 \cdots d\mathbf{x}_N \tag{4.34}$$

where integration is over the spin coordinates of all electrons and the spatial coordinates of all but one electron. The integral is the probability of finding electron 1 in volume element $d\mathbf{r}_1$. Since all electrons are identical, the probability of finding any electron is N times the probability for one electron. The density function $\rho(\mathbf{r})$ is a non-negative function of only the three spatial coordinates integrated over the total number of electrons.

The main problem with the Thomas-Fermi model in the previous sections is the poor representation of the kinetic energy. In 1965 Kohn and Sham[80] envisioned an approach in which the starting point is to take a fictitious non-interacting reference system, given by a Slater Determinant, whose density is the same as the real system whose electrons do interact. The kinetic energy, T_s, of the non-interacting system is given by

$$T_s = -\frac{1}{2} \sum_{i=1}^{N} \langle \vartheta_i | \nabla^2 | \vartheta_i \rangle$$

where ϑ_i are the Kohn-Sham (KS) spin orbitals of the non-interacting Slater determinant similar to that of Hartee-Fock theory, but given a different symbol so as not to be confused with HF theory. Integration over all spin coordinates results in the electron density given as a function of the KS spatial orbitals only, as

$$\rho(\mathbf{r}) = \sum_{i=1}^{N} |\phi_i(\mathbf{r})|^2$$

The non-interacting kinetic energy is not equal to the true kinetic energy and the residual part is simply added to the non-classical contribution (exchange and correlation),

$$E[\rho(\mathbf{r})] = T_s[\rho(\mathbf{r})] + J[\rho(\mathbf{r})] + E_{xc}[\rho(\mathbf{r})] + V_{Ne}[\rho(\mathbf{r})]$$

where $T_s[\rho(\mathbf{r})]$ is the kinetic energy of the non-interacting Slater determinant, $J[\rho(\mathbf{r})]$ is the Coulomb interaction, $E_{xc}[\rho(\mathbf{r})]$ the exchange-correlation energy and $V_{Ne}[\rho(\mathbf{r})]$ the nucleus-electron interaction energy. The expression for the energy of the interacting system is thus

$$\begin{aligned} E[\rho(\mathbf{r})] = &-\frac{1}{2} \sum_{i=1}^{N} \langle \phi_i(1) | \nabla^2 | \phi_i(1) \rangle + \frac{1}{2} \sum_{i=1}^{N} \sum_{j=1}^{N} \int \int |\phi_i(\mathbf{r}_1)|^2 \frac{1}{r_{12}} |\phi_j(\mathbf{r}_2)|^2 \, d\mathbf{r}_1 d\mathbf{r}_2 \\ &+ E_{xc}[\rho(\mathbf{r})] - \sum_{i=1}^{N} \int \sum_{A}^{M} \frac{Z_A}{r_{1A}} |\phi_i(\mathbf{r}_1)|^2 \, d\mathbf{r}_1 \end{aligned} \tag{4.35}$$

where the terms are all given in terms of KS spatial orbitals. The unknown term (functional), $E_{xc}[\rho(\mathbf{r})]$, then still remains. A procedure similar to that of Lagrange multipliers within the Hartree-Fock approximation can be applied to result in the canonical Kohn-Sham equations, analogous to the Hartree-Fock equations,

$$\left[-\frac{1}{2}\nabla_1^2 + \int \frac{\rho(\mathbf{r}_2)}{r_{12}}\, d\mathbf{r}_2 + V_{xc}(\mathbf{r}_1) - \sum_{A=1}^{M} \frac{Z_A}{r_{1A}}\right] \phi_i(1) = \varepsilon_i \phi_i(1) \tag{4.36}$$

The form of the potential due to the exchange-correlation energy, V_{xc}, is still unknown and can simply be expressed as the functional derivative of E_{xc} with respect to the electron density,

$$V_{xc}(\mathbf{r}) = \frac{\delta E_{xc}(\mathbf{r})}{\delta \rho(\mathbf{r})}$$

A detailed derivation of the above equations was done by Parr and Yang.[81]

4.6.4 Exchange-Correlation Energy

In the Hartree-Fock model the assumption is made that the wave function can be given by a *single* Slater Determinant. The approximation is thus made from the start and can therefore never deliver the true solution. In DFT the approximation only enters through the unknown exchange-correlation functional, and if the exact exchange-correlation functional was known, the wave function would be the exact solution. The principal goal of DFT development is thus the determination of $E_{xc}[\rho(\mathbf{r})]$. It is useful to write the functional dependence of $E_{xc}[\rho(\mathbf{r})]$ as

$$E_{xc}[\rho(\mathbf{r})] = \int \rho(\mathbf{r}) \varepsilon_{xc}[\rho(\mathbf{r})]\, d\mathbf{r}$$

where ε_{xc} is the exchange-correlation energy per particle (energy density). We can further split this quantity into its exchange and correlation parts,

$$\varepsilon_{xc}[\rho(\mathbf{r})] = \varepsilon_x[\rho(\mathbf{r})] + \varepsilon_c[\rho(\mathbf{r})]$$

Exchange energy only involves electrons of similar spin. Since correlation between opposite spin electrons involves both inter- and intraorbital contributions it will always be larger than correlation between similar spin electrons. Exchange energy can thus be given as the sum of both α and β contributions, whereas correlation energy is given in terms of its $\alpha \leftrightarrow \alpha$, $\beta \leftrightarrow \beta$ and $\alpha \leftrightarrow \beta$ components,

$$E_x[\rho] = E_x^{\alpha}[\rho_\alpha] + E_x^{\beta}[\rho_\beta]$$
$$E_c[\rho] = E_c^{\alpha\alpha}[\rho_\alpha] + E_c^{\beta\beta}[\rho_\beta] + E_c^{\alpha\beta}[\rho_\alpha, \rho_\beta]$$

This leads to the definition of *spin polarisation*,

$$\zeta = \frac{\rho_\alpha(\mathbf{r}) - \rho_\beta(\mathbf{r})}{\rho(\mathbf{r})}$$

In the next sections we look at general methods of determining $E_{xc}[\rho(\mathbf{r})]$.

4.6.5 Local-Density Approximations

In the *local density approximation* (LDA) the assumption is made that the electron density can be treated as a uniform electron gas and that the value of ε_{xc} at some point $\mathbf{r}$ is a function solely of $\rho(\mathbf{r})$,

$$E_{xc}^{LDA}[\rho] = \int \rho(\mathbf{r})\varepsilon_{xc}\rho(\mathbf{r})\, d\mathbf{r}$$

The exchange part of the energy density is given by (cf. Slater and Dirac/Bloch formulas in Section 4.6.1)

$$E_x^{LDA}[\rho] = -\frac{3}{4}\left(\frac{3}{\pi}\right)^{1/3} \int \rho^{4/3}(\mathbf{r})\, d\mathbf{r}$$

$$\varepsilon_x^{LDA}[\rho] = -\frac{3}{4}\left(\frac{3}{\pi}\right)^{1/3} \rho^{1/3}$$

The more general form of the approximation is the *local spin density approximation* (LSDA), where the assumption is made that the α and β electron densities are not the same. In this case the prefactor changes by a factor of $2^{1/3}$ and the α and β densities are raised individually (not their sum, as in LDA) to the $4/3$ power.

No such explicit expression is known for the correlation part, but highly accurate Monte Carlo simulations done by Ceperly and Alder[82] led to the analytical expression of ε_c by Vosko, Wilk and Nusair.[83] Another, more recent representation has been given by Perdew and Wang.[84]

4.6.6 Generalised Gradient Approximations

A further extension is of course to express the electron density as a non-uniform gas. In this case the value ε_{xc} is not only a function of $\rho(\mathbf{r})$ but also of $\nabla\rho(\mathbf{r})$. In practice it is found that a Taylor expansion in which the first term is simply the LDA approximation performs even worse than the simple LDA approach. Functionals which have been adjusted to perform correctly are collectively known as *generalised gradient approximations* (GGA) and can be written in general form as

$$E_{xc}^{GGA}[\rho_\alpha, \rho_\beta] = \int f(\rho_\alpha, \rho_\beta, \nabla\rho_\alpha, \nabla\rho_\beta)\, d\mathbf{r}$$

In practice, the energy of the GGA functional can once again be split into exchange and correlation parts.

We now enter an area where it is not anymore the physics behind the concept that leads us to the functional. Mathematical complex constructs are formed which adhere to the relevant boundary conditions. We therefore refrain from explicit discussion of these functionals. For an adequate summary of the most popular exchange and correlation functionals the reader is referred to the work by Koch and Holthausen (p. 77).[73]

4.6.7 Hybrid Functionals

In practice it is found that the exchange contributions are significantly larger in absolute numbers than the corresponding correlation effects. Fortunately, the exchange energy of a Slater determinant can be calculated exactly. In HF theory the exchange energy is given by the exchange integral, K_{ab} (Equation 4.17). Expanded in terms of the Kohn-Sham orbitals, the exchange energy for a closed shell system is (cf. Equation 4.29)

$$E_x^{exact} = -\frac{1}{4}\sum_{i=1}^{N}\sum_{j=1}^{N}\langle\phi_i(1)\phi_j(2)|\frac{1}{r_{12}}|\phi_j(1)\phi_i(2)\rangle$$

where the factor $\frac{1}{4}$ is a result of the fact that here we sum over the electrons (or one-electron orbitals) whereas in Equation 4.29 the summation ran over the two-electron orbitals. Hybrid DFT functionals mix together the exact exchange, E_x^{exact} with the gradient-corrected $E_x[\rho]$ and $E_c[\rho]$ functionals. The most popular hybrid functional, B3LYP, is defined by[85]

$$E_{xc}^{B3LYP} = (1-a_0-a_x)E_x^{LSDA} + a_0E_x^{exact} + a_xE_x^{B88} + (1-a_c)E_c^{VWN} + a_cE_c^{LYP}$$

where *B*88 is the exchange functional proposed by Becke[86] and *LYP* the correlation functional of Lee, Yang and Parr.[87] The constants are $a_0 = 0.20$, $a_x = 0.72$ and $a_c = 0.81$.

4.7 Basis Sets

In this section we explain the "building blocks" of computational wave functions, basis sets. Finally, the basis set superposition error (BSSE) is explained and a method is introduced of approximating the size of this error.

Before continuing, a matter of notation: when referring to computational results it is common practice to state the basis set applied after the level of theory is given. This is shown in the notation B3LYP/6-311+G(d,p) or MP2/6-31+G(d). The first example indicates that a molecule was calculated using the DFT hybrid functional B3LYP combined with the 6-311+G(d,p) basis set, the second indicates a Hartree-Fock calculation with a Møller-Plesset 2nd-order perturbation correction, combined with the 6-31+G(d) basis set.

4.7.1 Slater-Type Orbitals

Slater-type orbitals (STOs) have the form

$$\varphi_{\zeta,n,l,m}(r,\theta,\phi) = NY_{l,m}(\theta,\phi)r^{n-1}e^{-\zeta r}$$

where N is a normalisation constant, n is the principal quantum number, $Y_{l,m}$ is the spherical harmonic function depending on the angular momentum quantum numbers l and m, and ζ is called the orbital exponent. Early on STOs were used as basis functions due to their similarity to the atomic orbitals of hydrogen. The functions have no radial nodes so higher angular momentum orbitals were approximated by linear combinations of STOs. Unfortunately, although these functions show the correct radial behaviour, they are not suitable for the calculation of two-electron integrals since the product of two STOs cannot be solved analytically and one has to resort to numerical integration, hampering computational efficiency to a large extent.

4.7.2 Gaussian-Type Orbitals

Gaussian-type orbitals (GTOs) have the form

$$\varphi_{\zeta,l_x,l_y,l_z}(x,y,z) = Nx^{l_x}y^{l_y}z^{l_z}e^{-\zeta r^2}$$

where N is a normalisation constant, ζ is the orbital exponent and l_x, l_y and l_z are integral exponents. The sum of these exponents determine the type of orbitals, for example,

$$\begin{aligned}
2p_x &= Nxe^{-\zeta r^2}; \qquad L = l_x + l_y + l_z = 1+0+0 = 1\\
3d_{xy} &= Nxye^{-\zeta r^2}; \qquad L = l_x + l_y + l_z = 1+1+0 = 2\\
4f_{xyz} &= Nxyze^{-\zeta r^2}; \qquad L = l_x + l_y + l_z = 1+1+1 = 3
\end{aligned}$$

These functions are computationally much more efficient since products of gaussian functions can be solved analytically. A problem exists with d-type and higher orbitals. There are five orthogonal and linearly independent canonical d-orbitals, xy, xz, yz, x^2-y^2 and $3z^2-r^2$, while there are six possible combinations in cartesian coordinates, x^2, y^2,z^2,xy, xz and yz. However, linear combinations of the cartesian functions can be made to produce the canonical d-orbitals, together with a sixth combination $x^2+y^2+z^2$, which is actually an s-type GTO. Similarly the 10 cartesian f-functions can be combined to form 7 canonical f-orbitals.

Together with the fact that Gaussian functions are differentiable at the nucleus ($r = 0$) they also show radial decay exponential in r^2, where hydrogenic real atomic orbitals decay exponentially in r. Therefore, in practice, linear combinations of GTOs have to be made to better approximate the true

shape of atomic orbitals. These combinations are called *contractions* and the individual Gaussians are called *primitives*. Furthermore, there are two ways of making the contractions, segmented or general contractions. In segmented contractions, each primitive is only used once. In general contractions, all primitives are used in each contraction. GTOs are thus defined by their contractions coefficients and the orbital exponents of each primitive.

4.7.3 Basis Set Classification

A minimum basis set is one which uses a single Gaussian contraction for each atomic orbital. For first row atoms this means two s-functions (1s and 2s) and one set of p-functions ($2p_x$, $2p_y$ and $2p_z$). The next improvement is to use two contractions for each orbital, leading to *double zeta* (DZ) basis sets. Similarly, three, four or five contractions can be used leading to *triple zeta* (TZ), *quadruple zeta* (QZ) and *quintuple zeta* (5Z). Since bonding occurs between valence orbitals, it makes sense to constrict the usage of more than one contraction to only the valence orbitals, leading to *split valence* basis sets.

Basis functions are atom centred and although this leads to a good description of individual atomic orbitals, bonding in terms of molecular orbitals cannot be described sufficiently. A better description can be obtained by including basis functions of one angular momentum quantum number higher. These GTOs are called *polarisation functions*. For first row atoms they are d-type functions and for hydrogen (and helium), p-type. The last type of augmentation that can be done is for describing anions, excited states and "loose" complexes. Adding additional basis functions with the same angular momentum quantum number as the highest atomic orbital, but with smaller exponents, allows the electron density to delocalise further away. These GTOs are called *diffuse functions*.

Finally, we give the notation for showing the degree of contraction. The following example is for 6-311G first row atoms, $(11s, 5p) \rightarrow [4s, 3p]$. Parentheses indicate the total number of primitives, in order of increasing angular momentum quantum number. Square brackets show the number in the resulting contractions. Additionally, how the contraction was done can be shown by $(6311, 311)$. Summing up, this means that 11 s-type primitives were contracted to 4 s-type functions, the first consisting of 6 primitives, the second of 3 and the last two of one each. Also, 5 p-type basis functions were contracted to 3 p-types consisting of 3 primitives in the first functions and one each in the remaining two.

4.7.4 Effective Core Potentials

Systems involving third row atoms or heavier elements contain a large number of chemically unimportant but energetically important core electrons. Calculations can be sped up significantly if the core electrons are replaced

by analytical functions that approximate the core electron interactions. Such functions are called *effective core potentials* (ECPs) or *pseudopotentials*. Another advantage is that relativistic effects, which become significant for heavy elements, can be introduced implicitly through ECPs.

4.7.5 The Basis Set Superposition Error

In practice it is impossible to use infinite basis sets and we approximate the "electronic space" of each atom with a finite set of atom centred basis functions. If we consider a bimolecular interaction between fragments A and B where we have assigned basis set a to fragment A and basis set b to fragment B, the interaction energy is given by

$$\Delta E_{int} = E_{HF}^{a\cup b}(A \bullet B) - E_{HF}^{a}(A) - E_{HF}^{b}(B)$$

where $E_{HF}^{a\cup b}(A \bullet B)$ is the Hartree-Fock energy of the complex, calculated with the combined basis sets of both fragments and $E_{HF}^{a}(A)$ is the energy of fragment A in the geometry of the complex with its assigned basis set. The basis set used for the complex is thus larger than the one used for the individual fragments. The atoms of fragment A in the complex $A \bullet B$ may thus be described by basis functions not available to the atoms in the isolated fragment A. This leads to an unphysical lowering of the energy of the complex and hence the interaction energy. An approximate way of assessing this *basis set superposition error* (BSSE) is the *counterpoise correction* (CP) of Boys and Bernardi,[88]

$$E^{CP} = E_{HF}^{a\cup b}(A) + E_{HF}^{a\cup b}(B) - E_{HF}^{a}(A) - E_{HF}^{b}(B)$$

The fragments are all calculated with their geometry in the complex $A \bullet B$. The energy term $E_{HF}^{a\cup b}(A)$ is obtained by calculating the A fragment in the presence of its own atom centred functions plus the functions centred on the B fragment, but without any of the atoms of the B fragment present.

It must be noted that the "borrowing" of basis functions is not a mathematical artifact only. Charge transfer and polarisation takes place when the complex is formed and some borrowing simply reflects this reality. The CP correction thus always overestimates the BSSE.

4.8 Population Analysis

This section deals with methods of partitioning the electron density in terms of atoms and subsequently assigning atomic charge. The most basic method, Mulliken analysis, is discussed. Although this method delivers the worst results, many informative principles and concepts, also present in more refined approaches, are defined within this method and it serves as an adequate basis. Additionally, a much better technique frequently applied in this work, natural population analysis (NPA), is also discussed. Finally, Merz-Kollman charge determination, derived from the electrostatic potential, is discussed.

4.8.1 Mulliken Population Analysis

One of the first methods of associating a number of electrons (or charge) to a given atom was introduced by Mulliken.[89] The total number of electrons is given by

$$N = \sum_{i=1}^{N} \int \psi_i(\mathbf{r})\psi_i(\mathbf{r})\, d\mathbf{r}$$

Expanded in terms of K basis functions gives

$$\begin{aligned} N &= \sum_{i=1}^{N}\sum_{\mu=1}^{K}\sum_{\nu=1}^{K} \int c_{i\mu}\varphi_\mu(\mathbf{r})c_{i\nu}\varphi_\nu(\mathbf{r})\, d\mathbf{r} \\ &= \sum_{i=1}^{N}\sum_{\mu=1}^{K}\sum_{\nu=1}^{K} c_{i\mu}c_{i\nu} \int \varphi_\mu(\mathbf{r})\varphi_\nu(\mathbf{r})\, d\mathbf{r} \\ &= \sum_{i=1}^{N}\left(\sum_{\mu=1}^{K} c_{i\mu}^2 + \sum_{\mu\neq\nu}^{K} c_{i\mu}c_{i\nu}S_{\mu\nu}\right) \end{aligned}$$

where $c_{i\mu}$ and $c_{i\nu}$ are the coefficients of basis functions $\varphi_\mu(\mathbf{r})$ and $\varphi_\nu(\mathbf{r})$ in the ith molecular orbital and $S_{\mu\nu}$ is the overlap matrix element between basis functions $\varphi_\mu(\mathbf{r})$ and $\varphi_\nu(\mathbf{r})$. The second sum in parentheses represents the amount of electrons "shared" between basis functions. Mulliken suggested that this may be divided up equally between the two atoms on which basis functions $\varphi_\mu(\mathbf{r})$ and $\varphi_\mu(\mathbf{r})$ reside. The total atomic population on atom A, N_A, then becomes

$$N_A = \sum_{i}^{N}\left(\sum_{\mu\in A} c_{i\mu}^2 + \sum_{\mu\in A,\nu\notin A} c_{i\mu}c_{i\nu}S_{\mu\nu}\right)$$

In those cases where $\varphi_\mu(\mathbf{r})$ and $\varphi_\nu(\mathbf{r})$ both reside on A the corresponding overlap integrals will be zero due to the orthonormality of basis functions on the same atom. The atomic charge is given by

$$q_A = Z_A - N_A$$

Unfortunately there are various problems with Mulliken analysis, such as severe basis set dependence and unphysically negative or Pauli-violating populations.

4.8.2 Natural Population Analysis

Many of the problems associated with Mulliken population analysis are eliminated by *natural population analysis* (NPA).[90,91] Natural orbitals, introduced

by Löwdin,[92] arise as the eigenvectors of the one-electron reduced density operator,

$$\hat{\Gamma}(\mathbf{x}_1, \mathbf{x}_1') = N \int \Psi(\mathbf{x}_1, \mathbf{x}_2, \ldots, \mathbf{x}_N)\Psi^*(\mathbf{x}_1', \mathbf{x}_2, \ldots, \mathbf{x}_N)\, d\mathbf{x}_2 \cdots d\mathbf{x}_N$$

where the integral is the probability of finding an electron in the volume element $d\mathbf{x}_1$ at coordinates $\mathbf{x}_1$ and integration is over the space and spin coordinates of the remaining electrons $2, 3, \ldots, N$. Note the coordinates of Ψ and Ψ^* are different. The matrix elements associated with this operator, in terms of spin orbitals, are

$$\Gamma_{ij} = \int \chi_i^*(\mathbf{x}_1)\hat{\Gamma}(\mathbf{x}_1, \mathbf{x}_1')\chi_j(\mathbf{x}_1')\, d\mathbf{x}_1 d\mathbf{x}_1'$$

All NPA-related methods start with the determination of the *natural atomic orbitals* (NAOs). The reduced density matrix can be written in terms of localised blocks of basis functions centred on a specific centre, A. The eigenvectors $\{\theta_i^A\}$ of this localised $\hat{\Gamma}^A$ operator then give the pre-orthogonal NAOs. The final NAOs are then formed by means of an occupancy-weighted symmetric orthogonalisation procedure. The natural population q_i^A of orbital θ_i^A on atom A is given by the diagonal elements of the reduced density operator in the NAO basis,

$$q_i^A = \langle \theta_i^A | \hat{\Gamma} | \theta_i^A \rangle$$

With the density matrix transformed to the NAO basis, the *natural bond orbitals* (NBOs) can now be determined. Each one-centre block in the reduced density matrix is first searched for eigenvectors of occupancy ≥ 1.90. These one-centre orbitals are then identified as either core or lone pair orbitals and subtracted from the subsequent blocks. Next, all two-centre blocks are searched for eigenvectors of occupancy ≥ 1.90. This gives the NBOs. If no sufficient set of $N/2$ localised electron pairs can be found, the threshold is lowered. Each bond orbital, which can subsequently be decomposed into its constituent hybrids, also has an antibonding counterpart,

$$b_{AB} = c_A h_A + c_B h_b$$
$$b_{AB}^* = c_A h_A - c_B h_b$$

Finally, the residual density is partitioned into low occupancy Rydberg orbitals.

The optimal set of NBOs mimics the best Lewis structure of a given system. However, electrons do not strictly adhere to a specified set of localised two-electron orbitals and delocalisation of electron density is possible. Within NPA theory an estimate of the delocalisation can be obtained by perturbation theory. The Fock matrix in the NBO basis can be separated into diagonal and off-diagonal portions to serve as the unperturbed operator and

the perturbation, respectively. The eigenfunctions of the diagonal portion are simply the Lewis-type NBOs $\{b_{AB}\}$ with eigenvalues ε_{AB}. This leads to an estimate of the second-order energy lowering due to delocalisation given by

$$\Delta E^{(2)}_{\sigma\to\sigma^*} = \frac{\langle\sigma|\hat{\mathcal{F}}|\sigma^*\rangle}{\varepsilon_{\sigma^*} - \varepsilon_\sigma}$$

where $\hat{\mathcal{F}}$ is the Fock operator in the NBO basis, σ is a bonding NBO with orbital energy ε_σ and σ^* is an antibonding NBO with orbital energy ε_{σ^*}.

4.8.3 Charges Derived from the Electrostatic Potential

The molecular electrostatic potential is an observable which can be directly calculated from the wave function. Cox and Williams[93] have introduced a method which allows charges to be determined easily using the electrostatic potential. In their method the electrostatic potential is derived quantum mechanically for a system of N_{atom} atoms using a grid of N_{pnt} points,

$$V(\mathbf{r}) = \sum_A^M Z_A T(\mathbf{r}, \mathbf{r_A}) - \sum_\mu^K \sum_\nu^K P_{\mu\nu} \int \varphi^*_\mu(\mathbf{r}')\varphi_\nu(\mathbf{r}') T(\mathbf{r}, \mathbf{r}')\, d\mathbf{r}'$$

where $T(\mathbf{r}, \mathbf{r}')$ is defined as $|\mathbf{r} - \mathbf{r}'|^{-1}$. Restricting the expansion to only monopole terms, the set of charges $\{q_i\}$ can then be calculated by minimising the functional

$$F[\{q_i\}] = \sum_k^{N_{pnt}} \left[V(\mathbf{r}_k) - \sum_i^{N_{atom}} q_i T(\mathbf{r}_k, \mathbf{r}_i) \right]^2$$

Lagrange functionals can be employed to constrain the sum of charges to the exact total molecular charge. Singh and Kollman[94,95] proposed a modification where the points at which the potential is derived are defined on the van der Waals envelope.

4.9 Atoms in Molecules

Atoms in molecules (AIM) is a very powerful tool for understanding and interpreting chemical structure.[96,97] The strength of the technique lays in its ability to narrow the gap between quantum mechanics and "everyday chemistry". It is based on the electron density, an observable which can be calculated through computational means, but also verified experimentally. Using a quantum mechanically calculated variable AIM has the ability to verify the existence of bonds, characterise interactions and and provide an astounding array of information in a clear and understandable manner. A brief introduction to some fundamentals of the technique will be be given. Benzene will be used to illustrate the concepts.

Table 4.2: Summary of the four types of critical points. In addition to their names the three eigenvalues of the Hessian matrix at each CP is given, as well as the common (*r*,*s*) notation.

Name	λ_1	λ_2	λ_3	(*r*,*s*)
Nuclear attractor	+	+	+	(3,3)
Bond critical point	+	-	-	(3,-1)
Ring critical point	+	+	-	(3,1)
Cage critical point	- +	-	-	(3,-3)

Calculating the electron density from the wave function has already been introduced in Section 4.6.3 in Equation 4.34,

$$\rho = N \int |\Psi_0(\mathbf{x}_1, \mathbf{x}_2, \ldots, \mathbf{x}_N)|^2 \, d\omega_1 d\mathbf{x}_2 \cdots d\mathbf{x}_N$$

Integration is over the spin coordinates of all the electrons and the spatial coordinates of all but one electron. Once the wave function has been determined, the electron density can be calculated and a number of operations performed on the result. Figure 4.1(a) shows a contour diagram of the electron density in the plane of a benzene ring. The gradient vectors at each point on the electron density surface point in the direction of the greatest increase. Following these vectors results in the construction of gradient paths. A property of a gradient path is that at every point it is perpendicular to an envelope of constant scalar value. A collection of gradient paths is called a gradient vector field. The majority of paths terminate at a nucleus (or a nuclear attractor). However, there exists a collection of paths that start at infinity but terminate at a point between nuclei. These paths form a surface around each atom and their collective name is an interatomic surface or zero-flux surface. The area inside each surface is called the atomic basin of the particular atom and the gradient vector field consisting of the vectors starting at infinity and terminating at a nucleus span the atomic basin of that nucleus. Properties derived from the electron density for a particular atom (eg. the atomic charge) is usually determined through integration across the atomic basin of that atom. Figure 4.1(b) shows the gradient vector field spanning the atomic basins of each of the atoms in benzene, as well as the interatomic surface paths.

The points mentioned above, at which interatomic surface paths terminate, are called *critical points* (CPs) because the gradient vector becomes zero at these points. There exists four different kinds of critical points in three dimensional space, characterised by the number of nonzero eigenvalues (the rank, *r*) of the Hessian matrix ($\nabla\nabla\rho$) and the algebraic sum of the signs of the eigenvalues (the signature, *s*). The accepted notation is to write a CP as (*r*,*s*). Table 4.2 lists the different kinds of critical points.

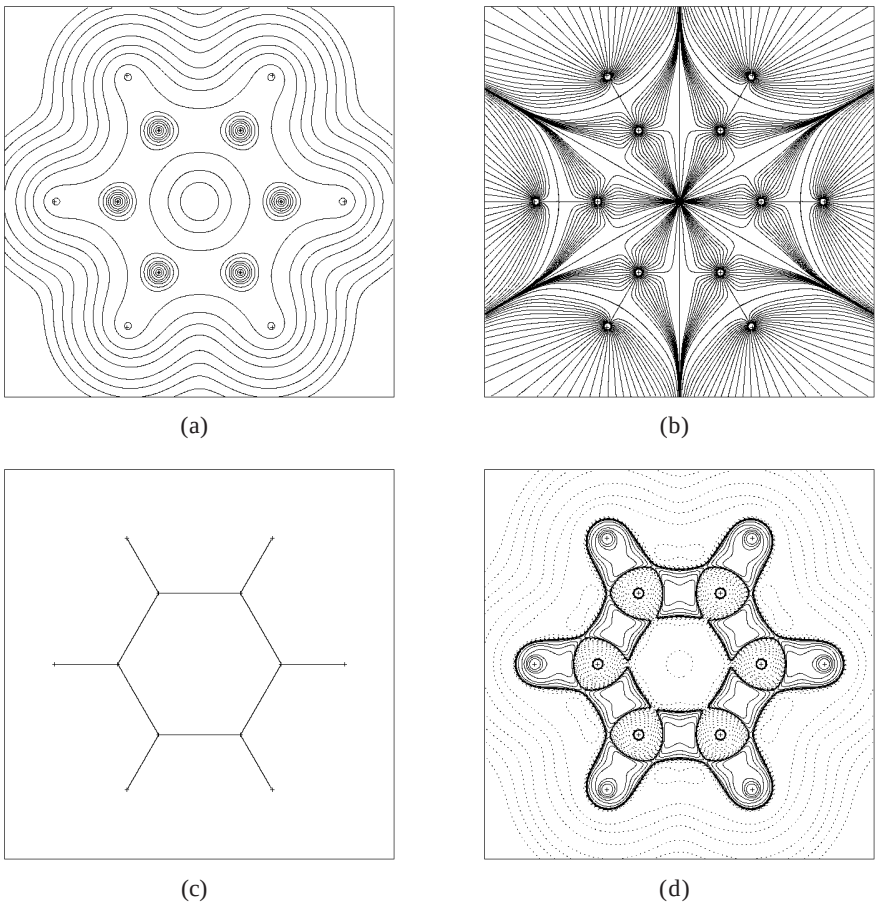

Figure 4.1: (a) A contour diagram of the electron density in benzene. (b) The gradient vector field, showing the atomic basins. The interatomic surface paths in the plane are also shown. (c) The bond paths in benzene. (d) A contour diagram of the Laplacian of the electron density, solid lines indicate regions of local charge concentration, dotted lines indicate regions of local charge depletion.

There exists a set of two gradient vector paths of maximum ascent leading away from a BCP. Tracing these two paths in both directions leads to two atoms. In general, such a line can exists between any interacting atoms, in which case it is merely called an atomic interaction path. In the specific case that the forces on the nuclei are zero the interaction path becomes a bond path. Figure 4.1(c) shows the bond paths in the benzene molecule.

Another insightful procedure is to plot the second derivitive of the electron density, the Laplacian $\nabla^2\rho$. This generates a contour diagram indicating regions of local charge concentration and charge depletion. By convention, solid lines indicate isodensity lines with a negative Laplacian value - thus a local maximum - and dotted lines indicate positive Laplacian values - thus a local minimum. Figure 4.1(d) shows $\nabla^2\rho$ for benzene.

Chapter 5

A Computational Study of B–N Clusters

5.1 Introduction

In this chapter we will present attempts to simulate the large changes between selected gaseous and crystalline species and explore a fundamental question related to them: is this solely the work of dipole-dipole interaction or is there an additional factor or even factors responsible for this astounding phenomenon?

Our investigation will start with a model which explicitly simulates the effects of the surroundings. The dipole-dipole interaction potential between two point dipoles is given by[98]

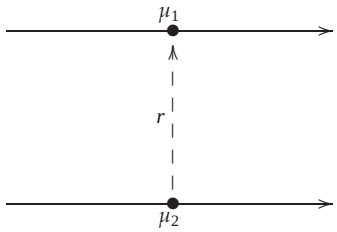

$$V(r) = \frac{\vec{\mu}_1 \cdot \vec{\mu}_2}{4\pi\epsilon_0 r^3} - 3\frac{(\vec{\mu}_1 \cdot \vec{r})(\vec{\mu}_2 \cdot \vec{r})}{4\pi\epsilon_0 r^5} \tag{5.1}$$

The potential is a maximum when the two dipoles are parallel. As the dipoles turn away from parallel the dot product between them becomes smaller until it vanishes completely when the dipoles are aligned perpendicularly. The force will be attractive if the two dipoles are in opposite directions and repulsive in the same direction.

A SCRF calculation in which the surroundings are described as a continuous dielectric have successfully simulated the structural changes in HCN–BF_3 and CH_3CN–BF_3.[31] This model is based on dipole and/or induced di-

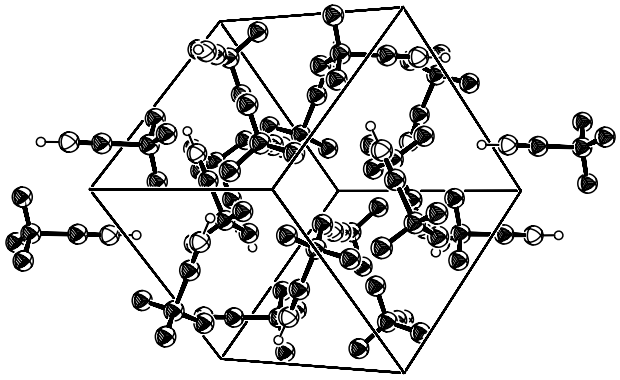

(a) The HCN–BF_3 unit cell.

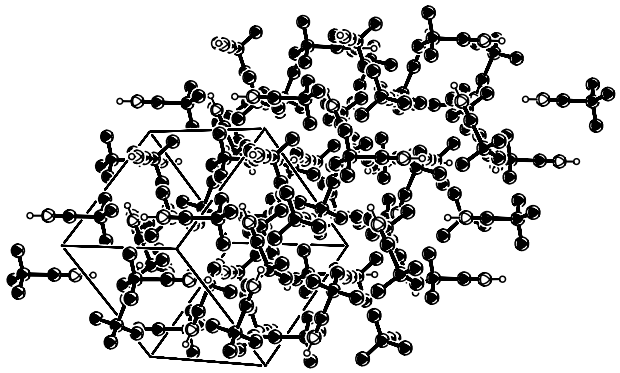

(b) A compounded representation of HCN–BF_3 unit cells.

Figure 5.1: The crystallographic unit cell of HCN–BF_3 (a, top). A compounded representation in which the unit cell is doubled along the *a*-axis and *b*-axis is also shown (b, bottom).

pole interactions between molecules in solution. Figure 5.1 shows the HCN–BF_3 unit cell as well as a compounded representation of four unit cells (a total of four units cells, two along the *a*-axis, two along the *b*-axis) in order to illustrate the arrangement of the molecules within the crystal. The related methylated CH_3CN–BF_3 is not shown but shows similar packing. Within each unit cell there is a dimeric unit consisting of two antiparallel molecules separated by 3.8 Å. The other surrounding molecules lay at near perpendicular orientations to this pairing. Since such an orientation minimises the dipole-dipole interaction energy the principle goal of the first section is to investigate whether dipole-dipole interactions are the main protagonist in the phase-dependent structural changes.

Similar success with the SCRF method and $H_3N–SO_3$ has also been achieved.[26] This molecule crystallises in the same space group as $HCN–BF_3$ and although crystal models were built, they add little additional information to the situation.

As already mentioned, the largest structural effects are found in $HCN–BF_3$. The methylated species presents the second largest change, however in principle the nonmethylated compound provides the same chemical environment for investigation. The most important factor governing which systems are studied is the availability of experimental structures. With this kept in mind, there are only three borontrifluoride compounds of interest, $HCN–BF_3$, $CH_3CN–BF_3$ and $H_3N–BF_3$. Only one sulphurtrioxide complex shares this property of having both its gas phase and crystalline structure experimentally known, $H_3N–SO_3$. The $H_3N–BF_3$ and $H_3N–SO_3$ complexes have surely received their fair share of interest throughout the literature. A search in the Chemical Abstracts lists 106 results for $H_3N–BF_3$ with over 500 hits for the zwitterionic and acidic form of the sulphur trioxide complex.

In our work, the nitrile species will thus receive the most attention, with the nonmethylated species a representative of this type of interaction. From a computational viewpoint, the amine adducts very quickly become quite complex with the rotational freedom of the NH_3 group. This is of course not a factor when dealing with the unsaturated nitriles.

5.2 Computational Models and Methods

The aim is to build a model from which the effect of individual molecules on a central molecule or molecules can be assessed. The procedure for setting up the model will be explained in general terms since it is similar for both $HCN–BF_3$ and $CH_3CN–BF_3$.

The $HCN–BF_3$ molecule crystallises in the orthorhombic space group *Pbca*, translating to centre of inversion point group symmetry, C_i. The methylated compound crystallises in *Pnma* and in terms of point group symmetry consists of inversion plus an additional mirror plane. The mirror plane however, adds no additional complications to the procedure. Figure 5.3 (given together with the discussion of the results, Section 5.4.1) illustrates the different models. In this case, centre of inversion symmetry can only be achieved with an even number of molecules. To retain the point group symmetry, the crystal model was thus started at the dimer level with the next higher level a tetramer, then a hexamer and finally an octamer. A sphere of inclusion with the centre of inversion at the origin was created around the dimer and gradually enlarged until four, six and finally eight molecules were included in total. In the experimental crystal structure of $CH_3CN–BF_3$ there is rotational disorder of the methyl groups leading to a 50(6) % distribution of both staggered and eclipsed conformers.[13] The exact positions of the hy-

drogen atoms were determined by doing an optimisation of only the hydrogen atoms in a 222 representation of the unit cell, keeping the heavy atoms constrained to the crystal structure coordinates. Due to the size of the system involved this calculation was done using the universal force field (UFF).[99–101]

The other calculations were done with B3LYP.[85] Two Pople basis sets were used, 6-31G(d) and 6-31+G(d). The largest HCN–BF_3 model, $(HCN–BF_3)_8$, consists of 56 atoms in total. With the computational power of modern computers, this might not seem large enough to justify the use of the very small double-zeta basis set. However, due to a very flat potential energy surface (see Figure 5.2 in Section 5.3.2) the calculations had to be done by recalculating analytical second derivatives at every step of the optimisation. This added considerable computational effort and hence the choice of basis set had to be limited to double zeta with little additional functions.

Calculations were also done on systems restricted to only monomer and dimer levels, and these were done at B3LYP / 6-311+G(2df,p).

Calculations were performed with both the Gaussian 98[102] and Gaussian 03 program packages.[103]

5.3 Quality of Results

Weakly bound, van der Waals-type complexes, like HCN–BF_3 and CH_3CN–BF_3, are known to possess very flat potential energy surfaces and often high levels of theory and large, balanced basis sets are needed to accurately describe them. It is thus of benefit to first explore the effect of theory and basis set on the representative complex HCN–BF_3.

5.3.1 Density Functional and Basis Set Comparison

Tests of MP2 theory and various DFT functionals in predicting the structures and bond dissociation energies of amine-borane complexes suggests that B3LYP performs poorly for dative B–N bonds.[104] This prompted us to do a study of various DFT functionals in conjunction with different basis sets and compare the results with those obtained with MP2 theory. The DFT functionals used, are

- B3LYP: This is the very popular three-parameter hybrid functional originally proposed by Becke[105] in 1993. The current form was proposed by Stevens *et al.*[85] and uses the B (or B88) exchange functional of Becke[86] and the LYP correlation functional of Lee, Yang and Parr.[87]

- B97-1: Another hybrid functional originally introduced by Becke[106] as B97, based on an elaborate fitting procedure. This form is a modification done by Hamprecht and coworkers.[107] This functional was found to give geometries comparable with the very popular B3LYP but more accurate energies.[108]

- mPW1PW91: A hybrid one-parameter functional proposed by Adamo and Barone[109] which uses modified Perdew-Wang exchange and the PW91 correlation functional.
- mPW1K: This hybrid functional, originally designed to model incompletely bound transition states, is suggested by Truhlar et al.[110] as a better approach for B–N dative bonds. It differs only from the mPW1PW91 model in the percentage of exact HF exchange.
- mPWPW91: This is the exchange functional first introduced by Perdew and Wang and modified by Adamo and Barone,[109] mPW. It is combined with the gradient-corrected correlation part of the PW91 Perdew-Wang functional.[111] Note that this is a pure DFT functional and no exact HF exchange is included.

Basis sets used are the Pople 6-31G and 6-311G sets of DZ and TZ quality in conjunction with diffuse and polarisation functions. The molecules were all calculated with C_{3v} symmetry. All stationary points were characterised as minima by frequency analysis. Table 5.1 shows the results of the basis set and level of theory comparisons for a HCN–BF_3 monomer.[I] The hybrid B3LYP functional compares very well with the computationally intensive MP2 results. The difference between the average value and the experimental value over all the tested basis sets is indeed slightly smaller for B3LYP than MP2. Surprising is the near *exact* correlation between the experimental value and the B3LYP/6-31G(d) result. This should, however, be seen as coincidental rather than a genuine measure of quality, since calculations with larger basis sets deviate to a much larger degree. Another surprising result is that the mPW1K functional, explicitly designed for incompletely bound complexes, performs the worst of all the tested methods. The high average error is due to the fact that this functional calculates both a long and short minimum based on the inclusion of diffuse functions in the basis set. This phenomenon, which has also been witnessed by Cabaleiro-Lago and Ríos,[36] will be further investigated in later sections. The mPW1PW91 functional also consistently calculates a shorter minimum with the inclusion of a diffuse function. The accuracy of the functionals tested is thus

$$\text{B3LYP} < \text{MP2} < \text{B97}-1 < \text{mPWPW91} < \text{mPW1PW91} < \text{mPW1K}$$

Functional tests were also done on the $(HCN–BF_3)_2$ dimer. In this case the system was constrained to C_i symmetry and once again all stationery points were characterised as minima by means of frequency analysis. Results are shown in Table 5.2. This time B3LYP befalls a similar fate to many of the

[I] A complex between molecules A and B is sometimes referred to as a dimer $A-B$ in the literature. We restrict the use of dimer and higher order "polymers" to molecules of the type $(A-B)_n$ and refer to single $A-B$ molecules as monomers.

Table 5.1: Comparison of B–N bond lengths in $HCN–BF_3$ calculated with MP2 and selected DFT functionals and various Pople basis sets.[a]

	MP2	B3LYP	B97-1	mPW1 PW91	mPW1K	mPW PW91
6-31G(d)	2.439	2.474	2.444	2.350	2.287	2.416
6-31+G(d)	2.430	2.511	2.461	1.828	1.806	1.854
6-31G(d,p)	2.443	2.474	2.444	2.350	2.285	2.417
6-31+G(d,p)	2.437	2.512	2.462	1.828	1.805	1.854
6-311G(d)	2.493	2.494	2.420	2.345	2.285	2.416
6-311+G(d)	2.435	2.483	2.420	1.979	1.882	2.296
6-311G(d,p)	2.503	2.495	2.451	2.351	2.288	2.418
6-311+G(d,p)	2.447	2.484	2.421	2.055	1.887	2.302
Average	2.453	2.491	2.440	2.136	2.066	2.247
Experimental	2.473	...	...	...	...	...
$\lvert\Delta Exp\rvert$[b]	0.020	0.018	0.033	0.337	0.407	0.226

[a] Distances in Å. [b] Difference between the average and experimental values.

Table 5.2: Comparison of B–N bond lengths in $(HCN–BF_3)_2$ calculated with selected DFT functionals and various Pople basis sets.[a]

	B3LYP	B97-1	mPW1PW91	mPW1K	mPWPW91
6-31G(d)	1.806	1.781	1.751	1.735	1.762
6-31+G(d)	1.735	1.727	1.709	1.697	1.720
6-31G(d,p)	1.800	1.776	1.747	1.732	1.757
6-31+G(d,p)	1.736	1.728	1.710	1.698	1.721
6-311G(d)	2.330	1.825	1.773	1.750	1.802
6-311+G(d)	1.772	1.750	1.727	1.713	1.741
6-311G(d,p)	2.329	1.826	1.773	1.751	1.800
6-311+G(d,p)	2.484	1.752	1.728	1.715	1.743
Average	1.999	1.771	1.740	1.724	1.756

[a] Distances in Å.

functionals tested for the monomer in that two minima are found. This leads to an average value that is much higher than the other functionals. The conclusion would therefore have been very clear if only the results from Table 5.1 were considered, especially since B3LYP delivers good monomer results with small basis sets such as 6-31G(d) and 6-31+G(d). However, results for the dimer cast some doubt on the decision. It should be taken into account that all minima shown in Tables 5.1 and 5.2 are not necessarily global minima (with the inherent computational difficulties in modelling this complex this would require a rigourous potential energy surface scan in many degrees of freedom for the dimer). Also, MP2 theory, which is generally regarded as producing better results than density functional methods, does indeed also give two minima.[36] The conclusion is thus that B3LYP is an adequate functional for our purposes.

5.3.2 The Effect of BSSE

An important factor when dealing with weakly interacting systems is the influence of the basis set superposition error (BSSE). The counterpoise correction was used to evaluate the BSSE.[112,113] Table 5.3 shows the results using B3LYP and the same set of basis sets as previously employed. The values can be divided into two classes, those for basis sets with diffuse functions, and those without. The basis sets without diffuse functions, in order of increasing size, have values of 2.06, 2.06, 1.79 and 1.78 kcal.mol^{-1}. Those with diffuse

Table 5.3: The basis set superposition error (BSSE) in HCN–BF_3 calculated at B3LYP and various basis sets. The dative bond length is also given, as well as the value resulting from a geometry optimisation in which the BSSE between the HCN and BF_3 fragment is removed from the SCF energy at each consecutive step. [a]

	BSSE	r(B–N)	r(B–N)^{BSSE}[b]
6-31G(d)	2.06	2.474	2.685
6-31+G(d)	0.58	2.511	2.605
6-31G(d,p)	2.06	2.474	2.685
6-31+G(d,p)	0.60	2.512	2.607
6-311G(d)	1.79	2.494	2.653
6-311+G(d)	0.70	2.483	2.569
6-311G(d,p)	1.78	2.495	2.651
6-311+G(d,p)	0.63	2.484	2.569
6-311+G(2df,p)	0.44	2.554	2.553

[a] Distances in Å. Energies in kcal / mol.
[b] Calculated on a BSSE corrected PES.

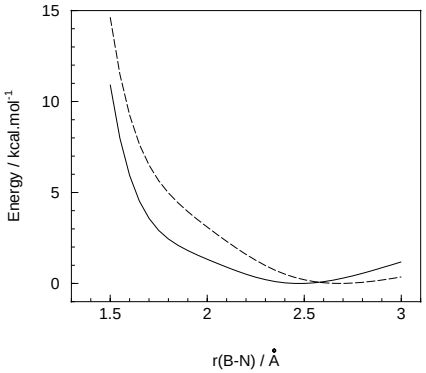

(a) r(B–N) at B3LYP / 6-31G(d).

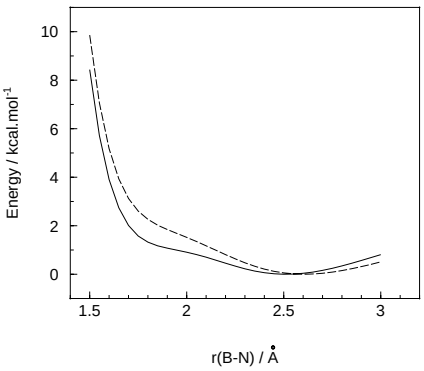

(b) r(B–N) at B3LYP / 6-31+G(d).

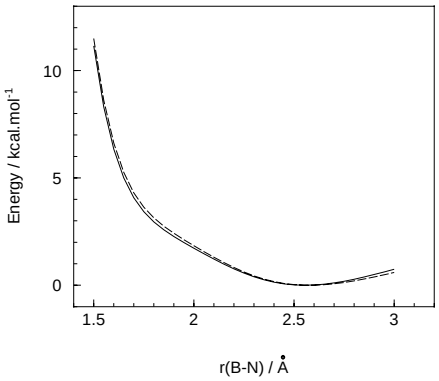

(c) r(B–N) at B3LYP / 6-311+G(2df,p).

Figure 5.2: Potential energy curves for the B–N bond stretching coordinate in HCN–BF_3. Solid lines indicate the uncorrected curve, broken lines indicate the BSSE corrected curve.

functions have 0.58, 0.60, 0.70 and 0.63 kcal.mol^{-1}. Comparing the functionals that calculate two substantially different minima with basis functions only differing with the addition of a diffuse function, high values of BSSE are associated with minima with long B–N bonds and small values with minima with short B–N bonds.

Figure 5.2 shows potential energy curves for the stretching r(B–N) coordinate, calculated with the cluster basis sets and another considerably larger basis set, 6-311+G(2df,p). Incorporating BSSE between the HCN and BF_3 fragments into the potential energy surface clearly shifts the minimum to a longer distance for both the DZ basis sets. It is also very interesting to notice the shape of the curve. There seems to be signs of a second possible minimum at a shorter r(B–N), albeit a stationary point is never actually reached. The effect is also clearly more pronounced with 6-31+G(d). As expected, the effect of BSSE on the optimisation has largely been eliminated when using

the heavily augmented TZ basis set. It is comforting to note the resemblance between the potential energy curve corrected for BSSE and the uncorrected curve.

It is important to note that BSSE for the basis set used in the cluster calculations amounts to between one-half and one-third of the complex dissociation energy, which was calculated to be 4.8 kcal.mol^{-1} at B3LYP / 6-31G(d) (uncorrected for zero-point vibrational energy). When a bond is formed and electron pair density is shared, and even more so donated as is the case here, a natural consequence is for orbitals of one of the bonded atoms to use / occupy the orbitals of the other atom. The counterpoise correction makes no distinction between "natural" orbital overlap and "unnatural" overlap. However, following this argument one expects that the shorter bond should have more BSSE, which is in fact the opposite of the observed trend. Also, diffuse functions provide more "freedom" to the electron density, in particular at distances relatively removed from the other standard basis functions, and should necessarily result in less superposition. The argument that large BSSE values necessarily indicate erroneous calculations should not be taken without careful thought regarding the system and the specific property or properties of interest.

In general though, some doubt is cast on the usefulness of these small sets, however, our primary goal is to achieve comparable results for very large systems and we envision that the existing error is incorporated into *all* the crystal models and can thus be ignored when comparisons are made.

5.4 Crystal Model Results

The $(HCN–BF_3)_n$ and $(CH_3CN–BF_3)_n$ crystal models will be discussed separately. Where results are given in tabular and graphical form, they are given together in order to allow easy comparison. Addendum A gives the distance matrices of the optimised structures with accompanying pictures. The pictures given in the main text are smaller versions of these and the reader is referred to Addendum A for a more detailed version.

5.4.1 $(HCN–BF_3)_n$ Crystal Simulations

The results from the crystal models for $HCN–BF_3$ are shown in Table 5.4. These calculations were carried out at both B3LYP / 6-31G(d) and B3LYP / 6-31+G(d). Ball and stick representations of the optimised structures are shown in Figure 5.3(a)-(d).

The addition of one antiparallel molecule at B3LYP / 6-31G(d) leads to a shortening of 0.668 Å, or 80% of the experimental shortening of 0.835 Å. The

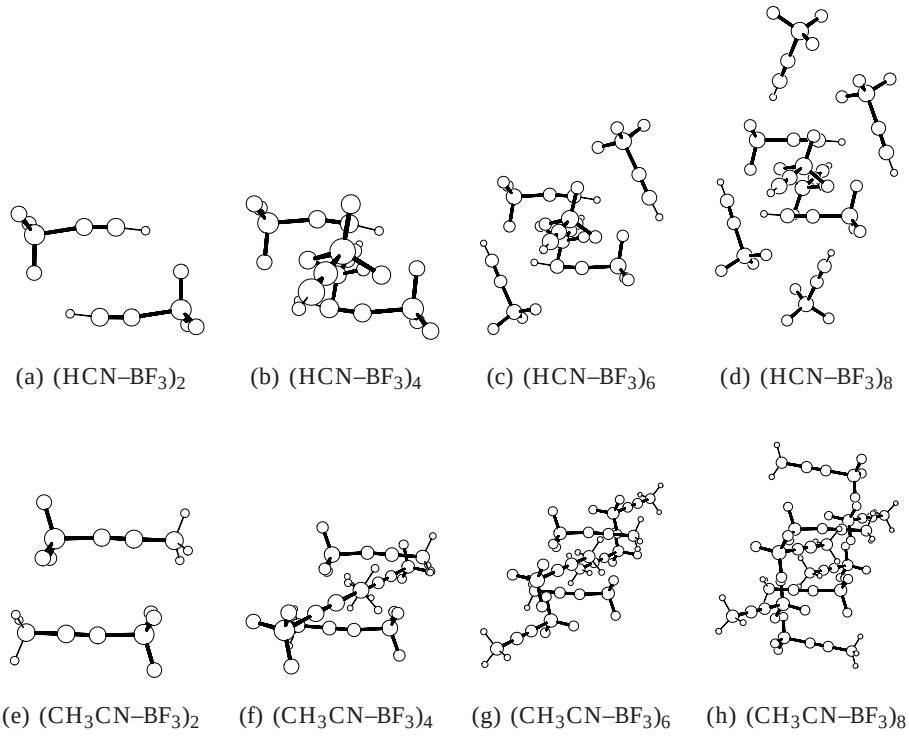

(a) $(HCN–BF_3)_2$ (b) $(HCN–BF_3)_4$ (c) $(HCN–BF_3)_6$ (d) $(HCN–BF_3)_8$

(e) $(CH_3CN–BF_3)_2$ (f) $(CH_3CN–BF_3)_4$ (g) $(CH_3CN–BF_3)_6$ (h) $(CH_3CN–BF_3)_8$

Figure 5.3: The $(HCN–BF_3)_n$ and $(CH_3CN–BF_3)_n$ crystal models; $n = 2, 4, 6, 8$. The central in-plane molecular pair was optimised, with the surrounding molecules kept frozen.

diffuse basis set[II] calculates a longer monomer bond length but also a shorter dimer bond length than the nondiffuse set. Thus the change is even more pronounced at B3LYP/6-31+G(d), where the value is 0.777 Å. The monomers are bent along the H–C–N axis due to the formation of C–H$\cdots$F hydrogen bonds. These hydrogen bonds are also the cause of the difference between the in-plane N–B–F angle ($\angle$(NBF1) in Table 5.4) and the two out-of-plane angles.[III] It is important to emphasise that the orientation of the molecules in the dimer model is so as to maximise the dipole-dipole interaction. The next addition shortens the bond a further 0.077 Å in the nondiffuse case but only 0.012 Å when calculated with the diffuse basis set. These molecules are added (a reminder that the additions exactly reflect the arrangement in the crystal structure) near-perpendicular to the plane and therefore a smaller change is expected. From this point onwards the addition of molecules

[II]The 6-31+G(d) basis set will be referred to as the diffuse basis set and 6-31G(d) the nondiffuse set.

[III]The plane is defined in such a manner that it contains the H–C–N–B linkages of both molecules of the central dimer. Due to the low symmetry this is not strictly an exact plane but for discussion purposes it will suffice.

Table 5.4: Results of the $(HCN–BF_3)_n$ and $(CH_3CN–BF_3)_n$ crystal model optimisations. The parameters for the isolated molecules are also shown. Calculations were done at B3LYP / 6-31G(d) and B3LYP / 6-31+G(d)[a]

	r(B–N)	∠(NBF1)[b]	∠(NBF2)[c]	∠(NBF3)[c]	$\angle\overline{(NBF)}$[d]
			6-31G(d)		
$HCN–BF_3$	2.474	93.0	93.0	93.0	93.0
$(HCN–BF_3)_2$	1.806	99.4	102.5	102.3	101.4
$(HCN–BF_3)_4$	1.739	100.3	104.5	103.6	102.8
$(HCN–BF_3)_6$	1.670	102.1	105.6	105.6	104.4
$(HCN–BF_3)_8$	1.665	103.8	106.1	103.5	104.5
$CH_3CN–BF_3$	2.281	94.9	94.9	94.9	94.9
$(CH_3CN–BF_3)_2$	1.684	105.2	103.8	103.1	104.0
$(CH_3CN–BF_3)_4$	1.666	106.4	103.3	103.8	104.5
$(CH_3CN–BF_3)_6$	1.645	107.1	103.4	104.3	104.9
$(CH_3CN–BF_3)_8$	1.627	105.9	104.5	106.0	105.5
			6-31+G(d)		
$HCN–BF_3$	2.511	93.0	93.0	93.0	93.0
$(HCN–BF_3)_2$	1.734	101.4	103.5	103.5	102.8
$(HCN–BF_3)_4$	1.722	101.0	104.8	104.2	103.3
$(HCN–BF_3)_6$	1.661	102.6	105.7	106.0	104.8
$(HCN–BF_3)_8$	1.659	103.9	106.2	104.2	104.8

[a] Distances in Å. Angles in degrees. [b] ∠NBF1 is the in-plane angle. Note that in $(HCN–BF_3)_n$ the in-plane F1-atom points towards the closest antiparallel neighbour whereas in $(CH_3CN–BF_3)_n$ the in-plane F1-atom points away from the antiparallel neighbouring molecule. [c] ∠NBF2 and ∠NBF3 are the out-of-plane angles.
[d] The average value of the three NBF angles.

results in almost identical changes for both basis sets. The order of change thus converges, independent of the diffuse nature of the basis set. By the time six molecules have been added at B3LYP / 6-31G(d), 97% of the experimental change has been simulated. Due to the longer monomer bond length at B3LYP / 6-31+G(d) the change is even larger using this combination.

Hydrogen bonds involving fluorine are known to be weak since the large electronegativity and low polarisability of fluorine renders it a weak hydrogen acceptor. Howard *et al.*[114] even argued that C–F$\cdots$H–C contacts are not to be judged as being hydrogen bonds as they are weak, with energies similar to van der Waals complexes. In the dimer the in-plane N–B–F angle, whose fluorine is hydrogen bonded[IV] to the opposite hydrogen, is almost three degrees less than the out-of-plane angles. Similar observations are made in the

[IV] We will not debate whether this is a true hydrogen bond or a weak van der Waals interaction.

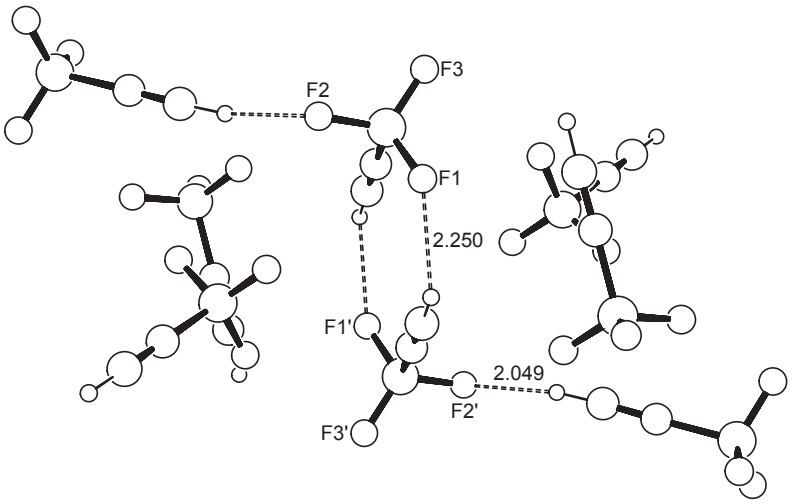

Figure 5.4: The $(HCN–BF_3)_8$ system with C–H$\cdots$F contacts shown. The contact distance are indicated in Ångstrom. For the relevant angles see Table 5.4.

tetramer and hexamer. The two out-of-plane angles in the tetramer are also not equivalent. Although this effect is not due to hydrogen bonding, the larger N–B–F angle lies closer to a fluorine atom on an adjacent molecule, leading to more electrostatic repulsion and hence the larger angle. The sum of van der Waals radii of fluorine (1.47 Å) and hydrogen (1.2 Å) is 2.67 Å. In the octamer, one of the two molecules added lays close enough to one of the out-of-plane fluorine atoms to be involved in hydrogen bonding and this angle is considerably less than the remaining out-of-plane angle. Figure 5.4 illustrates the hydrogen bonds in the $(HCN–BF_3)_8$ crystal. The C–H$\cdots$F1 distance is 2.250 Å and the C–H$\cdots$F2 distance is 2.049 Å (F1 and F2 are identified in Figure 5.4). Accepting a correlation between the bond length and bond strength of the hydrogen bonds, the size of the N–B–F angle thus corresponds with the strength of the associated hydrogen bond. This correlation should not be seen in absolute terms. If the angle between the boron, fluorine and hydrogen atom is smaller than 180° (measured anticlockwise from the boron to the hydrogen) the hydrogen bond will ”pull” the fluorine atom towards the boron and decrease the N–B–F angle. Similarly the fluorine can also by ”pulled” away if the angle is larger than 180°, leading to a larger N–B–F angle. On average though, the values correlate well with the change in B–N bond length, in that the average N–B–F angle becomes larger as the dative bond length decreases.[12,38]

5.4.2 $(CH_3CN–BF_3)_n$ Crystal Simulations

The results from the crystal models for $CH_3CN–BF_3$ are also shown in Table 5.4. Ball and stick representations of the optimised structures are shown in

Figure 5.3(e)-(h). Adding the pairs of molecules in a manner based strictly on which lays closest to the central dimer leads to difficulties in this optimisation. The addition of the seventh and eighth molecules occur along the same axis as all the previous additions, leading to an oblong shaped model. This creates open ends on two sides for the cavity in which the dimer unit resides and causes the dimer to move around to an undesirable extent, inflicting serious convergence issues on the optimisation. The final addition was thus made neglecting the distance criterium in the $(CH_3CN–BF_3)_8$ model, in order to block at least one end of the cavity and ease the optimisation. The $(HCN–BF_3)_8$ model also has open ends, but the calculation did not suffer similar problems.

The methylation of $HCN–BF_3$ adds an additional degree of freedom with the rotation of the methyl group. The most stable monomer conformation first needed to be obtained. The conformation in which the methyl and borontrifluoride are eclipsed is found to be a minimum at B3LYP / 6-31+G(d). The staggered conformer is a one-dimensional maximum on the PES (with the negative frequency being a rotation from staggered to eclipsed). At B3LYP / 6-31G(d), however, neither the staggered nor eclipsed forms display negative frequencies. The eclipsed conformation, however, is less than 0.0025 kcal.mol^{-1} more stable. More important though is that the diffuse basis set calculates short B–N bonds for both the eclipsed (minimum) and staggered (1D-maximum) conformers, 1.752 Å and 1.754 Å, respectively. The nondiffuse set, on the other hand, calculates near-identical long B–N bond distances of 2.281 Å ($\pm$ 0.0007) for both minimum conformations! Clearly this erratic behaviour of basis set dependence, first noticed by Giesen and Phillips,[48] is much more evident in this case than with $HCN–BF_3$. The structures reported for both basis sets are thus eclipsed minima.

The geometrical changes brought on by adding only two molecules are considerably larger than in the case of $HCN–BF_3$. The B–N bond length is already shortened to 1.684 Å in $(CH_3CN–BF_3)_2$. Adding two more molecules shortens the bond to 1.666 Å. Another two leads to 1.646 Å. Finally, the addition of six molecules in total shortens the bond to 1.627 Å, a few thousandths of an Ångstrom *less* than the value in the crystal structure, 1.630 Å.

Once again, the values of the N–B–F angles are found to be influenced by the formation of hydrogen bonds. The interactions involving hydrogens atoms in the methylated compound however, are slightly more complex. As explained earlier, in Section 5.2, the positions of the hydrogen atoms in the crystal models were determined by doing a UFF optimisation with constraints on the heavy atoms. This resulted in near-eclipsed conformers for each molecule in the energy minimum of the whole system. In this case, near-eclipsed equates to an "improper" H–C(–C–N–)B–F dihedral angle of roughly 10°. Near-eclipsed conformers are also the result of the DFT calculations on the dimer. From a purely computational point of view, this is allowed by the fact that all the crystal systems were calculated with C_i sym-

metry. This of course provides the freedom to alter all three H–C(–C–N–)B–F dihedral angles independently. The dimer was also calculated with C_{2h} symmetry but the resultant structure was found to be a second-order transition state. The two negative frequencies correspond with symmetric and antisymmetric rotations of the methyl groups. The near-eclipsed conformations result in nonidentical C–H$\cdots$F contact distances which immediately alerts one to the existence of different hydrogen bonds. An atoms in molecules (AIM) analysis was done in order to verify the existence of hydrogen bonds.[96] The AIMPAC program package was used. A (3,-1) bond critical point was found *only between the shorter of the two C–H$\cdots$F contacts.* This is in agreement with studies on dihydrogen bonding in $(H_3N–BH_3)_2$ dimers in which topographical analysis of the electron density showed that dihydrogen bonds only form between one pair of $H^{\delta+}\cdots H^{\delta-}$ contacts.[115,116] These authors also found a dimer with C_i symmetry to be the minimum energy structure, with the C_{2h} structure a transition state. This explains the tendency of the methyl groups to rotate slightly away from the completely eclipsed conformation (which is the energy minimum for the monomer) so that the contact distance with the hydrogen bonded fluorine atom (2.321 Å) is less than the nonbonded pairing (2.608 Å). Although there is no bond critical point, the distance between the nonbonded hydrogen and fluorine suggests a weak attractive van der Waals interaction.

The above interactions are very clearly reflected in the three N–B–F angles in the dimer. The largest of the angles, at 105.1°, means that the fluorine points away from the opposite molecule and no interaction is possible. The second largest angle, at 103.9°, is that of the fluorine interacting through very weak van der Waals forces with the opposite molecule. The smallest angle, at 103.1°, is that of the fluorine atom involved in hydrogen bonding. Once again the strength of the interaction with fluorine atoms influences the corresponding N–B–F angle.

In the larger $(CH_3CN–BF_3)_n$ models the existence of hydrogen bonds becomes less clear cut. It has to be kept in mind that the basis set used in these calculations is not suited at all for a thorough description of hydrogen interactions. Even more so, C–H$\cdots$F interactions are known to be weak and in some cases it is doubtful whether they should even be called hydrogen bonds.[114] Whether the interactions are true hydrogen bonds, very weak van der Waals or electrostatic in nature, the fact remains that the N–B–F angles are clearly influenced by their existence. This result will take on more meaning once the findings of Section 5.6 have been incorporated.

5.5 The Relationship Between the Dipole-Dipole Interaction and Structure

The relationship between the dipole-dipole interaction and the structural changes in r(B–N) was investigated by considering each molecular dipole as a point dipole lying at the geometric centre of the linear atoms (H–C–N–B and C–C–N–B for $HCN–BF_3$ and $CH_3CN–BF_3$, respectively) of each molecule. The direction of the dipole vector at this point was determined by the orientation of the linear atoms in space. The interaction energy was calculated classically using Equation 5.1 (p. 50) and plotted against the values of r(B–N) in all the crystal models for both $HCN–BF_3$ and $CH_3CN–BF_3$. The value of each molecular dipole was determined based on the length of the B–N bond of each molecule in the cluster, compared to a quadratic polynomial fitting of r(B–N) with the molecular dipoles of a series of r(B–N) constrained optimised single molecules. This method does neglect the effect of polarisation by adjacent molecules on the dipole moment. All DFT calculations were done at B3LYP / 6-31G(d). Figure 5.5(a)-(d) (p. 65) shows the results.

To test the validity of this model, a similar graph was constructed for $H_3N–BH_3$, based on the results by Dillen and Verhoeven.[34] They calculated larger systems consisting of 8, 10, 18, 20 and 30 molecules surrounding a single $H_3N–BH_3$ molecule. As simplification the dipole moment of the gas phase species was used in our calculation.[8] Figure 5.5(e)-(f) shows the results. In the case of $H_3N–BH_3$ there is a striking similarity between the calculated bond changes and the dipole-dipole interaction energy. Note that the final model was constructed with the intention of lessening the stabilisation and this is clearly reflected in the graphs. The same conclusion cannot be made for $HCN–BF_3$ and $CH_3CN–BF_3$. In these systems the bond length clearly does not respond in the same fashion as would be expected based on purely dipole-dipole stabilisation.

It has to be kept in mind that the models of Dillen and Verhoeven are much larger than those employed in thus study and this may aid in the similarities. Nevertheless, these results do suggest that there may be alternative forces at work.

5.6 Electron Delocalisation in $HCN–BF_3$ and $CH_3CN–BF_3$

The changes in structure have successfully been simulated using explicit molecular models. The next step is to elucidate some information on the bonding in these complexes. This was done for isolated $HCN–BF_3$ and $CH_3CN–BF_3$ in terms of natural orbitals.[90,91] The NBO 5.0 code was used.[117] Since the systems are now considerably smaller, the basis set has been enlarged to 6-311+G(2df,p), and the level of theory remains B3LYP. This should also lead

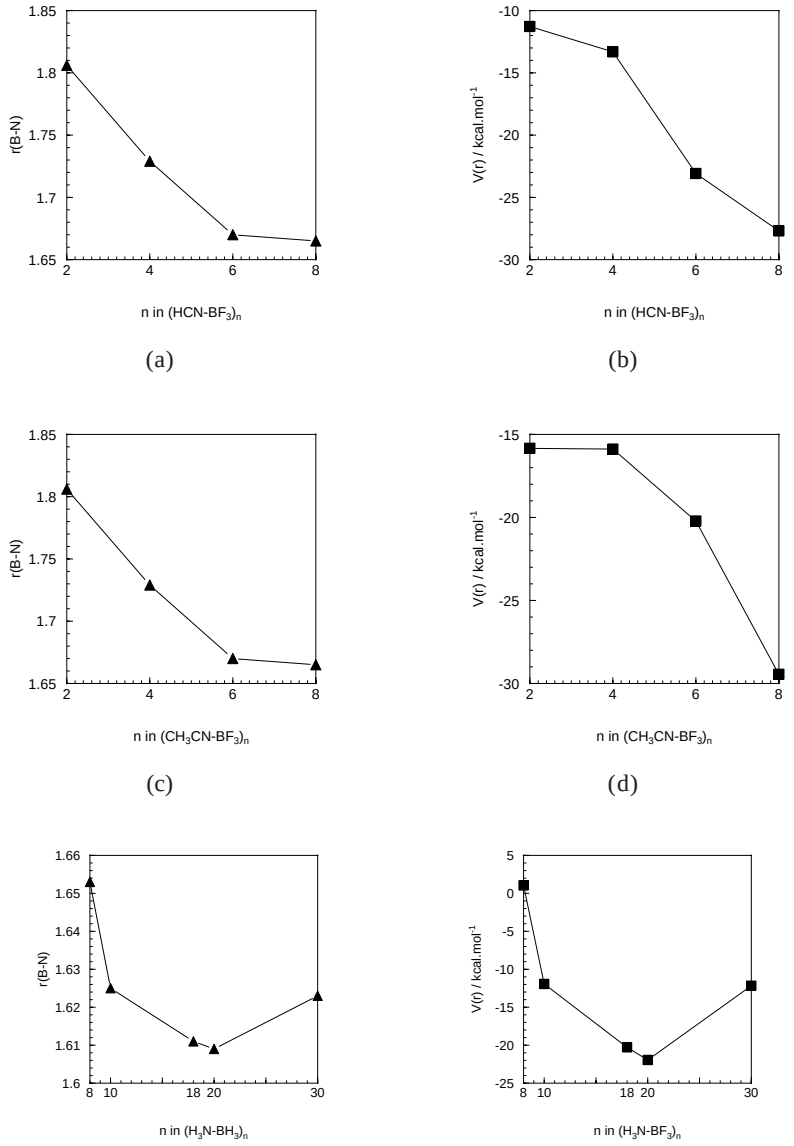

Figure 5.5: The trend between the length of the dative bond (r(B–N),triangles) as well as the dipole-dipole interaction energy (V(r),squares) and the model size in $(HCN–BF_3)_n$ (a and b, top) and $(CH_3CN–BF_3)_n$ (c and d, middle) and $(H_3N–BH_3)_n$ (e and f, bottom). Data for a-d was obtained at B3LYP/6-31G(d). Data for e and f was taken from the work of Dillen and Verhoeven.[34]

to considerably lower BSSE (see Section 5.3.2, with specific reference to Table 5.3). The optimised structures are shown in Figure 5.6, together with bond distances and angles. Both structures were calculated with C_{3v} symmetry

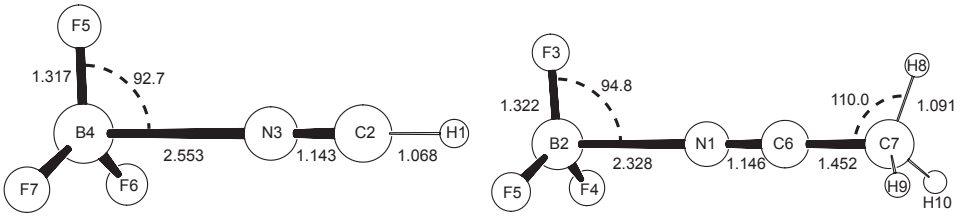

(a) (b)

Figure 5.6: Minimum energy structures of $HCN–BF_3$ (a, left) and $CH_3CN–BF_3$ (b, right) optimised at B3LYP / 6-311+G(2df,p)

and the stationary points characterised as minima by frequency analysis. The intended Lewis structure had to be requested, since the default searching algorithm of the NBO 5.0 program did not calculate a natural bond orbital (NBO) between the donor and acceptor fragment. A measure of the quality of the NBO structure can be done by comparing the amount of electrons in Lewis-type orbitals with those in non-Lewis natural orbitals. The resultant $HCN–BF_3$ structure has 98.75% of its electrons in Lewis-type natural orbitals and 1.25% in non-Lewis natural orbitals. For $CH_3CN–BF_3$ these percentages are 98.7% and 1.3%.

Second-order perturbation analysis between all "filled" (donor) Lewis-type NBOs and "empty" (acceptor) non-Lewis NBOs estimates the energetic importance of these interactions. Since this leads to a loss of occupancy of the idealised Lewis structure they are referred to as delocalisation corrections to the zeroth-order natural Lewis structure. The dominant delocalisation interactions in $HCN–BF_3$ and $CH_3CN–BF_3$ are shown in Table 5.5. The three largest entries are the consequence of $n \rightarrow \sigma^*$ delocalisation from the third lone pair on each of the fluorine atoms into the antibonding natural orbital of the nitrogen-boron bond. Another interesting set of entries is the delocalisation of the second lone pair on each of the fluorine atoms into the antibonding natural orbital of its boron-fluorine bond. These are related to the partial double bond character of the boron-fluorine bonds in borontrifluoride, which has been used to qualitatively explain the relative strengths of the boron-halogens as acceptors.[58] The third lone pair has much better delocalisation into σ^*(B–N) than any of the other fluorine lone pairs into σ^*(B–F), not only because of better overlap, but more importantly because the orbital energies of the lone pair and the antibonding orbital lie closer together. (cf. E(j)-E(i) and F(i,j) in Table 5.5).

The bonding and antibonding natural orbitals of the boron-nitrogen bond in $HCN–BF_3$ has the following compositions,

$$\sigma(\text{B–N}) = 0.9984(\text{sp}^{0.99})_N(98.7\%) + 0.1143(\text{sp}^{6.70})_B(1.3\%)$$
$$\sigma^*(\text{B–N}) = 0.1143(\text{sp}^{0.99})_N(1.3\%) - 0.9984(\text{sp}^{6.70})_B(98.7\%)$$

Table 5.5: Important delocalisation interactions in the NBO basis of $HCN–BF_3$ and $CH_3CN–BF_3$.[a]

donor (i)[b]	acceptor (j)[c]	$E^{(2)}$ [d]	E(j)-E(i)[e]	F(i,j)[f]
	$HCN–BF_3$			
BD(1) N3-B4	RY*(1) C2	17.32	1.92	0.163
LP(1) F5	RY*(1) B4	11.87	2.39	0.150
LP(2) F5	BD*(1) B4-F6	12.32	0.86	0.092
LP(2) F5	BD*(1) B4-F7	12.32	0.86	0.092
LP(3) F5	BD*(1) N3-B4	41.13	0.50	0.134
LP(2) F6	BD*(1) B4-F5	12.32	0.86	0.092
LP(2) F6	BD*(1) B4-F7	12.32	0.86	0.092
LP(3) F6	BD*(1) N3-B4	41.13	0.50	0.134
LP(2) F7	BD*(1) B4-F5	12.32	0.86	0.092
LP(2) F7	BD*(1) B4-F6	12.32	0.86	0.092
LP(3) F7	BD*(1) N3-B4	41.13	0.50	0.134
	$CH_3CN–BF_3$			
BD(1) N1-B2	RY*(1) C6	18.61	1.76	0.162
LP(1) F3	RY*(2) B2	12.40	2.33	0.152
LP(2) F3	BD*(1) B2-F4	12.28	0.84	0.091
LP(2) F3	BD*(1) B2-F5	12.28	0.84	0.091
LP(3) F3	BD*(1) N1-B2	38.55	0.52	0.132
LP(2) F4	BD*(1) B2-F3	12.28	0.84	0.091
LP(2) F4	BD*(1) B2-F5	12.28	0.84	0.091
LP(3) F4	BD*(1) N1-B2	38.55	0.52	0.132
LP(2) F5	BD*(1) B2-F3	12.28	0.84	0.091
LP(2) F5	BD*(1) B2-F4	12.28	0.84	0.091
LP(3) F5	BD*(1) N1-B2	38.55	0.52	0.132

[a] Delocalisation energy in kcal / mol. All other values in a.u.
[b] Donor NBOs are indicated as bond orbitals (BD) or lone pairs (LP). Where more than one LP is possible, they are numbered. The atom labelling is shown in Figure 5.6. [c] Acceptor NBOs are indicated as low occupancy non-Lewis Rydberg orbitals (RY*) or antibonding NBOs (BD*). [d] The second-order stabilisation energy. [e] The difference in energy between the donor and acceptor NBOs. [f] The off-diagonal NBO Fock matrix elements for NBO *i* and NBO *j*. This indicates the overlap.

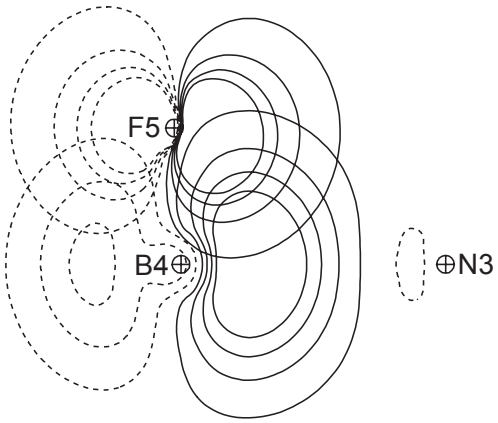

Figure 5.7: A superimposed contour diagram showing the overlap of the fluorine lone pair with the antibonding boron-nitrogen natural bond orbital in $HCN–BF_3$.

The bonding interaction is thus mainly localised in a sp-hybrid on the nitrogen atom, with the antibonding interaction in a p-orbital (strictly speaking a $sp^{6.7}$-hybrid with a very large contribution from the p-orbital, 86.3%) on the boron atom. The occupation of the bonding orbital is slightly less than expected from a fully occupied orbital, 1.98 e. The most influential result however, is that the considerable delocalisation discussed earlier leads to a very large antibonding orbital occupation of 0.302 e. The occupation of the lone pair natural orbitals involved in the delocalisation are consequently reduced as well. The bonding in the gas phase is thus determined to a very high degree by the properties of the donor, with the acceptor only influencing the nature of the bond through antibonding contributions. Figure 5.7 shows a superimposed contour diagram of the n(F) pre-orthogonal natural bond orbital (PNBO) and the σ(B–N) PNBO. The pre-orthogonal orbitals are plotted simply because they present better visual representations. The natural bond orbitals differ from them only in that they have been made orthogonal to each other. However, this creates "orthogonality tails" which may leave unwanted visual artifacts.[90]

Similarly the dative bond in $CH_3CN–BF_3$ consists of

$$\sigma(\text{B–N}) = 0.9842(\text{sp}^{0.99})_N(96.9\%) + 0.1770(\text{sp}^{4.82})_B(3.1\%)$$
$$\sigma^*(\text{B–N}) = 0.1770(\text{sp}^{0.99})_N(3.1\%) - 0.9842(\text{sp}^{4.82})_B(96.9\%)$$

The same observations can be made. The bonding interaction is again localised on the donor atom, with the destabilising influence being exerted through a high occupation of the antibonding orbital, localised on the p-orbital (in this case, one with slightly less pure p-character, 82.3%) of the boron. The antibonding occupation is 0.278 e. Less n(F)$\rightarrow$ σ^*(B–N) delocalisation takes place due to slightly less overlap and also a larger difference

in energy between the antibonding NBO and the fluorine lone pair orbitals. The fact that the methylated compound has a shorter bond in the gas phase than $HCN–BF_3$ is thus reflected through comparison of their bonding / antibonding NBO occupation.

A final interesting NBO-based calculation is presented to further demonstrate the importance of the above-explained delocalisation. It is possible to identify the specific elements in the NBO Fock matrix (strictly speaking the Kohn-Sham matrix in DFT) that represent a certain delocalisation. These elements can then be *deleted* from the NBO Fock matrix, the matrix diagonalised and then used to determine the new density matrix which will be used in the SCF evaluation. Optimising with this density matrix then produces an electronic system unaffected by the specific delocalisation. At B3LYP / 6-311+G(2df,p) an optimisation with the $n(F) \rightarrow \sigma^*(B–N)$ delocalisation removed calculates a boron-nitrogen bond length of only 1.526 Å and an N–B–F angle of 104.4°. It should be noted that the NBO 5.0 manual warns against the use of this technique with DFT methods. Since the densities calculated by DFT differ in nature from pure *ab initio* densities, caution should be exercised in interpreting energetic results when DFT methods are employed. Nevertheless, this does illustrate the importance of the delocalisation. It is interesting to note that although the bond distance is considerably shorter than the crystal structure value of 1.638 Å, the N–B–F angle is more than one degree less than the value of 105.6° in the crystalline phase.

The intricate relationship between the dative bond length and the hybridisation angle at the boron atom has been known for some time.[12,38] NBO analysis now casts some light on this phenomenon. In classical terms, competition for occupation of the boron p-orbital exists between the fluorine lone pairs on the acceptor and the lone pair on the donor. In quantum chemical terms, delocalisation from the fluorine lone pairs into the p-orbital of the boron atom, which after bond formation has become the antibonding orbital of the dative interaction, has a considerable effect on the strength of the interaction. The amount of delocalisation is firstly determined by the overlap between the orbitals on the relevant atoms, which is influenced in a static sense by their type, but even more so by their relative spatial orientation. This variable is affected during the optimisation of the structure as the atoms change their coordinates and we thus label this as being a nonstatic influence. Secondly, the energy gap between the orbitals also determines the delocalisation. This variable is open to very specific change, since it is determined by the electronic environment and type of donor and acceptor atom. It is thus possible to maximise this by carefully choosing the donor and acceptor species. The lone pair orbital on the donor might be well suited to enhance donation by lying close in energy to the accepting orbital, but combined with the acceptor, its antibonding counterpart must be much lower or higher in energy than the acceptor lone pair carriers in order to nullify the delocalisation effect.

Were the lone pairs to be completely absent, this should have a considerable effect on the strength of the dative bond, and this is indeed clearly demonstrated by the bond length in hydrogenated boron species such as $H_3N–BH_3$, in which the dative bond length is 1.672 Å in the gas phase.[8] For reference, a calculation was done on the hypothetical species $HCN–BH_3$. At B3LYP / 6-311+G(2df,p) it has an optimised boron-nitrogen bond length of 1.543 Å.

5.7 Changes in $(HCN–BF_3)_2$

The results from Sections 5.4.1 and 5.4.2 show that the dominant structural changes occur with the addition of a single antiparallel neighbour, in agreement with the work of Cabaleiro-Lago and Ríos.[36] In this section the interaction between two molecules in a $(HCN–BF_3)_2$ dimer is studied at B3LYP / 6-311+G(2df,p). At first the calculations were done enforcing C_i symmetry , as was the case in the model mentioned earlier. However, it soon became apparent that a higher symmetry would be beneficial. Higher symmetry results in more symmetry species and this will be of great assistance in the correlation of molecular orbitals. More on this later in the section. The main idea behind these calculations is to obtain a measure of the response of a monomer to the approaching antiparallel molecule in the dimer. This can be done by optimising the dimer at a series of frozen perpendicular separations.

5.7.1 Structural Changes

The $(HCN–BF_3)_2$ system was thus constructed to conform to C_{2h} symmetry, with some additional constraints. The individual molecules were kept linear, with the exception of the fluorine atoms and the hydrogen atom. The hydrogen atom was allowed to deviate towards the opposite molecule so that the hydrogen bond formation could occur. The two molecules were also kept parallel to maximize the dipole-dipole interaction.

Stationary points for both a “normal” C_{2h} dimer as well as the system with the additional constraints (henceforth labelled C'_{2h}) were determined. This gives a measure of the influence of the additional constraints. Figure 5.8(a,b) gives fully detailed optimised structures of both the C_{2h} and C'_{2h} dimer. The normal C_{2h} dimer is a minimum on its PES. The constrained structure, however, features one negative frequency, corresponding to a rotation of the BF_3 groups. A few interesting structural results need some commenting on. Firstly, the boron-nitrogen bond length is shorter by 0.079 Å in the C'_{2h} dimer, which is quite astounding if we consider the limited effect the additional constraints should be expected to have on the geometry of the molecules. The dipole-dipole interaction is surely strengthened by the parallel constraint, but the two molecules are further away (judged by the fluorine-hydrogen contact distance, 2.179 Å for C_{2h} compared to 2.443 Å for C'_{2h}), which in turn lessens

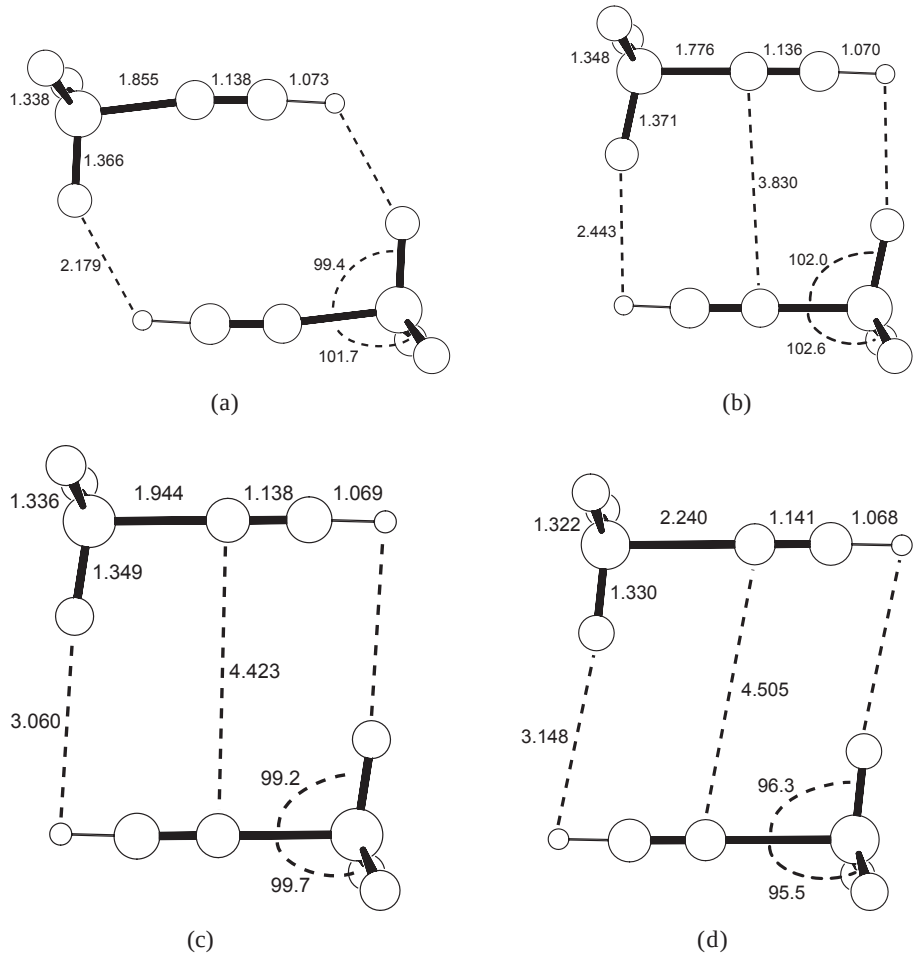

Figure 5.8: The optimised $(HCN–BF_3)_2$ dimer with C_{2h} symmetry (a, top left) and with additional constraints of being linear and parallel (b, top right). The two points between which the bond change occurs are also shown (c and d, bottom).

the interaction. The dipole-dipole interaction is additionally strengthened by the fact that in the latter case the two molecules align nearly horizontally. The hydrogen-fluorine contact distances create no doubt that the hydrogen-fluorine interaction is much weaker when the dative bond is shorter.

Scans were done with the scanning variable the perpendicular distance between the two molecules, starting from 2.5 Å to 5.5 Å, in steps of 0.1 Å. This was followed by another, similar scan, but now with a smaller window of change, between 4.0 Å and 5.0 Å, and in smaller steps of 0.02 Å. Figure 5.9(a) shows the dative bond length as a function of the intermolecular separation distance. The boron-nitrogen bond length slowly increases as the distance between the two molecules is increased. Between 4.42 Å and 4.44 Å, however, a sudden change occurs. The geometries at these separations are given in

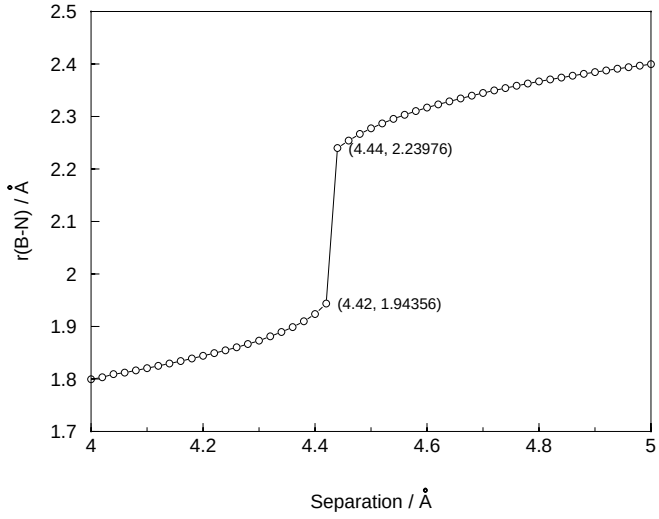

(a)

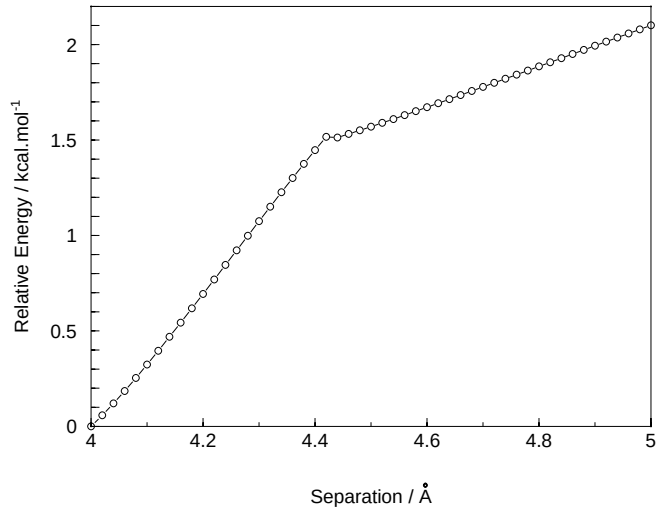

(b)

Figure 5.9: The dative bond length as a function of the perpendicular distance between two molecules in the $(HCN–BF_3)_2$ dimer (a, top). The two points between which the change in bond length occurs, are marked. The change in energy as the complex geometry changes, relative to the energy at the starting separation of 4.00 Å, -836.3119705 Hartree (b, bottom).

Figure 5.8(c,d). The structures are fully detailed to include bond distances and angles. The bond changes from 1.944 Å to 2.240 Å and the in-plane N–B–F angle changes from 99.2° to 96.3°. The nitrile bond is not greatly affected

by the change in dative bond, it shortens by only 0.003 Å as the dative bond shortens. This clashes with the *first bond length variation rule* of Gutmann,[66] which states: "The smaller the intermolecular distance D → A, the greater the induced lengthening of the adjacent intramolecular bonds both in the donor and acceptor components". The changes in the boron-fluorine bond lengths, however, do correlate with this rule. The shorter donor-acceptor bond leads to a higher partial charge on the acceptor, which in turn leads to a lengthening of the substituent bonds to the acceptor. The out-of-place behaviour of the nitrile bond again alerts one to its important role in the structural changes. Although the existence of a formal hydrogen bond is inconclusive at this point, the hydrogen-fluorine contact distance is shorter in the case where the associated boron-fluorine bond is longer. Another very interesting result stems from this calculation. The dative bond length change occurs at a hydrogen-fluorine contact distance between 3.060 Å and 3.148 Å, which is considerably longer than their combined van der Waals radius of 2.67 Å. This can be seen as strong proof that the hydrogen bond plays little role in the changes happening, at least at fundamental level.

After the sudden structural transformation, the changes happen gradually once again as the molecules move further away from one another. Figure 5.9(b) shows the change in energy of the dimer as the structural changes occur. The potential energy surface is extremely flat, with a change in the order of only 2.0 kcal.mol^{-1} in total for this specific window of separation distances. There does seem to be a "barrier" as the bond length changes. This value, however, is 0.004 kcal.mol^{-1} and it is doubtful whether this is associated with a barrier or if it is an artifact of the calculation method. Another interesting observation is that the gradient of energy change lessens after the sudden jump in bond length, although the tempo at which the separation distance changes is unaffected. An investigation into the changes happening in the electronic composition of the molecule might explain this behaviour and this is the topic of the next subsection.

5.7.2 Electronic Changes

The abrupt changes in structure as well as the difference in tempo of energy change can be interpreted as a significant alteration in the electronic composition of the molecule. A rearrangement of the electronic energy levels within the molecule would support a rapid mechanism in favour of one prompting a gradual change. In this regard, it has to be stressed once again that the potential energy surface of dative bond change is very flat, and substantial changes are possible with very little energy input or consequence. Decomposition of the bond energy has been used to determine that boron-nitrogen complexes with a long bond in the gas phase differ from those having a shorter bond and that the long and short bonds should be seen as different types, at least in terms of their composition.[50] An investigation into the electronic changes

of the dimer was undertaken by doing a correlation between the molecular orbitals of the system with the short bond compared to the system with the longer bond. Since the correlation is done visually, it thus becomes important to have a system with the maximum amount of symmetry species to help with the correlation. This then explains our choice to model the system with strict C_{2h} symmetry.

As expected, no change takes places in the low energy core and valence orbitals, the first 24 orbitals remain unaffected in their ordering. From the 25th orbital onwards, rearrangements start. A full listing, accompanied by pictures of the molecular orbitals, is given in Addendum B. However, an investigation of the ten highest energy occupied orbitals of the dimer with a short B–N bond and their counterparts of the dimer with a long B–N bond, is sufficient to cast light on the changes in electronic structure that happen. Figure 5.10 shows the correlation diagram of the relevant orbitals, labelled according to their symmetry. Figure 5.11 shows graphical representations of these orbitals. The numbering is assigned in the order that they are discussed and does not match the energy ordering. The changes in molecular orbital composition (or likewise, wave function composition) will be presented in the same order as the separation calculation was done, in other words from a short bond to a long bond, or from the crystalline state to the gas phase. The first change is the shifting of the HOMO (**1**) and HOMO-1 (**2**) of the "short-bond" dimer to the HOMO-5 (**16**) and HOMO-4 (**15**) positions of the "long-bond" dimer.[V] The HOMO-2 (**3**) of the short-bond dimer correlates with the HOMO (**11**) of the long-bond dimer. Next is the HOMO-3 (**4**), HOMO-4 (**5**) and HOMO-5 (**6**) of the short-bond dimer that correlate with the HOMO-2 (**13**), HOMO-3 (**14**) and HOMO-1 (**12**), respectively, of the long-bond dimer. Following these, the next two orbitals of the short-bond dimer, **7** and **8**, correlate to the same relative positions in the long-bond complex, **17** and **18**, but with slightly higher energy. The following two orbitals, **9** and **10**, correlate with orbitals that fall below the ten highest in energy of the long-bond dimer. On the graph they are shown as **19** and **20**, but they are actually the 36th and 31st in terms of energy (out of 46 occupied molecular orbitals in total). The reader is reminded that the full correlation graph and accompanying pictures are given in Addendum B.

In Section 5.6 the role of the fluorine atoms, or rather the lone pairs on the fluorine atoms, in the structure of the molecule, was explained. In the correlation of the molecular orbitals the involvement of the fluorine lone pairs is again evident. The HOMO and HOMO-1 orbitals of the short-bond dimer are largely localised on the fluorine atoms (see Figure 5.11(**1**) and (**2**)), and their energies are considerably lowered as the complex progresses to a longer

[V] The changes are briefly discussed in the text, in a fashion that may prove rather difficult to follow. For a better understanding it is recommended that the changes are followed by comparing Figures 5.10 and 5.11.

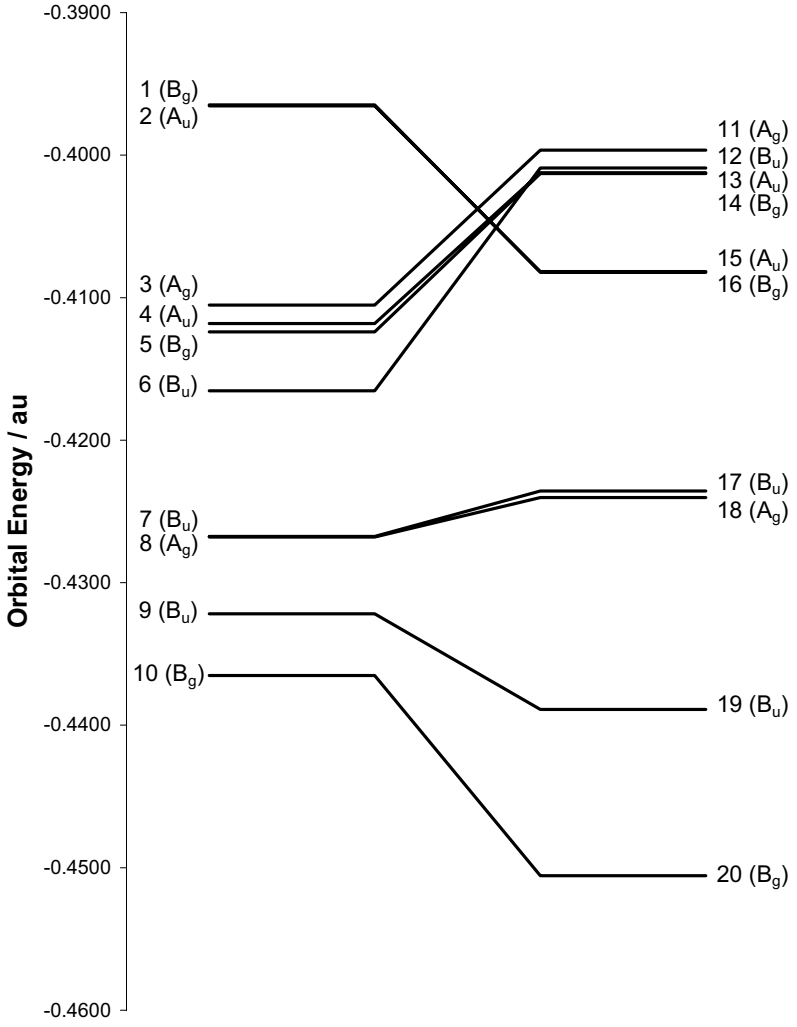

Figure 5.10: A correlation diagram between molecular orbitals of the "short-bond" $(HCN–BF_3)_2$ dimer (left) and the "long-bond" dimer (right). This correlation is only between the ten highest energy occupied MOs of the short-bond dimer and the associated MOs of the long-bond dimer. The MOs of the long-bond dimer that do not correlate with any of the ten highest energy occupied MOs of the short-bond dimer are not shown.

dative bond. The other large change is the rearrangement of the next four orbitals in the short-bond dimer. Inspection of their composition reveals that they consist of the *gerade* and *ungerade* combinations of both perpendicular π-bonds of the triple bond of the nitrile group, together with contributions of antibonding nature from the fluorine lone pairs. Their energies are all raised in the formation of the long-bond complex. An absolute conclusion from

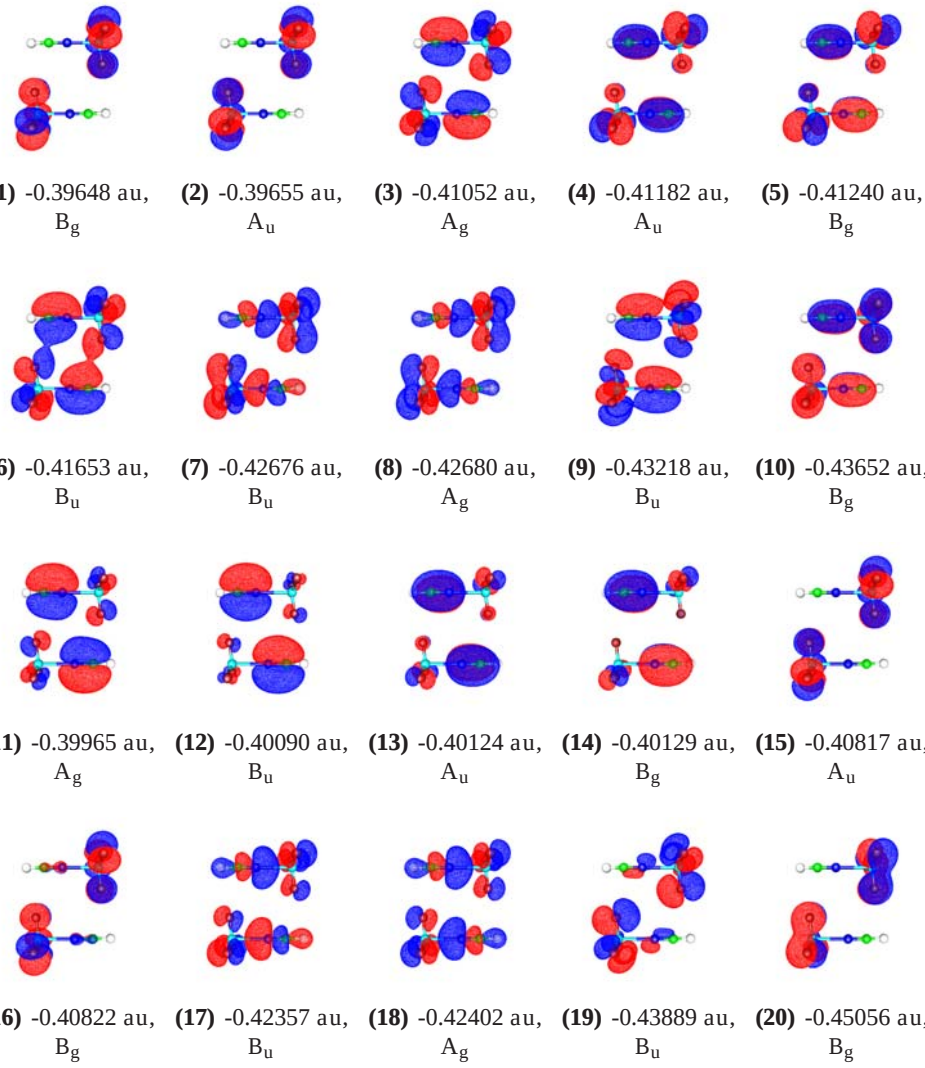

Figure 5.11: Representations of the ten highest energy occupied molecular orbitals of $(HCN–BF_3)_2$ with an intermolecular separation of 4.42 Å (**1** to **10**) and those corresponding to them with an intermolecular separation of 4.44 Å (**11** to **20**).

this behaviour is difficult to make, since the "meaning" of molecular orbitals (including, of course, their physical interpretation) is largely open for discussion. The orbitals in which the lone pairs are the only constituent parts (**1** and **2** as well as **15** and **16**) represent the localisation of the lone pair density on the fluorine atoms. Since they are localised away from the B–N bond region they contribute very little to bonding. The orbitals in which both fluorine lone pair and nitrile π-electron density feature play a considerably larger role in the bonding, since these contributions come from both fragments. However, these all exhibit antibonding interorbital overlap in the B–N bond region. All

these orbitals thus have "negative" effects on the strength of the B–N bond. With regard to the significance of the change in ordering, the lone pairs in the short-bond dimer are higher in energy; and the lowering of their energy as the bond lengthens might indicate an increase in their importance to the specific structure. In other words, the need for the lone pairs to be localised on the fluorine atoms is higher when the B–N bond is longer. However, this is acceptedly an *ad hoc* explanation and perhaps the only conclusion one can draw is that this analysis once again points to the importance of the lone pairs in the structure and resulting structural changes.

5.8 "Basis Set Effects" Revisited

Enough information has now been gathered on the changes happening in $HCN–BF_3$, both in its molecular and electronic structure, to review the effect of the basis set again, as explained in Section 5.3.1. Our aim is to determine whether the differences in electronic structure, as seen in the two discrete points at which the bond change occurs, are also evident in the two minima with a long and short bond, calculated with the same density functional but with only the addition of a diffuse function separating them. For this purpose, the MPWK1 / 6-31G(d) and MPWK1 / 6-31+G(d) results will be compared. This was the only functional that constantly preferred a long dative bond without a diffuse function and a short bond with one (see Table 5.1).

Figure 5.12 shows the five highest energy occupied molecular orbitals of MPWK1 / 6-31G(d) $HCN–BF_3$, compared with those calculated at MPWK1 / 6-31+G(d). The 6-31G(d) structure with a boron-nitrogen bond length of 2.287 Å has a doubly degenerate HOMO and HOMO-1 consisting of nitrile π and fluorine lone pair density. The 6-31+G(d) structure with a bond length of 1.806 Å has a HOMO consisting of localised fluorine density, followed by the doubly degenerate pairing. The electronic properties distinguishing the two structures calculated with the same basis set, 6-311+G(2df,p) in Section 5.7.2 are thus just as evident in this case. In general, such erratic behaviour of a basis set would suggest sever inadequacy in terms of its composition. However, our results lead us to conclude that these smaller basis sets do not necessarily give a "worse" description of the molecule; the availability of diffuse functions alters the calculation at a much more fundamental level of its electronic makeup.

5.9 Energetics of $HCN–BF_3$ and $(HCN–BF_3)_2$

Before concluding with this chapter, we include some energetic properties of the $HCN–BF_3$ and $(HCN–BF_3)_2$ system. It has already been shown in this work that this system is plagued with basis set superposition error and minima that might be considered "untrustworthy". Results for analogous

(a) -0.44549 au, E (b) -0.44549 au, E (c) -0.45570 au, A_1 (d) -0.47555 au, A_2

(e) -0.48751 au, E (f) -0.44868 au, A_2 (g) -0.46700 au, E (h) -0.46700 au, E

(i) -0.48060 au, A_2 (j) -0.49108, E

Figure 5.12: Representations of the five highest energy occupied molecular orbitals of HCN–BF_3, calculated at MPWK1/6-31G(d) (a to e) and MPWK1/6-31+G(d) (f-j). The orbitals are given in order of increasing energy, labelled by their energy and symmetry species within the C_{3v} point group.

CH_3CN–BF_3 have been found to only start converging at B3LYP/aug-cc-pVQZ, and even at this level are still hampered by BSSE.[48] The results given here should thus be taken with some caution. Nevertheless, all calculations were once again performed at B3LYP/6-311+G(2df,p).

The dissociation energy (D_e) of HCN–BF_3, corrected for BSSE, is 3.45 kcal.mol^{-1}. This value lessens to 2.80 kcal.mol^{-1} when the value is corrected for zero-point vibrational energy (ZPVE) as well (D_0). This agrees with the evidence that the gas phase compound is extremely weakly bound. Since it remains impossible to obtain a second minimum with a short bond, the best one can do is to also calculate the energy of the $(HCN–BF_3)_2$ dimer and compare these values. The difference in energy between the optimised dimer and the sum of the two monomers, at the geometries they have in the dimer, gives the interaction energy associated with the hydrogen bonds, 10.90 kcal.mol^{-1}. This equates to 5.45 kcal.mol^{-1} for each hydrogen bond. One hydrogen bond is thus stronger than the total dissociation energy of the gas phase monomer! Finally, the difference in energy between the optimised dimer and two op-

timised monomers gives an indication of the energy needed to perform the structural changes, 4.89 kcal.mol^{-1}. This value has not been corrected for ZPVE or BSSE. This compares well with the potential energy curve for the stretching r(B–N) coordinate, Figure 5.2(c), which indicates that the energy needed for one monomer to progress from ca. 2.5 Å to ca. 1.9 Å, is more or less 2 kcal.mol^{-1}.

5.10 Conclusions

The claim that dipole-dipole interactions are responsible for the large changes in structure of HCN–BF_3 and CH_3CN–BF_3 as these molecules change from the gas to the crystalline phase was initially doubted, since the crystal structure of these two molecules features an arrangement which largely minimises dipole-dipole interaction. Structural changes brought on by explicitly placing molecules in the immediate vicinity of a (HCN–BF_3)$_2$ and (CH_3CN–BF_3)$_2$ dimer have been investigated. In the case of HCN–BF_3 the dative bond length is shortened from 2.474 Å to 1.665 Å with the addition of six molecules. The CH_3CN-BF_3 molecule shows a change from 2.281 Å to 1.627 Å under similar conditions. This corresponds very well with the experimental crystalline phase bond lengths of 1.630 Å and 1.638 Å respectively. Also interesting was the evidence that the N–B–F angle, which also changes dramatically, was largely influenced by the hydrogen bond formation.

A calculation of the classic dipole-dipole interaction between point dipoles, using the structures determined in the (HCN–BF_3)$_n$ and (CH_3CN–BF_3)$_n$ models, shows that the dipole-dipole interaction energy does not correlate exactly with the calculated change in dative bond length, casting some doubt on an exclusive dipole-dipole mechanism being responsible for the bond change.

NBO analysis of the two systems produces the most interesting findings. It was found that fluorine lone pair delocalisation into the boron-nitrogen natural antibonding orbital greatly influences the structure of these molecules. In the absence of the delocalisation the dative bond length is very close to the sum of the individual covalent radii of boron and nitrogen. Since the delocalisation is dependent on the relative proximity of the fluorine lone pair density and boron-nitrogen antibonding orbital, which resides primarily on the boron atom, the importance of the N–B–F angle in the structure follows. This then provides some theoretical backing to the relationship between the N–B–F angle and r(B–N) previously determined.[12,38] Hydrogen bond formation, which was shown to be evident to a great extent in the crystal structures, might thus be linked to the structural changes.

An investigation of the exact point at which the bond changes from short to long, and along with this more information on the path by which it happens, was done by increasing the distance between two HCN–BF_3 molecules

in a $(HCN–BF_3)_2$ dimer. This showed that the changes occur in an abrupt fashion, and is not at all a gradual phenomenon. Analysis of the molecular orbitals and how they change when the dative bond changes once again confirms that fluorine lone pair delocalisation is important. The changes in electronic composition of the molecule agrees with previous determinations that the two different bond lengths are evidence that the complexes have different donor-acceptor type bonding.[50] A final conclusion from this calculation is that the bond changes in the absence of any hydrogen-fluorine bond interaction (based on the van der Waals radii of hydrogen).

The main conclusion from this chapter is thus that dipole-dipole interactions are primarily responsible for the difference between the gas phase and crystalline structures in that it provides the energetic basis for the progression from a weak partially formed dative bond to a completely formed dative bond. However, the influence of hydrogen bonds, propagated through their effect on the value of the N–B–F angle, which in turn influences the dative bond length, is undeniable.

In the next chapter a much more in depth look will be taken into the changes that can be catalysed by dipole-dipole interaction, facilitated through an electric field, on a wide array of datively bound complexes.

Chapter 6

The Effect of an External Electric Field on the Dative Bond

6.1 Introduction

Up till now our efforts have gone primarily into $HCN–BF_3$ and $CH_3CN–BF_3$, which are the two molecules that display the largest phase dependent bond differences based on both experimental and computational studies. Fortunately, the gas phase and crystal structures of both compounds have been determined as well. However, a much better picture can of course be obtained by comparing these molecules with a wider set of other datively bound complexes. In order to have more freedom and construct a better comparison, this set was constructed without the constraint of the availability of experimental gas and crystal phase structures. Two important aspects, as determined in the previous chapter, are the effect of the sp-hybridised nitrile nitrogen as opposed to a sp^3-hybridised nitrogen, as well as the availability of lone pairs on the substituent atoms of the acceptor. Donor fragments where thus chosen to be H_3N, CH_3CN and HCN. Acceptors were chosen to be BH_3, BF_3 and SO_3.

Since it is very clear that consistently large basis sets are needed to provide an accurate wave function, the effect of the surrounding molecules has to be introduced via a technique that adds comparatively little computational cost to that needed to model the single, unperturbed molecule. The previous chapter has shown that dipole-dipole interactions, at least in the $(HCN–BF_3)_2$ dimer, can be used to simulate the bond changes. The effect of dipoles and/or induced dipoles on the other molecules in a medium are propagated through their influence on the charge distribution and the resulting polarisation in the other molecules. Similar changes can be brought on in a molecule by simply applying an external electric field. This is evident by examining reaction field theory, which has achieved tremendous success in simulating the phase dependent changes.[26,31] In this model, the electrostatic solvent effect is taken as an additional term in the Hamiltonian of the

isolated molecule. The perturbation describes the coupling between the molecular dipole moment and the reaction (electric) field.[26]

Computationally, the effect of a finite homogeneous electric field (strictly speaking a dipole electric field in this work) can be factored into the wave function of a molecule by supplementing the existing one-electron integrals with integrals of the form $\langle\varphi_\mu|z|\varphi_\nu\rangle \times F$, where φ_μ and φ_ν are basis functions and z is the z-component of the dipole moment operator. The integrals are scaled by multiplication with the field strength, F. The nature of the electric field as a dipole electric field is determined by the choice of multipole moment operator. In this example-integral the electric field lays purely along the z-axis but it is possible to construct any alignment by factoring the electric field into its components along the z-, y-, and x-axes.

6.2 Computational Methods and Models

The molecules were built in traditional Z-matrix format. The Gaussian 03 manual states that in order to do geometry optimisations in the presence of an electric field the input geometry must be given in traditional Z-matrix format (in fact, symbolic cartesian coordinates should also work, as long as the optimisation is done in redundant internal coordinates) and symmetry should be disabled. The disabling of symmetry prevents the rotation of the molecule from the input orientation to the standard orientation, and since the applied field is given in terms of the input orientation, the rotation of the molecule would result in an erroneous calculation. Although specific symmetry was therefore not utilised in constructing the wave functions, the Z-matrix was constructed in order to result in C_{3v} structural symmetry for all complexes.

Since this study originally evolved from one primarily concentrating on $HCN–BF_3$ and $CH_3CN–BF_3$, the general electric field strength range was chosen based on those values which were found to catalyse the changes in these complexes. Therefore, all complexes were optimised in electric fields of 0.0010 au, 0.0025 au, 0.0050 au, 0.0075 au and 0.0100 au. In specific cases, however, the electric field was modelled much larger, but these cases will be discussed in full detail. The direction of the field was taken to be both along the dipole moment of the molecule as well as in the opposite direction. The atomic unit of electric field in SI units is equal to $5.1423 \times 10^{11} V.m^{-1}$ (cf. Table 4.1).

All normal optimisations within an electric field were performed with Gaussian 03, at B3LYP / 6-311+G(2df,p).[103] The nature of the stationary points in the absence of an electric field were verified as minima through means of frequency analysis.

6.2.1 Atoms in Molecules

Analysis of the topology of the electron density was done within the paradigm of atoms in molecules (AIM).[96] The AIMPAC suite of programs, developed by Bader's group, was used. The fundamentals of the theory have already been discussed in Section 4.9, and only a quick reference to the relevant information that can be obtained from it will be given here.

Bond critical points (BCPs) in the electron density can be determined and various properties calculated at these points provide information on the bond. Firstly, the value of the electron density at the BCP, $\rho(\mathbf{r_c})$, gives a measure of the strength of the bond. As no absolute scale for these values exist, they should only be compared within collections of similar bond types. The sign of the Laplacian of the electron density at the BCP, $\nabla^2\rho(\mathbf{r_c})$, can be used to extract information on the type of bond. Since the position of the BCP is exactly on the "border" (where interatomic surfaces touch) between the two atoms, a positive Laplacian, associated with a local minimum in the electron density, indicates that the maximum electron density value occurs closer to one of the two atoms. This means that the bond electron pair is not shared, but lays towards one of the atoms and that the bond is therefore non-covalent / ionic. Similarly, a negative Laplacian, and therefore a local maximum in the electron density, indicates a shared bond electron pair and therefore a covalent bond. The energy density at the BCP, given by the sum of the kinetic and potential energy densities($H_b(\mathbf{r_c}) = G_b(\mathbf{r_c}) + V_b(\mathbf{r_c})$), is found to be negative for interactions which result from the accumulation of electron density at the CP, and therefore indicative of covalent interactions.[118] Lastly, the ellipticity at the BCP can be calculated as $\frac{\lambda_1}{\lambda_2} - 1$, where λ_1 and λ_2 are the two eigenvalues of the density matrix Hessian at the bond critical point that correspond to the two eigenvectors lying perpendicular to the bond path. This value gives an indication of the extent that charge is accumulated perpendicular to the bond path. Since σ-bonds have a cylindrical charge distribution and thus an ellipticity of zero or close to zero, this value is an indication of the π-character of the bond. It can also be used as a guide to instability in the bond.[97]

An additional remark regarding the calculations: the AIMPAC software interprets the wave function as being calculated from basis functions consisting of cartesian functions, which is not the case in the standard 6-311G (plus augmentations) basis set. Since there are only five pure d-type functions, and six cartesian combinations, linear combinations of cartesian functions are made to obtain the five pure d-type functions plus an additional s-type function. Similarly, the ten cartesian f-type functions are converted to the seven pure functions through appropriate linear combinations as well. The basis set used in the calculation needs to be altered to consist of six cartesian d-type functions and ten cartesian f-type functions. The wave functions used in the AIM calculations were thus calculated from separate single point cal-

culations at the stationary geometries, with adjusted basis sets. This is done in Gaussian 03 by adding *6d 10f* to the specification of the basis set, i.e. *6-311+G(2df,p) 6d 10f*.

6.2.2 Bond Energy Partitioning

The nature of the donor-acceptor bonds were investigated with the energy partitioning (EPA) method initially developed by Morokuma and Kitaura[119] and later modified for DFT by Ziegler and Rauk[120] as implemented in ADF 2004.1.[121–123] According to this method, the bond dissociation energy between two fragments is partitioned into two major contributions,

$$-D_e = \Delta E_{prep} + \Delta E_{int}$$

ΔE_{prep} is the deformation energy necessary to promote the fragments from their equilibrium geometry to the geometry in the complex.

The most meaningful term, however, is ΔE_{int}, which is the instantaneous interaction energy between the donor and acceptor. This term can be subdivided further into physically meaningful terms,

$$\Delta E_{int} = \Delta E_{elstat} + \Delta E_{Pauli} + \Delta E_{orb}$$

ΔE_{elstat} is the classical electrostatic interaction energy, calculated with the frozen electron density of the two fragments as they are brought from an infinite distance to their complex geometry. ΔE_{Pauli} gives the Pauli repulsion and is calculated by enforcing antisymmetry and normalisation on the determinant resulting from superimposing the fragments. Finally, ΔE_{orb} is calculated by allowing the fragment orbitals to relax to the form they have in the complex. This term is also linked to covalent interactions in the complex.

The EPA method as implemented within the ADF program package was used.[121–123] Unfortunately, B3LYP and Gaussian basis functions are not available within ADF, so for these calculations the complexes were optimised using the exchange functional of Becke[86] and the correlation functional of Perdew[124] (BP86) and a triple-ζ Slater-type basis set, augmented with one set of polarisation functions (TZP).[125]

6.2.3 Density of States Plots

The main use of density of states (DOS) plots is to provide a pictorial representation of molecular orbital populations. One can obtain a view of the character of the molecular orbitals within a specified energy range. It is possible to find out which orbitals give a large contribution and whether this contribution is bonding, nonbonding or antibonding with respect to particular bonds. In this chapter overlap population density of states (OPDOS) plots will be used. These plots are also referred to as crystal orbital overlap population (COOP) diagrams in the literature.

In the calculation of Mulliken populations of atoms the gross population, N_A, of an atom, A, written in term of a summation over all molecular orbitals, is given by

$$N_A = \sum_i n_i \sum_{a \in A} \sum_k c_{ia} c_{ik} S_{ak}$$

where n_i is the occupation number of the molecular orbital, k are all the basis functions and a are those localised on atom A and S_{ak} is the overlap matrix element between basis functions a and k. The coefficients of basis functions a and k in the i^{th} molecular orbital are given by c_{ia} and c_{ik}. With the assumption that the electrons are shared equally between basis functions, the overlap population between atoms A and B, OP_{AB}, once again summed over all molecular orbitals, is given by

$$OP_{AB} = \sum_i n_i \sum_{a \in A} \sum_{b \in B} 2 c_{ia} c_{ib} S_{ab}$$

A positive overlap population, being a function of the overlap element, indicates bonding overlap, a negative overlap indicates antibonding overlap. The OPDOS between fragments atoms A and B at energy E is given by

$$OPDOS_{AB}(E) = \sum_i OP_{AB,i} F(E - \varepsilon_i) \tag{6.1}$$

where the summation goes over all i one-electron energy levels, $OP_{AB,i}$ is the overlap population between atoms A and B at the specific energy level and F is a pseudo-Voigt function approximating the difference $E - \varepsilon_i$. The system can be subdivided into fragments, X and Y, each consisting of a number of atoms and the basis functions localised on these atoms, $a \in X$ and $b \in Y$. The term $\sum_{a \in X} \sum_{b \in Y} 2 c_{ia} c_{ib}$ then gives the contribution of molecular orbital i to bonding overlap between fragments X and Y.

Analysis of the bonding in the complexes, based on these principles, was done by examining the molecular orbitals using the AOMix code.[126,127]

6.3 Effects of a Varying Electric Field

First, a matter of convention: the direction of the dipole moment for all the complexes is from the boron / sulphur atom (the accepting fragment with an overall negative partial charge) to the nitrogen / oxygen atom (the donating fragment with an overall positive partial charge). An electric field that further polarises the charge distribution in a manner that stabilises the negative partial charge of the accepting pole, will lead to better donation. The convention is made that such an electric field is “positive”. Likewise, a “negative” electric field discourages electron donation and therefore is orientated with the molecular dipole moment. The discussion of the results of the different molecules will be grouped according to those complexes with the same donating species.

6.3.1 Molecular Structure

The results of the geometry optimisations of all the complexes in the presence of an electric field are shown graphically in Figure 6.1. The total change in bond length of the complexes over this arbitrarily chosen interval of electric field strengths, in decreasing order, are

$$\mathrm{HCN{-}BF_3} > \mathrm{CH_3CN{-}BF_3} > \mathrm{CH_3CN{-}SO_3} > \mathrm{HCN{-}SO_3} > \mathrm{H_3N{-}SO_3} > \mathrm{H_3N{-}BF_3} > \mathrm{HCN{-}BH_3} > \mathrm{H_3N{-}BH_3} > \mathrm{CH_3CN{-}BH_3}$$

A more detailed summary of the changes are given in the following subsections (where the full tables are more relevant) in Tables 6.1 to 6.9.

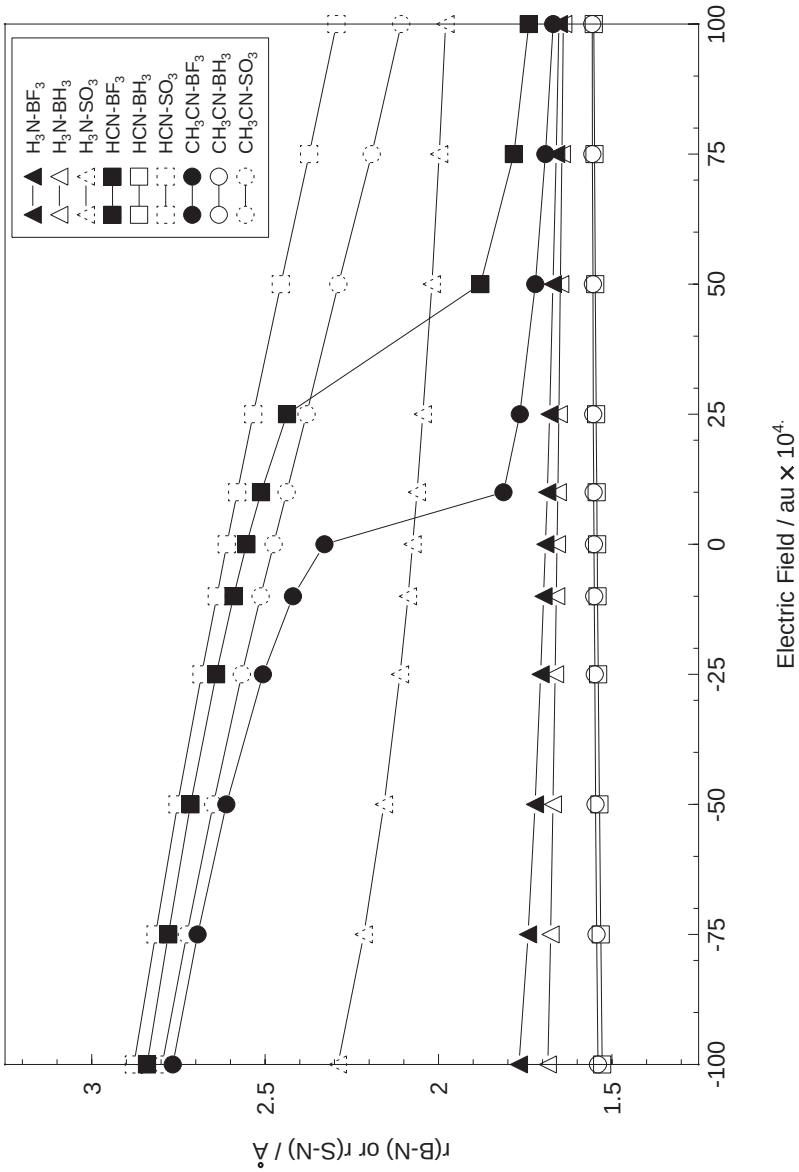

Figure 6.1: The optimised dative bond length in a selection of B–N and S–N complexes, as a function of the applied external electric field. The positive electric field stabilises the bond and is orientated against the molecular dipole moment, the negative electric field destabilises the bond and is orientated opposite the dipole moment.

Amine Donors

The complexes discussed in this section are those with H_3N as donor species: H_3N–BF_3, H_3N–BH_3 and H_3N–SO_3. The gas phase and crystal structures of all these complexes have been determined.

The boron-nitrogen bond length in H_3N–BF_3 progresses from 1.637 Å to 1.60 Å[10,11] from the gas to crystal phase. The calculated value is 1.691 Å in the absence of an electric field. The application of an electric field, aligned opposite the dipole moment with a strength of 0.01 au, shortens the bond to 1.653 Å, a 0.038 Å change. The oppositely aligned field of the same strength lengthens the bond by 0.077 Å, to 1.768 Å. The changes to the bond length are relatively small and without any surprises: the bond is shortened, as expected, in a stabilising electric field. The N–B–F angle increases as the field becomes stabilising and the bond length decreases.

The experimental data for the dative bond in H_3N–BH_3 is a shortening from 1.658 Å to 1.564 Å.[8,9] The calculated value without an applied field is also 1.658 Å, an exact match with the experimental value! A stabilising electric field of 0.01 au shortens the bond by 0.018 Å to 1.640 Å. The opposite field of the same strength lengthens the bond by 0.027 Å to 1.685 Å. Here the bond changes are much smaller. However the magnitude of change observed experimentally is not reached using the conventional range of field strengths. To investigate this, the complex was optimised in field strengths from +0.02 au to +0.1 au, in steps of 0.01 au. From +0.02 au to +0.05 au the nitrogen-boron bond length decreases from 1.629 Å to 1.613 Å. From +0.06 au the bond length starts to increase until the complex completely disintegrates (as signified by the fragments moving away to about 8.5 Å and the consequent inability to reach SCF convergence) at +0.08 au. We thus conclude that the full effects of the condensed medium cannot be simulated by simply applying an external dipole electric field to the H_3N–BH_3 molecule.

The zwitterion $^{+}H_3N$–SO_3^{-} has a gas phase bond of 1.957 Å which shortens to 1.771 Å in the solid state.[14,15] The B3LYP / 6-311+G(2df,p) isolated optimisation calculates a bond length of 2.074 Å. Once again, using the conventional range of field strengths the experimentally observed changes cannot be simulated. The stabilising field of 0.01 au shortens the bond to 1.979 Å, the reversed field lengthens the bond to 2.290 Å. In the previous HF / 6-31G(d) reaction field study on the effects of the medium on the geometry by Wong *et al.*, it was found that a polar medium with a dielectric constant of 2 shortens the bond to 1.893 Å; increasing the dielectric constant to 40 changes the bond length to 1.836 Å, which still falls short of the experimental value of 1.771 Å.[26] In the reaction field study by Jiao and von Ragué Schleyer[31] on HCN–BF_3, our reference compound, the changes occur much sooner at a dielectric constant of between 15 and 20. This is in agreement with our findings that a stronger electric field (and thus external polarisation) is needed to catalyse the changes in H_3N–SO_3 than in HCN–BF_3 (although the actual

structural changes are less). As was the case with H_3N–BH_3, the complex was also optimised in stronger electric fields, from +0.02 au to +0.1 au. The minimum bond length obtained is 1.874 Å in a +0.05 au electric field. From this point onwards application of the the electric field leads to a bond lengthening and at +0.08 au the complex disintegrates. The conclusion in this case is thus also that the electric field technique cannot be used to simulate the phase dependent changes quantitatively.

Hydrogen Cyanide Donors

The complexes discussed in this section are those with HCN as donor species: HCN–BF_3, HCN–BH_3 and HCN–SO_3. The gas phase and crystalline state structures of one of these complexes, HCN–BF_3 is known, the structure of HCN–SO_3 has only been published for the gas phase and HCN–BH_3 is a completely hypothetical compound.

The gas phase and condensed phase bond lengths and angles of HCN–BF_3 need no further statement. In an electric field of +0.01 au, r(B–N) has a value of 1.739 Å. Between +0.0050 au and +0.0025 au the bond length changes from 1.879 Å to 2.436 Å. As seen previously in the "separation-calculations" the sudden jump, which has been absent in the other molecules till now, is thus evident here. The N–B–F angle changes accordingly. Stronger field strengths were also applied: r(B–N) is 1.657 Å in +0.02 au, 1.615 Å in +0.03 au and 1.587 Å in +0.04 au, showing that the changes seen through phase change are satisfactorily simulated using electric fields.

In the previous chapter the importance of fluorine lone pair delocalisation was discussed. The claim was made that an intricate relationship exists between r(B–N) and the N–B–F angle and bond changes of the observed order would not be possible if the N–B–F angle did not change correspondingly. The HCN–BF_3 molecule was partially optimised in the electric fields of different strengths with the dative bond length kept frozen at the gas phase calculated value; as well as with the N–B–F angle kept frozen. Results are shown in Figure 6.2 and clearly show the inability of the bond to progress to its shortened condensed phase value if the N–B–F angle does not change correspondingly. Similarly, the N–B–F angle does not show the full change when r(B–N) is kept frozen. Interestingly, in the absence of the sudden bond change, the changes in the partial optimisations follow a linear trend.

The next question is how to obtain a measure of the accuracy of this method and whether it is capable of reproducing the point of bond change as obtained through the separation-calculations in Section 5.7.1. The electric field perpendicular to a point dipole is given by $E = \frac{D}{4\pi\varepsilon_0 r^3}$, where D is the dipole strength and r the distance from the point dipole. This formula was used to calculate the electric field generated by the molecular dipole (simplified to a point dipole at the centre) of one molecule in the optimised dimer at the centre of the opposite molecule. The value of the actual molecular dipole

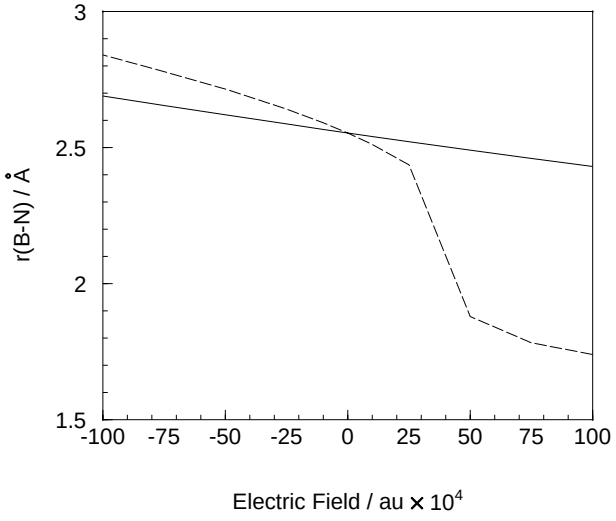

(a)

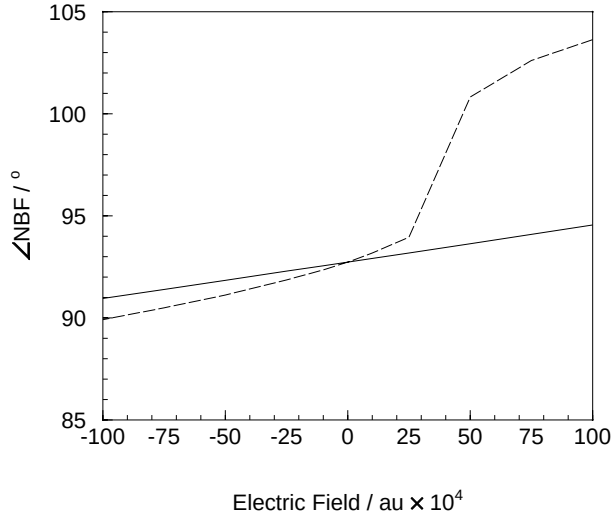

(b)

Figure 6.2: Changes in the structure of HCN–BF_3 in an electric field of varying strength. The molecule was optimised with ∠NBF kept frozen at the computed gas phase value of 92.7° (a, top) and with r(B–N) frozen at 2.554 Å (b, bottom). Results of the partial optimisations are shown with solid lines. Results of full optimisations are also shown, with broken lines.

was determined by fitting r(B–N) to a set of partial optimisations in which the molecular dipole of an isolated molecule was determined as a function of r(B–N). This process was repeated at separations of 4.00 Å to 5.00 Å, in steps

of 0.02 Å. Recall that the bond change occurs at separations between 4.42 Å, where r(B–N) is 1.944 Å, and 4.44 Å, where r(B–N) is 2.240 Å. This means that the change occurs between field strengths of +0.0042 au and +0.0034 au (keeping our sign convention). Optimisations of monomers in electric fields of +0.0042 au and +0.0034 au leads to dative bond lengths of 2.298 Å and 2.376 Å. Although r(B–N) at the lower field strength correlates well, the value at the higher field does not. Although an exact correlation does not exist, in a field that is 0.0045 au, only 0.0003 au stronger, r(B–N) is 1.974 Å, which is much closer to the value from the separation-calculation. This shows two things: firstly it verifies that using electric fields to simulate the effect of surrounding molecules has considerable merit, and secondly it underlines the dominance of dipole-dipole interactions in the bond change.

The $HCN–BH_3$ molecule is the first case which shows fundamentally different results. This completely "computational molecule" has the very interesting behaviour that its dative bond length *increases* as the electric field becomes more stabilising. Although the changes are very small in size, 0.024 Å over the total variation in field strength of 0.02 au, this is certainly unexpected. The N–B–H angle does not change as expected in relation to the B–N bond length. The largest angle corresponds to the longest bond length, and the smallest to the shortest bond length. Based on steric arguments one would expect a larger angle when the bond is shorter, however the steric interactions due to the small hydrogen atoms BH_3 acceptor interacting with the HCN electron density is very low. The stabilising field is in the direction of the boron atom from the nitrogen atom, and thus also in the direction of N–B–H angle increase. It seems reasonable that the change in N–B–H angle is thus due to the electric field interacting with the hydrogen atom density. This is even more so a factor since the hydrogen atoms on the acceptor have a partial negative charge. According to the argument of electron delocalisation of the previous chapter, the N–B–H angle should indeed not be influenced to any great extent by the value of r(B–N). All these unexpected changes might seem like a flaw of the method used, therefore a calculation similar to the "separation-calculation" of $HCN–BF_3$ in the previous chapter, was employed. Two antiparallel $HCN–BH_3$ molecules in a $(HCN–BH_3)_2$ dimer were partially optimised with the variable representing the distance of separation frozen at set intervals. Exactly the same technique was used as discussed in Section 5.7.1. The distance between the two molecules was increased and the dative bond length monitored. The results are shown in Figure 6.3. Starting at a perpendicular separation of 3.00 Å the B–N bond length increases as the two molecules move further away, but at ca. 4.10 Å where r(B–N) is 1.551 Å, the bond suddenly starts to decrease in length until it stabilises at a value of 1.547 Å. The energy profile for this calculation is also shown and has the very familiar form of a potential energy curve of a system possessing a single energy minimum at a specific geometry.

With the $HCN–SO_3$ molecule the structural changes return to the expec-

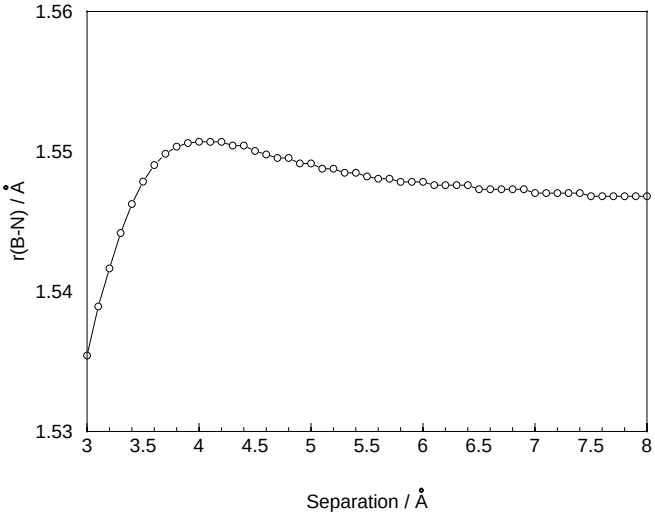

(a)

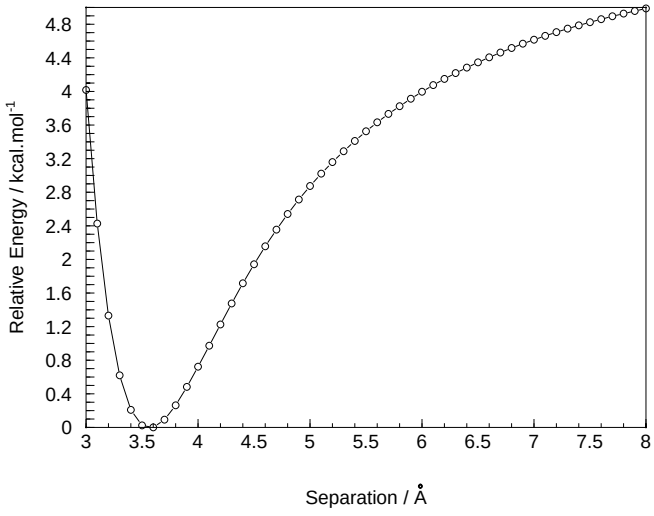

(b)

Figure 6.3: The dative bond length as a function of the perpendicular distance between two molecules in a $(HCN–BH_3)_2$ dimer (a, top). The change in total energy of the system is also shown (b, bottom)

ted trend, again. The gas phase dative bond length of this molecule is 2.577 Å.[16] In an electric field of +0.01 au, r(S–N) is 2.294 Å, a considerable change from the normal calculated bond length of 2.610 Å. Likewise, at the other side of the spectrum, the bond length is 2.878 Å in an electric field of -0.01 au. The N–S–O angle changes according to the length of the dative bond, becoming

smaller as r(S–N) increases. Although the changes are thus quite substantial a sudden jump in the bond length, as occurring in $HCN–BF_3$, is absent.

Acetonitrile Donors

The complexes discussed in this section are those with CH_3CN as donor species: $CH_3CN–BF_3$, $CH_3CN–BH_3$ and $CH_3CN–SO_3$. The gas phase and crystalline state structures of one of these complexes, $CH_3CN–BF_3$ is known, $HCN–SO_3$ has only been identified in the gas phase and $CH_3CN–BH_3$ is a completely hypothetical compound. This is equivalent to the situation with the nonmethylated compound and similar results should be expected in this case as those discussed in the previous subsection.

$CH_3CN–BF_3$ has a gas phase dative bond length of 2.011 Å which decreases to 1.630 Å in the condensed phase.[12,13] Our calculations result in a r(B–N) value of 2.329 Å in the absence of an electric field, 1.669 Å in a strongly stabilising field of +0.01 au and 2.766 Å in a strongly destabilising field of -0.01 au. It is well known that $CH_3CN–BF_3$ is difficult to calculate accurately.[48] This is also the only other molecule besides $HCN–BF_3$ in our test set which shows a sudden bond length change, occurring here between no field and a field of +0.0025 au (cf. Figure 6.1). The N–B–F angle changes accordingly.

A similar situation arises with $CH_3CN–BH_3$ as that encountered with $HCN–BH_3$, the bond length *inceases* as the electric field becomes more stable, and the N–B–H angle also increases.

Finally, the $CH_3CN–SO_3$ bond length, which was determined to be 2.466 Å in the gas phase, is 2.475 Å in our calculations without an electric field.[16] The stabilising +0.01 au field decreases the bond length to 2.107 Å, the destabilising field increases it to 2.797 Å. The N–S–O angle holds no surprises.

Looking at the curves in Figure 6.1, it is interesting to note the similar slope and bond lengths at high stabilising fields of $HCN–BF_3$, $CH_3CN–BF_3$, $HCN–SO_3$ and $CH_3CN–SO_3$. Only in destabilising fields (in fact, starting some time before the field becomes really destabilising) do the r(B/S–N) values differ greatly. The phenomenon of huge structural difference between phases can thus be seen as a property related to the gas phase behaviour of the molecules, since in the condensed phase similar compounds have similar dative bonds.

Table 6.1: Selected properties of H_3N–BF_3 at different applied electric field strengths[a]

	Field Strength								
	+0.0100	+0.0075	+0.0050	+0.0025	None	-0.0025	-0.0050	-0.0075	-0.0100
r(B–N)	1.653	1.660	1.670	1.680	1.691	1.705	1.722	1.742	1.768
∠(NBF)	105.9	105.4	105.0	104.5	104.0	103.5	102.9	102.3	101.6
$\rho(\mathbf{r_c})$ [b]	0.124	0.121	0.118	0.117	0.111	0.106	0.102	0.097	0.091
$\nabla^2\rho(\mathbf{r_c})$ [c]	0.123	0.125	0.125	0.133	0.119	0.117	0.109	0.099	0.083
$H(\mathbf{r_c})$ [d]	-0.106	-0.102	-0.098	-0.097	-0.090	-0.084	-0.080	-0.074	-0.068
q(N)[e]	-0.673	-0.712	-0.747	-0.783	-0.818	-0.851	-0.884	-0.925	-0.953
q(H)	0.350	0.355	0.359	0.362	0.365	0.368	0.370	0.374	0.374
q(H)	0.349	0.353	0.357	0.361	0.364	0.366	0.368	0.372	0.372
q(H)	0.349	0.353	0.357	0.361	0.364	0.366	0.368	0.372	0.372
q(Donor)	0.374	0.350	0.325	0.300	0.275	0.250	0.224	0.193	0.165
q(B)	0.985	0.994	1.004	1.014	1.024	1.035	1.045	1.065	1.075
q(F)	-0.452	-0.447	-0.442	-0.437	-0.432	-0.427	-0.422	-0.418	0.412
q(F)	-0.453	-0.448	-0.443	-0.439	-0.434	-0.429	-0.424	-0.420	-0.414
q(F)	-0.453	-0.448	-0.443	-0.439	-0.434	-0.429	-0.424	-0.420	-0.414
q(Acceptor)	-0.374	-0.350	-0.325	-0.300	0.275	-0.250	-0.224	-0.193	-0.165

[a] Electric field strength in au (5.1423×10^{11} V.m^{-1}). Distances in Ångstrom, angles in degrees. [b] Electron densities at the B–N bond critical point in e.Bohr^{-3}. [c] Laplacian of the electron density at the B–N bond critical point in e.Bohr^{-5}. [d] Energy densities at the B–N bond critical point in Hartree.Bohr^{-3}. [e] Partial atomic charges in e, calculated by fitting on the electrostatic potential using the Merz-Kollman scheme.

Table 6.2: Selected properties of H_3N–BH_3 at different applied electric field strengths[a]

	Field Strength								
	+0.0100	+0.0075	+0.0050	+0.0025	None	-0.0025	-0.0050	-0.0075	-0.0100
r(B–N)	1.640	1.644	1.648	1.653	1.658	1.663	1.670	1.677	1.685
∠(NBH)	106.2	105.9	105.6	105.3	105.0	104.7	104.3	104.0	103.6
$\rho(\mathbf{r_c})$ [b]	0.113	0.111	0.109	0.107	0.105	0.103	0.101	0.098	0.096
$\nabla^2\rho(\mathbf{r_c})$ [c]	0.354	0.360	0.364	0.369	0.372	0.376	0.377	0.378	0.377
$H(\mathbf{r_c})$ [d]	-0.082	-0.080	-0.077	-0.075	-0.072	-0.069	-0.067	-0.064	-0.061
q(N)[e]	-0.299	-0.343	-0.391	-0.436	-0.490	-0.534	-0.581	-0.627	-0.674
q(H)	0.252	0.259	0.265	0.272	0.282	0.288	0.294	0.301	0.308
q(H)	0.251	0.257	0.264	0.271	0.280	0.286	0.292	0.299	0.305
q(H)	0.251	0.257	0.264	0.271	0.280	0.286	0.292	0.299	0.305
q(Donor)	0.455	0.430	0.403	0.378	0.352	0.325	0.298	0.272	0.244
q(B)	0.296	0.304	0.318	0.329	0.339	0.351	0.364	0.378	0.392
q(H)	-0.249	-0.243	-0.239	-0.234	-0.229	-0.224	-0.219	-0.215	-0.211
q(H)	-0.251	-0.246	-0.241	-0.236	-0.231	-0.226	-0.221	-0.217	-0.213
q(H)	-0.251	-0.246	-0.241	-0.236	-0.231	-0.226	-0.221	-0.217	-0.213
q(Acceptor)	-0.455	-0.430	-0.403	-0.378	-0.352	-0.325	-0.298	-0.272	-0.244

[a] Electric field strength in au (5.1423×10^{11} V.m^{-1}). Distances in Ångstrom, angles in degrees. [b] Electron densities at the B–N bond critical point in e.Bohr^{-3}. [c] Laplacian of the electron density at the B–N bond critical point in e.Bohr^{-5}. [d] Energy densities at the B–N bond critical point in Hartree.Bohr^{-3}. [e] Partial atomic charges in e, calculated by fitting on the electrostatic potential using the Merz-Kollman scheme.

Table 6.3: Selected properties of H_3N–SO_3 at different applied electric field strengths[a]

	Field Strength								
	+0.0100	+0.0075	+0.0050	+0.0025	None	-0.0025	-0.0050	-0.0075	-0.0100
r(S–N)	1.979	1.998	2.019	2.045	2.074	2.111	2.159	2.215	2.290
∠(NSO)	98.9	98.4	97.9	97.4	96.9	96.3	95.6	94.8	93.8
$\rho(\mathbf{r_c})$ [b]	0.123	0.117	0.112	0.105	0.099	0.091	0.082	0.071	0.060
$\nabla^2\rho(\mathbf{r_c})$ [c]	-0.050	-0.030	-0.010	0.010	0.030	0.049	0.067	0.081	0.090
$H(\mathbf{r_c})$ [d]	-0.061	-0.056	-0.050	-0.043	-0.037	-0.030	-0.023	-0.016	-0.010
q(N)[e]	-0.588	-0.642	-0.698	-0.751	-0.718	-0.758	-0.797	-0.833	-0.865
q(H)	0.356	0.361	0.366	0.371	0.349	0.348	0.347	0.343	0.337
q(H)	0.355	0.360	0.365	0.370	0.348	0.347	0.345	0.341	0.334
q(H)	0.355	0.360	0.365	0.370	0.348	0.347	0.345	0.341	0.334
q(Donor)	0.478	0.439	0.400	0.359	0.327	0.285	0.240	0.191	0.140
q(S)	1.068	1.091	1.111	1.130	1.165	1.182	1.201	1.221	1.240
q(O)	-0.516	-0.510	-0.504	-0.497	-0.498	-0.490	-0.481	-0.471	-0.461
q(O)	-0.515	-0.510	-0.503	-0.496	-0.497	-0.489	-0.480	-0.470	-0.460
q(O)	-0.515	-0.510	-0.503	-0.496	-0.497	-0.489	-0.480	-0.470	-0.460
q(Acceptor)	-0.478	-0.439	-0.400	-0.359	-0.327	-0.285	-0.240	-0.191	-0.140

[a] Electric field strength in au (5.1423×10^{11} V.m^{-1}). Distances in Ångstrom, angles in degrees. [b] Electron densities at the S–N bond critical point in e.Bohr^{-3}. [c] Laplacian of the electron density at the S–N bond critical point in e.Bohr^{-5}. [d] Energy densities at the S–N bond critical point in Hartree.Bohr^{-3}. [e] Partial atomic charges in e, calculated by fitting on the electrostatic potential using the Merz-Kollman scheme.

Table 6.4: Selected properties of HCN–BF_3 at different applied electric field strengths[a]

	Field Strength								
	+0.0100	+0.0075	+0.0050	+0.0025	None	-0.0025	-0.0050	-0.0075	-0.0100
r(B–N)	1.739	1.783	1.879	2.436	2.554	2.641	2.715	2.779	2.840
∠(NBF)	103.6	102.6	100.8	94.0	92.7	91.9	91.1	90.5	89.9
$\rho(\mathbf{r_c})$ [b]	0.086	0.077	0.063	0.020	0.015	0.013	0.011	0.009	0.008
$\nabla^2\rho(\mathbf{r_c})$ [c]	0.173	0.136	0.069	0.053	0.047	0.043	0.039	0.035	0.032
$H(\mathbf{r_c})$ [d]	-0.056	-0.049	-0.036	0.001	0.002	0.002	0.002	0.002	-0.002
q(H)[e]	0.316	0.303	0.290	0.268	0.256	0.243	0.231	0.220	0.208
q(C)	0.121	0.122	0.111	0.071	0.069	0.073	0.076	0.076	0.078
q(N)	-0.107	-0.136	-0.165	-0.249	-0.258	-0.271	-0.277	-0.279	-0.282
q(Donor)	0.330	0.289	0.236	0.090	0.067	0.045	0.029	0.016	0.004
q(B)	0.874	0.908	0.921	0.940	0.923	0.972	0.998	1.026	1.056
q(F)	-0.401	-0.399	-0.386	-0.343	-0.330	-0.338	-0.341	-0.346	-0.352
q(F)	-0.401	-0.399	-0.386	-0.344	-0.330	-0.340	-0.343	-0.348	-0.354
q(F)	-0.401	-0.399	-0.386	-0.344	-0.330	-0.340	-0.343	-0.348	-0.354
q(Acceptor)	-0.330	-0.289	-0.236	-0.090	-0.067	-0.045	-0.029	-0.016	-0.004

[a] Electric field strength in au (5.1423×10^{11} V.m^{-1}). Distances in Ångstrom, angles in degrees. [b] Electron densities at the B–N bond critical point in e.Bohr^{-3}. [c] Laplacian of the electron density at the B–N bond critical point in e.Bohr^{-5}. [d] Energy densities at the B–N bond critical point in Hartree.Bohr^{-3}. [e] Partial atomic charges in e, calculated by fitting on the electrostatic potential using the Merz-Kollman scheme.

Table 6.5: Selected properties of $HCN–BH_3$ at different applied electric field strengths[a]

	Field Strength								
	+0.0100	+0.0075	+0.0050	+0.0025	None	-0.0025	-0.0050	-0.0075	-0.0100
r(B–N)	1.552	1.550	1.548	1.545	1.543	1.539	1.536	1.532	1.528
∠(NBH)	106.0	105.8	105.6	105.5	105.3	105.1	105.0	104.9	104.8
$\rho(\mathbf{r_c})$ [b]	0.121	0.121	0.121	0.121	0.121	0.122	0.122	0.123	0.124
$\nabla^2\rho(\mathbf{r_c})$ [c]	0.621	0.633	0.646	0.658	0.671	0.684	0.698	0.712	0.726
$H(\mathbf{r_c})$ [d]	-0.076	-0.075	-0.074	-0.074	-0.074	-0.074	-0.074	-0.074	-0.074
q(H)[e]	0.321	0.309	0.297	0.286	0.274	0.262	0.250	0.238	0.226
q(C)	-0.012	-0.008	-0.005	-0.004	-0.002	-0.002	-0.003	-0.005	-0.009
q(N)	0.091	0.071	0.052	0.034	0.016	-0.001	-0.017	-0.033	-0.048
q(Donor)	0.400	0.372	0.344	0.316	0.289	0.259	0.230	0.200	0.169
q(B)	0.076	0.084	0.091	0.098	0.105	0.113	0.120	0.128	0.136
q(H)	-0.158	-0.152	-0.145	-0.138	-0.131	-0.124	-0.116	-0.109	-0.101
q(H)	-0.159	-0.152	-0.145	-0.138	-0.131	-0.124	-0.117	-0.109	-0.102
q(H)	-0.159	-0.152	-0.145	-0.138	-0.131	-0.124	-0.117	-0.109	-0.102
q(Acceptor)	-0.400	-0.372	-0.344	-0.316	0.289	-0.259	-0.230	-0.200	-0.169

[a] Electric field strength in au (5.1423×10^{11} V.m^{-1}). Distances in Ångstrom, angles in degrees. [b] Electron densities at the B–N bond critical point in e.Bohr^{-3}. [c] Laplacian of the electron density at the B–N bond critical point in e.Bohr^{-5}. [d] Energy densities at the B–N bond critical point in Hartree.Bohr^{-3}. [e] Partial atomic charges in e, calculated by fitting on the electrostatic potential using the Merz-Kollman scheme.

Table 6.6: Selected properties of HCN–SO_3 at different applied electric field strengths[a]

	Field Strength								
	+0.0100	+0.0075	+0.0050	+0.0025	None	-0.0025	-0.0050	-0.0075	-0.0100
r(S–N)	2.294	2.373	2.455	2.534	2.610	2.683	2.752	2.816	2.878
∠(NSO)	95.2	94.3	93.4	92.6	91.9	91.3	90.7	90.2	89.8
$\rho(\mathbf{r_c})$ [b]	0.054	0.045	0.037	0.031	0.026	0.022	0.019	0.016	0.014
$\nabla^2\rho(\mathbf{r_c})$ [c]	0.099	0.098	0.092	0.084	0.076	0.069	0.061	0.055	0.049
$H(\mathbf{r_c})$ [d]	-0.007	-0.004	-0.001	0.000	0.001	0.002	-0.000	0.002	0.002
q(H)[e]	0.311	0.296	0.284	0.270	0.255	0.242	0.230	0.216	0.203
q(C)	0.084	0.087	0.083	0.087	0.093	0.094	0.095	0.102	0.108
q(N)	-0.136	-0.174	-0.202	-0.230	-0.253	-0.269	-0.280	-0.293	-0.306
q(Donor)	0.259	0.209	0.165	0.127	0.095	0.068	0.045	0.025	0.008
q(S)	0.997	1.026	1.064	1.095	1.126	1.163	1.193	1.224	1.258
q(O)	-0.418	-0.412	-0.410	-0.408	-0.407	-0.411	-0.412	-0.416	-0.422
q(O)	-0.419	-0.412	-0.410	-0.408	-0.407	-0.410	-0.413	-0.417	-0.422
q(O)	-0.419	-0.412	-0.410	-0.408	-0.407	-0.410	-0.413	-0.417	-0.422
q(Acceptor)	-0.259	-0.209	-0.165	-0.127	-0.095	-0.068	-0.045	-0.025	-0.008

[a] Electric field strength in au (5.1423×10^{11} V.m^{-1}). Distances in Ångstrom, angles in degrees. [b] Electron densities at the S–N bond critical point in e.Bohr^{-3}. [c] Laplacian of the electron density at the S–N bond critical point in e.Bohr^{-5}. [d] Energy densities at the S–N bond critical point in Hartree.Bohr^{-3}. [e] Partial atomic charges in e, calculated by fitting on the electrostatic potential using the Merz-Kollman scheme.

Table 6.7: Selected properties of $CH_3CN–BF_3$ at different applied electric field strengths[a]

	Field Strength								
	+0.0100	+0.0075	+0.0050	+0.0025	None	-0.0025	-0.0050	-0.0075	-0.0100
r(B–N)	1.669	1.692	1.721	1.765	2.329	2.506	2.611	2.695	2.766
∠(NBF)	105.2	104.5	103.7	102.6	94.8	92.9	91.8	91.0	90.3
$\rho(\mathbf{r_c})$ [b]	0.102	0.096	0.089	0.080	0.017	0.017	0.014	0.011	0.010
$\nabla^2\rho(\mathbf{r_c})$ [c]	0.234	0.217	0.192	0.152	0.059	0.051	0.045	0.040	0.036
$H(\mathbf{r_c})$ [d]	-0.072	-0.066	-0.059	-0.051	-0.001	0.001	0.002	0.002	0.002
q(N)[e]	-0.265	-0.292	-0.319	-0.355	-0.440	-0.462	-0.476	-0.489	-0.498
$q(C_{CN})$	0.413	0.435	0.456	0.479	0.452	0.467	0.484	0.505	0.524
$q(C_{CH_3})$	-0.441	-0.456	-0.471	-0.487	-0.487	-0.501	-0.515	-0.532	-0.549
q(H)	0.219	0.215	0.210	0.206	0.188	0.183	0.179	0.176	0.173
q(H)	0.218	0.214	0.210	0.206	0.188	0.183	0.179	0.176	0.173
q(H)	0.218	0.214	0.210	0.2056	0.188	0.183	0.179	0.176	0.173
q(Donor)	0.362	0.330	0.296	0.253	0.089	0.052	0.029	0.012	-0.003
q(B)	0.906	0.917	0.927	0.955	0.958	0.963	0.989	1.013	1.037
q(F)	-0.423	-0.416	-0.408	-0.403	-0.349	-0.338	-0.339	-0.340	-0.343
q(F)	-0.423	-0.415	-0.408	-0.403	-0.349	-0.338	-0.340	-0.342	-0.345
q(F)	-0.423	-0.415	-0.408	-0.403	-0.349	-0.338	-0.340	-0.342	-0.345
q(Acceptor)	-0.362	-0.330	-0.296	-0.253	-0.089	-0.052	-0.029	-0.012	0.003

[a] Electric field strength in au (5.1423×10^{11} V.m^{-1}). Distances in Ångstrom, angles in degrees. [b] Electron densities at the S–N bond critical point in e.Bohr^{-3}. [c] Laplacian of the electron density at the S–N bond critical point in e.Bohr^{-5}. [d] Energy densities at the S–N bond critical point in Hartree.Bohr^{-3}. [e] Partial atomic charges in e, calculated by fitting on the electrostatic potential using the Merz-Kollman scheme.

Table 6.8: Selected properties of $CH_3CN–BH_3$ at different applied electric field strengths[a]

	Field Strength								
	+0.0100	+0.0075	+0.0050	+0.0025	None	-0.0025	-0.0050	-0.0075	-0.0100
r(B–N)	1.556	1.556	1.554	1.553	1.552	1.549	1.547	1.544	1.540
∠(NBH	106.6	106.3	106.1	105.8	105.6	105.4	105.2	105.0	104.9
$\rho(\mathbf{r_c})$ [b]	0.121	0.120	0.120	0.120	0.119	0.119	0.119	0.120	0.120
$\nabla^2\rho(\mathbf{r_c})$ [c]	0.588	0.600	0.613	0.625	0.638	0.652	0.665	0.678	0.693
$H(\mathbf{r_c})$ [d]	-0.077	-0.076	-0.075	-0.074	-0.073	-0.072	-0.072	-0.071	-0.071
q(N)[e]	-0.079	-0.109	-0.138	-0.170	-0.201	-0.231	-0.262	-0.294	-0.323
q(C_{CN})	0.297	0.324	0.350	0.378	0.405	0.431	0.457	0.484	0.508
q(C_{CH_3})	-0.402	-0.420	-0.438	-0.455	-0.472	-0.489	-0.505	-0.521	-0.535
q(H)	0.201	0.198	0.194	0.191	0.187	0.183	0.180	0.175	0.171
q(H)	0.201	0.198	0.194	0.191	0.187	0.183	0.180	0.175	0.171
q(H)	0.201	0.198	0.194	0.191	0.187	0.183	0.180	0.175	0.171
q(Donor)	0.417	0.388	0.358	0.326	0.294	0.262	0.229	0.195	0.161
q(B)	0.124	0.127	0.13-	0.139	0.147	0.153	0.160	0.167	0.175
q(H)	-0.180	-0.171	-0.162	-0.155	-0.146	-0.138	-0.129	-0.121	-0.111
q(H)	-0.181	-0.172	-0.163	-0.155	-0.147	-0.139	-0.130	-0.121	-0.112
q(H)	-0.181	-0.172	-0.163	-0.155	-0.147	-0.139	-0.130	-0.121	-0.112
q(Acceptor)	-0.417	-0.388	-0.358	-0.326	-0.294	-0.262	-0.229	-0.195	-0.161

[a] Electric field strength in au (5.1423×10^{11} V.m^{-1}). Distances in Ångstrom, angles in degrees. [b] Electron densities at the B–N bond critical point in e.Bohr^{-3}. [c] Laplacian of the electron density at the B–N bond critical point in e.Bohr^{-5}. [d] Energy densities at the B–N bond critical point in Hartree.Bohr^{-3}. [e] Partial atomic charges in e, calculated by fitting on the electrostatic potential using the Merz-Kollman scheme.

Table 6.9: Selected properties of $CH_3CN–SO_3$ at different applied electric field strengths[a]

	Field Strength								
	+0.0100	+0.0075	+0.0050	+0.0025	None	-0.0025	-0.0050	-0.0075	-0.0100
r(S–N)	2.107	2.192	2.288	2.380	2.475	2.567	2.650	2.726	2.797
∠(NSO)	97.1	96.0	94.9	93.8	92.8	92.0	91.2	90.6	90.1
$\rho(\mathbf{r_c})$ [b]	0.054	0.045	0.037	0.031	0.026	0.022	0.019	0.016	0.014
$\nabla^2\rho(\mathbf{r_c})$ [c]	0.099	0.098	0.092	0.084	0.076	0.069	0.061	0.055	0.049
$H(\mathbf{r_c})$ [d]	-0.007	-0.004	-0.001	0.000	0.001	0.002	-0.000	0.002	0.002
q(N)[e]	-0.229	-0.288	-0.345	-0.392	-0.422	-0.456	-0.481	-0.494	-0.510
q(C_{CN})	0.374	0.401	0.427	0.452	0.463	0.488	0.510	0.522	0.543
q(C_{CH_3})	-0.433	-0.451	-0.468	-0.485	-0.494	-0.511	-0.525	-0.535	-0.551
q(H)	0.215	0.209	0.203	0.198	0.192	0.188	0.183	0.178	0.175
q(H)	0.215	0.209	0.203	0.198	0.192	0.187	0.183	0.178	0.174
q(H)	0.215	0.209	0.203	0.198	0.192	0.187	0.183	0.1778	0.174
q(Donor)	0.358	0.290	0.224	0.169	0.123	0.083	0.052	0.027	0.006
q(S)	1.000	1.023	1.048	1.076	1.117	1.147	1.181	1.216	1.249
q(O)	-0.453	-0.437	-0.424	-0.415	-0.413	-0.411	-0.411	-0.415	-0.418
q(O)	-0.453	-0.437	-0.424	-0.415	-0.413	-0.410	-0.411	-0.414	-0.418
q(O)	-0.453	-0.437	-0.424	-0.415	-0.413	-0.410	-0.411	-0.414	-0.418
q(Acceptor)	-0.358	-0.290	-0.224	-0.169	-0.123	-0.083	-0.052	-0.027	-0.006

[a] Electric field strength in au (5.1423×10^{11} V.m^{-1}). Distances in Ångstrom, angles in degrees. [b] Electron densities at the S–N bond critical point in e.Bohr^{-3}. [c] Laplacian of the electron density at the S–N bond critical point in e.Bohr^{-5}. [d] Energy densities at the S–N bond critical point in Hartree.Bohr^{-3}. [e] Partial atomic charges in e, calculated by fitting on the electrostatic potential using the Merz-Kollman scheme.

6.3.2 Topological Analysis and Charge Transfer

Topological analysis of the electron density of all the complexes was done. Atomic partial charges were also calculated, revealing information about the charge transfer and distribution in the complexes, as the bond length changes. Tables 6.1 to 6.9 show the charges and some important characteristics of the bond critical points in electric fields of different strengths. Contour plots of the Laplacian of the electron density are shown in Figures 6.4 to 6.6.

Amine Donors

Values of $\rho(\mathbf{r_c})$ at the dative bond critical points of all the complexes with amine donors decrease as the electric field moves from stabilising to destabilising. This corresponds to a weakening of the bond, as expected by analysis of the bond lengths. The actual values of $\rho(\mathbf{r})$ are also very similar in size, although the SO_3-acceptor has a dative bond that is considerably longer than the other complexes. Information on the nature of the interaction can be obtained by examining the Laplacian of $\rho(\mathbf{r_c})$ as well as the energy density at the bond critical point. The Laplacian is positive everywhere, for all complexes, except at the three points of H_3N–SO_3 in field strengths of 0.01 au, 0.0075 au and 0.0050 au. Since $\nabla^2\rho(\mathbf{r_c}) < 0$ in covalent bonds, this might be indicative of a bond with more covalent character at these three points. However, Cremer and Kraka[118] have shown that the energy density is a much better indicator of bond types in cases where the electron density values are very low at the BCP. This is predominantly the case for complexes with dative bonds. An example of this can be found if we compare $\rho(\mathbf{r_c})$ of the N–H bond with that of the N–B bond of the best known dative complex, H_3N–BH_3. The electron density at the covalent bond is 0.337 e.Bohr^{-3}, which is indeed three times more than the value of the dative bond. In this regard then, the energy densities, $H(\mathbf{r_c})$, are negative in all cases, which is representative of bonds with considerable covalent character. The values also become more negative as the electric field becomes more stabilising, indicating an increase in covalent character (or likewise, a decrease in electrostatic nature) as the bond weakens. Whichever values provide the correct picture, it is worth noting that the trend in Laplacian values differ in the complexes. In H_3N–BH_3 and H_3N–SO_3 $\nabla^2\rho(\mathbf{r_c})$ increases in stabilising fields, but in H_3N–BF_3 it first increases and then decreases. The Laplacian at a specified point is very sensitive to its surroundings and this trend should perhaps be disregarded at low values of $\rho(\mathbf{r})$.

In general though, the values of $\nabla^2\rho(\mathbf{r_c})$ and $H(\mathbf{r_c})$ produced by topological analysis of $\rho(\mathbf{r_c})$ are very low. This is most evident in H_3N–SO_3, where the values of $H(\mathbf{r_c})$ change from -0.061 Hartree.Bohr^{-3} to -0.010 Hartree.Bohr^{-3} over the wide spectrum of field strengths applied. It is thus

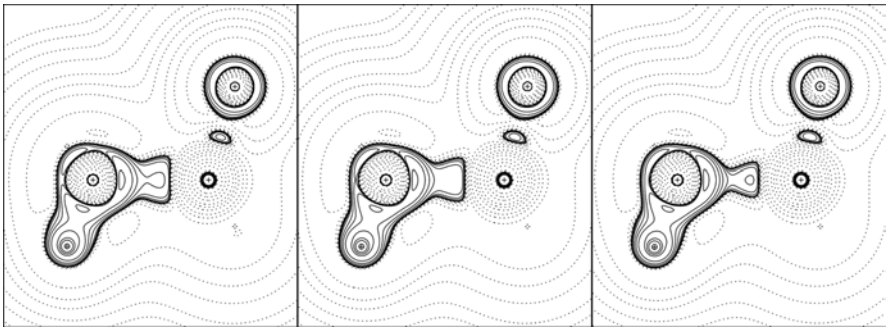

(a) H_3N–BF_3

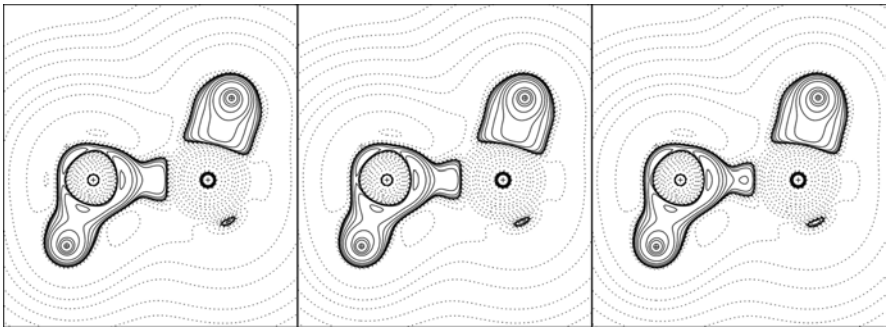

(b) H_3N–BH_3

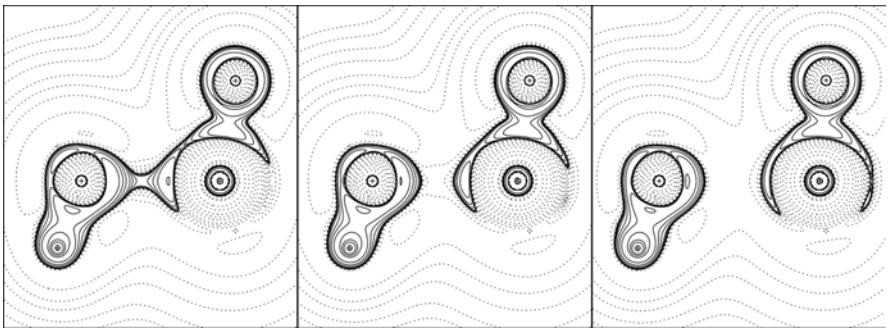

(c) H_3N–SO_3

Figure 6.4: Laplacian of the electron density in H_3N–BF_3 (a, top), H_3N–BH_3 (b, middle) and H_3N–SO_3 (c, bottom) in the absence of an electric field (centre), a stabilising field of 0.01 au (left) and a destabilising field of 0.01 au (right). Solid lines show areas of local charge concentration ($\nabla^2\rho(\mathbf{r}) < 0$), whereas dashed lines show areas of local charge depletion ($\nabla^2\rho(\mathbf{r}) > 0$). The H_3N fragments are on the left, and the BF_3 / BH_3 / SO_3 fragments on the right.

inconclusive in determining an exact point at which the interaction becomes dominated by electrostatic contribution.

Contour diagrams of $\nabla^2\rho(\mathbf{r_c})$ show the change in bond strengths graphically. Figure 6.4(a) shows a noticeable decrease in the electron density concen-

tration in the bonding region of H_3N–BF_3 as the bond weakens. This is also evident in H_3N–BH_3 and H_3N–SO_3. It is most noticeable in H_3N–SO_3, where the region of concentration completely disappears in no applied field and a destabilising field. The energy densities have already shown that the electrostatic nature of the bonds increase in destabilising fields, and the plots of $\nabla^2(\mathbf{r_c})$ for H_3N–SO_3 clearly support this finding. Deformation of the donor density, however, still clearly shows interaction between the fragments. Another interesting observation is the clear charge depletion at the donor atom and the concentration at the acceptor, as seen in these plots. The similarities between our conclusions of the change in characteristics of the bond based on $H_b(\mathbf{r})$ and the contour plots of $\nabla^2\rho(\mathbf{r_c})$ is an affirmation of the statement by Cremer and Kraka that energy densities rather than Laplacian values should be used to describe the bonding in these complexes.

Charge transfer in these complexes was investigated through atomic partial charges derived from the electrostatic potential, as per the Merz-Kollman scheme. The amount of charge transfer increases as the field becomes more stabilising, the negatively polarised end being the donor and the positive end the acceptor. In these cases, the donor and acceptor fragments are very simple, each having only one atom type directly bonded to the donor / acceptor atom. Excess charge on the nitrogen donor atom is thus channelled from the substituent hydrogen atoms, which concurrently carry a partial positive charge. Likewise, the partial positive charge on the accepting boron is sustained by the electronegative fluorine atoms carrying a partial negative charge. The atomic partial charges change as expected, based on the direction and strength of the polarisation introduced by the external electric field.

Hydrogen Cyanide Donors

Values of $\rho(\mathbf{r_c})$ in all these complexes support the trend in bond lengths. The HCN–BF_3 molecule, which has the largest change in structure, shows the largest change in electron density at the B–N BCP. In the absence of an electric field there exists a very small amount of electron density, 0.015 e.Bohr^{-3}, at the critical point. Between the two points at which the sudden bond change occurs, $\rho(\mathbf{r_c})$ increases by more than threefold. The SO_3 acceptor molecule has similar values of $\rho(\mathbf{r_c})$, but of course it lacks the sudden increase. HCN–BH_3, which shows a decrease in bond length where the others increase, has more or less constant electron density throughout the different electric fields, with a slight increase in the strongly destabilising fields.[I]

[I] It is worth reinvestigating our use of the word "destabilising". The origin of this term stems from its influence on donation in the complexes, which can be linked to bond lengths / strengths. Ultimately though, energetics should be employed to provide the required basis for such statements, and in this regard the energy of all the species indeed increases as

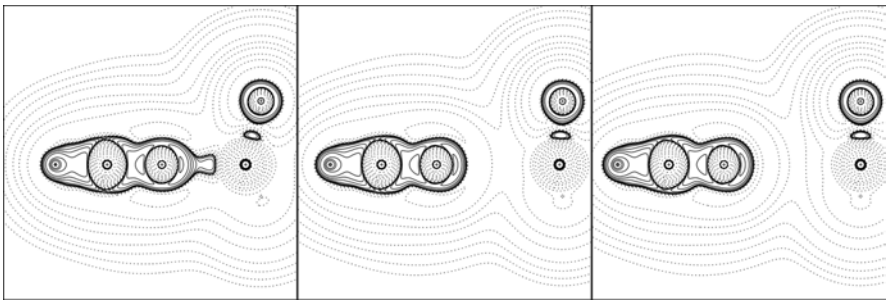

(a) $HCN–BF_3$

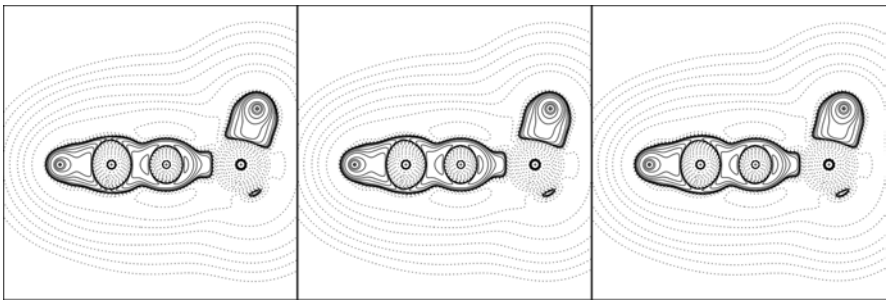

(b) $HCN–BH_3$

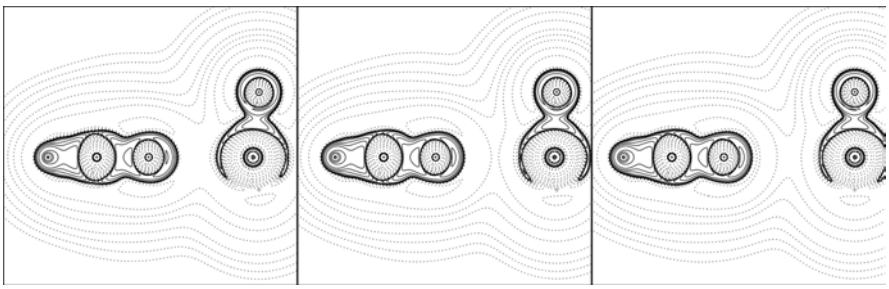

(c) $HCN–SO_3$

Figure 6.5: Laplacian of the electron density in $HCN–BF_3$ (a, top), $HCN–BH_3$ (b, middle) and $HCN–SO_3$ (c, bottom) in the absence of an electric field (centre), a stabilising field of 0.01 au (left) and a destabilising field of 0.01 au (right). Solid lines show areas of local charge concentration ($\nabla^2\rho(\mathbf{r}) < 0$), whereas dashed lines show areas of local charge depletion ($\nabla^2\rho(\mathbf{r}) > 0$). The HCN fragments are on the left, and the BF_3 / BH_3 / SO_3 fragments on the right.

The $\nabla^2\rho(\mathbf{r_c})$ values in $HCN–BF_3$ and $HCN–SO_3$ are all positive and increase in stronger stabilising fields. But once again, we rather use the energy density values as indicative of the bond character. In $HCN–BF_3$ they are negative in the strongly stabilising fields with a short dative bond, and positive or close to zero in destabilising fields with longer bonds, indicating

the electric field is applied against the direction of molecular donation. Whether this might then lead to a stronger or weaker bond, is not straightforward.

that whatever covalent contributions exist in the shorter bonded state disappear in the longer bonded state (e.g. the condensed phase and the gas phase). This agrees with the findings of Mo and Gao[50] that electrostatic contributions dominate weakly bound complexes. In HCN–SO_3 the $H_b(\mathbf{r_c})$ values remain close to zero throughout, indicating no real covalent character in the bonds, irrelevant of the bond lengths and field strengths. In HCN–BH_3 the values stay negative and show very little change, indicating considerable covalent character not influenced by the polarisation of the external electric field.

Contour plots of the Laplacian of $\rho(\mathbf{r})$ underline the changes in bond character reported. The HCN–BF_3 molecule shows some charge concentration in the bonding region (associated with covalent character of the bond) of the complex with a short bond, Figure 6.5(a), which gradually disappears as the bond becomes weaker. In HCN–BH_3 the charge concentration stays visible throughout the different field strengths, in correlation with the finding that the bond has a high covalent character relatively uninfluenced by the field strength. The complex with SO_3 as donor shows no charge concentration in the bonding region. There is even a very small increase in deformation of the nitrogen electron density in the direction of the acceptor.

A very interesting finding is the charge transfer in the complexes; this being the most sensitive indicator of the effect of the external electric field on the polarisation in the complexes. In *all* the complexes, even HCN–BH_3 the charge transfer decreases in the destabilising fields. Although the bond length thus becomes shorter and stronger, the charge transfer decreases, with no effect on the covalency of the bond. In HCN–SO_3 the charge transfer also decreases, having no effect on the bond character as well. Between the points of bond change, the charge transfer in HCN–BF_3 lessens from 0.236 e to 0.090 e, after which it becomes as little as 0.004 e in the strongest destabilising field of -0.01 au. Similarly, the charge transfer in HCN–SO_3 is as little as 0.008 e in the destabilising field of -0.01 au. The HCN–BH_3 complexes retains a relatively high value of charge transfer throughout the calculations. The reader is reminded of the conclusion made by both Jonas *et al.*[33] and Timoshkin *et al.*,[128] that charge transfer does not necessarily correlate with bond strength.

Regarding the atomic partial charges, in HCN–BF_3, the nitrogen atom remains partially negatively charged, with the carbon and hydrogen atoms carrying partial positive charges. As the donation increases, electron density is removed from the nitrogen atom and the partial negative charge decreases. The other atoms of the donor become more electron deficient, the hydrogen atom much more so than the carbon. The trend of change at the carbon atom is interesting. The charges on all of the other atoms of the donor fragment change either strictly increasing or decreasing, but the carbon atom decreases in positive charge as the bond length decreases in the lessening destabilising field. As the field then becomes stable, the positive charge increases, with a large change, as expected, at the point of sudden bond length change. At the acceptor, the positive charge on the boron decreases with more donation.

The fluorine atoms become less electron rich as the bond length decreases in the destabilising field. With the change in field direction, the negative charge increases again. In the HCN–SO_3 molecule the changes are similar on the acceptor fragment, except now of course the fluorine atoms are replaced by oxygens and the boron by a sulphur atom. On the donating fragment, the changes are also similar, except for a slight alteration on the carbon atom. In this case, the positive charge also decreases as the bond length decreases in the decreasingly destabilising field. However, in the stabilising field it is impossible to establish a trend, although the charge is continuously less than in the destabilising field. Irregularities in HCN–BH_3 are again apparent. Just as the trend in bond change differs, the partial atomic charges differ from the other molecules in the test set. As already mentioned, charge donation increases as the bond length decreases, which is the expected change based on the polarisation by the external electric field. On the donating fragment, the nitrogen atom carries a partial negative charge in the destabilising field which becomes positive as the field direction reverses. The hydrogen atom increases in positive charge as the electric field sweeps electron density from the donor to the acceptor. The charge on the carbon atom is nearly zero, but a trend can be established based on the little change that exists. Interestingly though, where the *positive* charge decreases on the carbon in the decreasingly destabilising field in the other molecules, here it is the *negative* charge that decreases. In the increasing stabilising field the negative charge increases, where it is the positive charge that increases in the other molecules. The trend of change is thus the same, although the signs are reversed. The boron atom has a partial positive charge which increases as donation decreases, the numerical value being much less than in the other molecules. The hydrogen atoms attached to the accepting boron strictly increase in negative charge as the donation increases.

Thus, summing up, as the external electric field promotes donation, charge density is transferred from the donating atom, the nitrogen, to the accepting atom, the boron. Charge density is also removed from the hydrogen atom attached to the nitrile group, as charge transfer increases. Unfortunately, the partial charges calculated by the Merz-Kollman scheme on the carbon atom of the nitrile group make a general conclusion as to the changes at this atom difficult.

Acetonitrile Donors

The values of $\rho(\mathbf{r})$ correlate with the dative bond lengths in the same fashion as was the case with the nonmethylated species. So also do the Laplacian values. Between the points of sudden bond change in CH_3CN–BF_3 $\rho(\mathbf{r})$ almost triples.

Similar results are obtained regarding the nature of the bond. The covalent character of the N–B bond in CH_3CN–BF_3 completely disappears as the

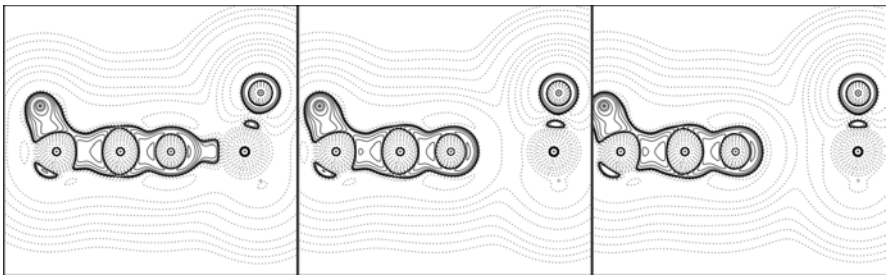

(a) $CH_3CN–BF_3$

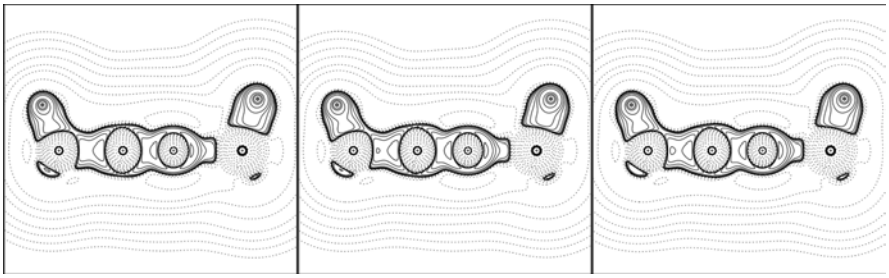

(b) $CH_3CN–BH_3$

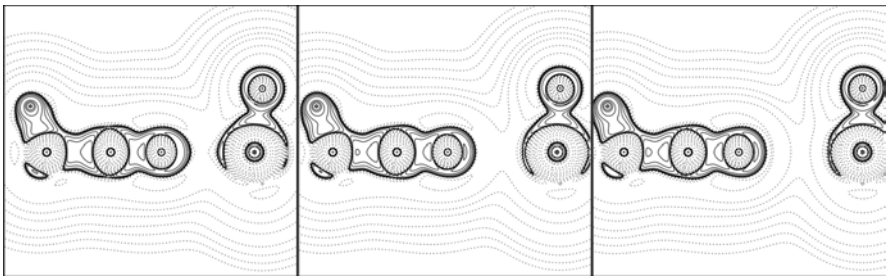

(c) $CH_3CN–SO_3$

Figure 6.6: Laplacian of the electron density in $CH_3CN–BF_3$ (a, top), $CH_3CN–BH_3$ (b, middle) and $CH_3CN–SO_3$ (c, bottom) in the presence of no electric field (centre), a stabilising field of 0.01 au (left) and a destabilising field of 0.01 au (right). Solid lines show areas of local charge concentration ($\nabla^2\rho(\mathbf{r}) < 0$), whereas dashed lines show areas of local charge depletion ($\nabla^2\rho(\mathbf{r}) > 0$). The CH_3CN fragments are on the left, and the BF_3 / BH_3 / SO_3 fragments on the right.

bond continues to lengthen after the sudden bond change, according to the energy density values. The covalent character of the N–B bond in $CH_3CN–BH_3$ decreases very slightly as the bond length decreases, but remains basically the same, and in $CH_3CN–SO_3$ there hardly seems to be any covalent character. The Laplacian contour diagrams once again support these arguments.

Charge transfer decreases as the bond length increases in $CH_3CN–BF_3$ and $CH_3CN–SO_3$. As seen previously, the charge transfer does increase as

the electric field promotes donation, although the bond length decreases in CH_3CN–BH_3.

We first point out the similarities between the partial charges in these complexes and the nonmethylated compounds. The nitrogen and boron atoms follow similar trends, as do the fluorine and hydrogen atoms. The trend of partial charges on the carbon atoms, of which there are two in this case, differs. In all complexes, the carbon atom in the nitrile group carries a partial positive charge which increases as charge donation decreases. The negative charge on the methyl carbon also increases with the decrease in charge donation.

Overall, thus, charge is removed from the donating nitrogen and added to the boron atom, as donation increases. At the same time, charge is added to the carbon nitrile atom, which seems to be originating from either the nitrogen or methyl carbon atom, as both of these decrease in partial negative charge. The methyl carbon is the most likely candidate, since donation in this direction correlates with the direction of the external field. In total, though, the nitrile group increases in positive charge as donation increases.

6.4 Bond Energy Partitioning

For the determination of the bond energy partitioning, the complexes were optimised using the exchange functional of Becke[86] and the correlation functional of Perdew[124] (BP86). A triple-ζ Slater-type basis set, augmented with one set of polarisation functions (TZP), was used.[125] The ADF 2004.1 package does not support geometry optimisations in the presence of an external electric field, therefore the energy partitioning was done at the unperturbed energy minimum in the gas phase. The results are given in Table 6.10

Table 6.10: Energy partitioning analysis of X–Y, with X = H_3N, HCN and CH_3CN and Y = BF_3, BH_3 and SO_3 at BP86/TZ2P.[a]

	r(B/S–N)	ΔE_{int}	ΔE_{Pauli}	ΔE_{elstat}[b]	ΔE_{orb}[b]
H_3N–BF_3	1.700	-40.14	125.15	-90.79 (54.8%)	-74.77 (45.2%)
H_3N–BH_3	1.658	-44.56	108.63	-76.94 (50.2%)	-76.25 (49.8%)
H_3N–SO_3	2.097	-24.23	111.85	-72.06 (53.0%)	-64.02 (47.0%)
HCN–BF_3	2.386	-4.52	15.43	-12.77 (64.0%)	-7.17 (36%)
HCN–BH_3	1.516	-40.10	128.54	-67.42 (40.0%)	-101.22 (60.0%)
HCN–SO_3	2.583	-5.36	17.70	-13.56 (59.0%)	-9.41 (41.0%)
CH_3CN–BF_3	2.188	-9.27	27.37	-22.05 (60.2%)	-14.60 (39.8%)
CH_3CN–BH_3	1.532	-41.96	124.54	-69.24 (41.6%)	-97.26 (58.4%)
CH_3CN–SO_3	2.443	-8.07	28.70	-20.96 (57.0%)	-15.80 (43%)

[a] Energies in kcal.mol^{-1}, distances in Ångstrom. [b] The values in parenthesis give the contribution to the total attractive interactions, $\Delta E_{elstat} + \Delta E_{orb}$.

The instantaneous interaction energies of the complexes, in decreasing order, are

$$H_3N–BH_3 > CH_3CN–BH_3 > H_3N–BF_3 > HCN–BH_3$$
$$> H_3N–SO_3 > CH_3CN–BF_3 > CH_3CN–SO_3 > HCN–SO_3 > HCN–BF_3$$

The strength of the Lewis donors are in decreasing order, $H_3N > HCN > CH_3CN$. Based on both the interaction energies and the dative bond lengths, two classes of complexes are found, in correlation with the work of Mo and Gao.[50] The first five complexes in the above comparison are the strongly interacting ones, the final four all have interaction energies below 10 kcal.mol^{-1}. The weakly interacting complexes are dominated by electrostatic interaction. The strongly interacting complexes, with the exception of $H_3N–BF_3$, are dominated by covalent (orbital) interactions. The complexes with the highest percentage of electrostatic contribution to the total attractive interaction, in decreasing order, are

$$HCN–BF_3 > CH_3CN–BF_3 > HCN–SO_3 > CH_3CN–SO_3$$
$$> H_3N–BF_3 > H_3N–SO_3 > H_3N–BH_3 > CH_3CN–BH_3 > HCN–BH_3$$

Comparing this ordering with the ordering of the structural change catalysed by an external electric field, one finds that the complexes which show the largest change in dative bond length are those with the highest electrostatic contribution to their bond energy in the gas phase minimum. This is the most evident in $HCN–BF_3$ and $CH_3CN–BF_3$, whose bond energy due to attractive terms is composed of over 60% electrostatic contributions.

The two complexes whose bond lengths do not change in accordance with what is suggested by the change in charge donation, $CH_3CN–BH_3$ and $HCN–BH_3$, have the largest contribution of covalent interaction to their bond energy. They are also the complexes with the shortest calculated dative bond lengths. The AIM analysis has already shown that these two complexes do indeed have considerable covalent character in their B–N bonds, and that this character shows little change upon an increase or decrease in donation (i.e. externally catalysed polarisation). Since electrostatic interaction is dependent on the charge separation, a bond with very little electrostatic character should indeed be much less sensitive to a change in charge separation or transfer. However, this still does not explain why an increase in donation seems to destabilise the bond in these two complexes.

It seems that the higher the electrostatic character of the bond in the gas phase equilibrium structure, the more the complex is prone to bond changes. Unfortunately, all the complexes that show a large change in bond distance are those with large separations in the gas phase and and because of this they universally fall in the same class. It is an expected result that electrostatic interaction should play a larger role in bonds where the fragments have a large separation, since orbital or covalent interaction in these cases become less possible as the interfragment distance increases.

6.5 Molecular Orbital Analysis

In the analysis of the nature of the bond, it has become clear that covalent contributions to the dative bond provide the key to the shortening: bond shortening goes hand-in-hand with an increase in the covalent character of the bond, or stated otherwise, an increase in orbital overlap. Whereas all the complexes show changes in their dative bond length, it is only the nitrile-borontrifluoride species whose bonds change in fundamental nature as they progress from predominantly electrostatic/ionic to predominantly covalent bonds. Those species whose bonds are dominated by electrostatic contributions remain predominantly electrostatic, although the bond lengths change considerably, e.g. r(S–N) in $HCN–SO_3$ and $CH_3CN–SO_3$ change by 0.584 Å and 0.690 Å respectively, in electric fields from +0.01 to -0.01 au. Likewise, bonds dominated by covalent contributions remain covalently dominated, e.g. r(B–N) in $H_3N–BF_3$ changes by 0.115 Å.

In this section, we will explicitly explore the bond in terms of its contributing molecular orbitals, negating electrostatics. All calculations were done with DFT and the analysis is thus actually in terms of Kohn-Sham (KS) molecular orbitals, which differ slightly from the true, "traditional" molecular orbitals. However, it has been shown on a great many occasions that conclusions made from KS orbitals are just as valid. We will investigate why the nitrile species are able to introduce such a high degree of covalency when paired with BF_3 as acceptor, enough to completely transform the bond. A simple and effective way to do this is by employing *density of states* (DOS) plots, in particular, *overlap population density of states* (OPDOS) plots. The latter gives a measure of the overlap in the molecular orbitals in terms of specified fragments, positive values indicating bonding interaction, and negative values antibonding interaction. The percentage of the particular molecular orbital localised on each fragment can also be calculated.

Since the acetonitrile and hydrogen cyanide complexes display similar bonding characteristics, for simplicity, the CH_3CN donors were dropped and the complexes under investigation are the H_3N and HCN donors with BF_3, BH_3 and SO_3 as acceptors. Also, since our main interest lays in the strengthening effect of the external field, a comparison will be made between the complexes without an electric field present and in a stabilising electric field of 0.01 au. The OPDOS plots are shown in Figures 6.7 to 6.12. The relevant molecular orbitals are also shown in the figures so that they are at hand when the results are explained. However, the same pictures are also given in Addendum C, where their size is considerably increased for easier viewing.

In $H_3N–BF_3$ (Figure 6.7), which shows a steadily increasing bond length and an increase in covalent nature, there are four orbitals contributing to the bonding character and five contributing to the antibonding character. Although this might at first seem to be a slightly unbalanced situation for creation of a stable bond, the bonding contributions come from orbitals that are

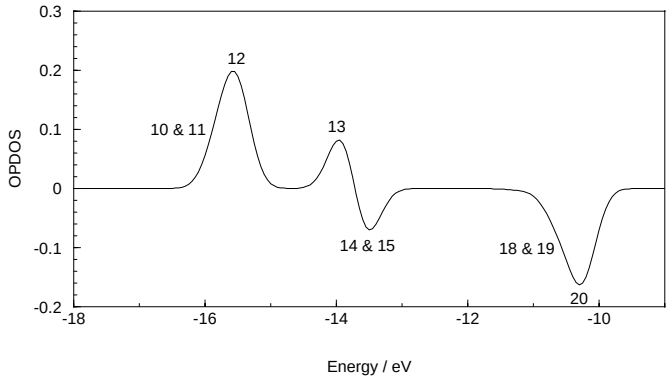

(a) Gas phase

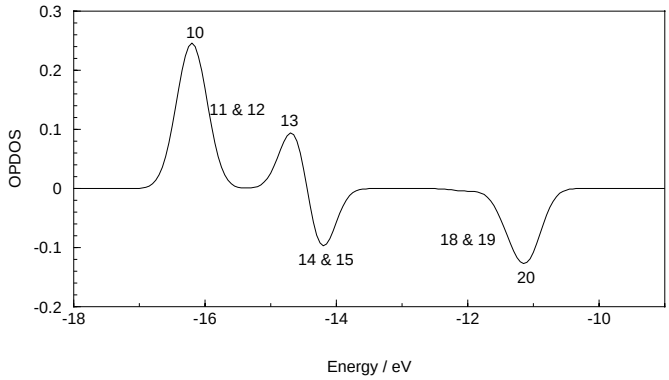

(b) 0.01 au stabilising electric field

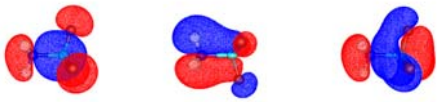

(c) 10 (d) 11 & 12 (e) 13

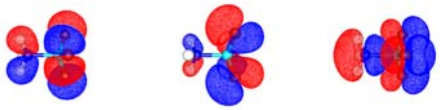

(f) 14 & 15 (g) 18 & 19 (h) 20

Figure 6.7: OPDOS plots of the B–N bond in H_3N–BF_3 in the gas phase (a, top) and in a stabilising electric field (b, bottom). The peaks / troughs are numbered with the corresponding molecular orbitals. A selection of the important orbitals are shown (in the molecule polarised by the electric field) with the donor fragment on the right and the acceptor fragment on the left

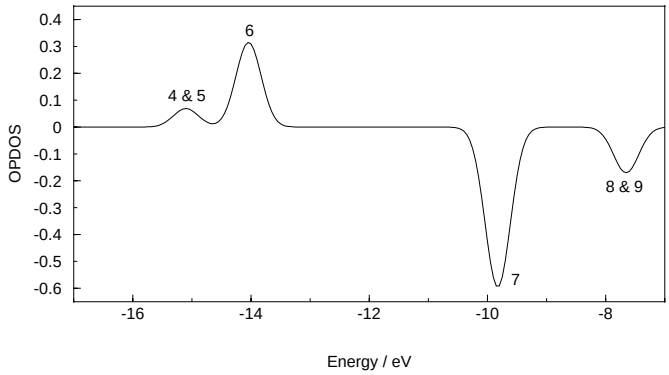

(a) Gas phase

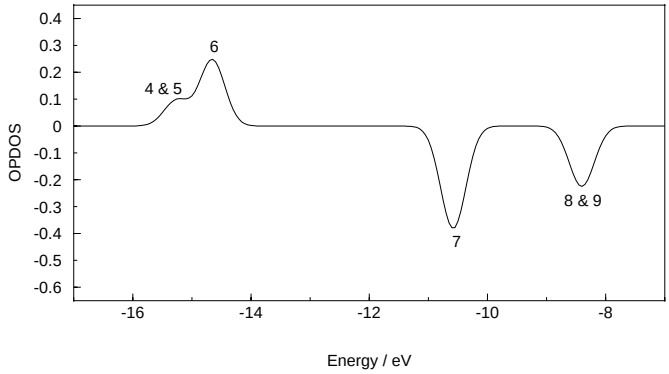

(b) 0.01 au stabilising electric field

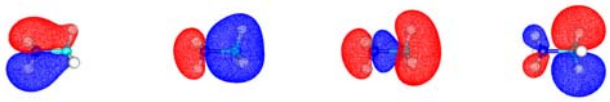

(c) 4 & 5 (d) 6 (e) 7 (f) 8 & 9

Figure 6.8: OPDOS plots of the B–N bond in H_3N–BH_3 in the gas phase (a, top) and in a stabilising electric field (b, bottom). The peaks / troughs are numbered with the corresponding molecular orbitals. A selection of the important orbitals are shown (in the molecule polarised by the electric field) with the donor fragment on the right and the acceptor fragment on the left

much lower in energy. As the external field is applied, there are no fundamental changes in the bonding, the only difference being a swap in ordering of **10** and **11**, which are doubly degenerate, and **12**. Considering the complex in the stabilising field, the largest contributors to bonding are **10** and **13**, which lie 79.2% and 73.9% respectively, on the BF_3 fragment. The contribution from the doubly degenerate pair, which lie mainly (89.8%) on the

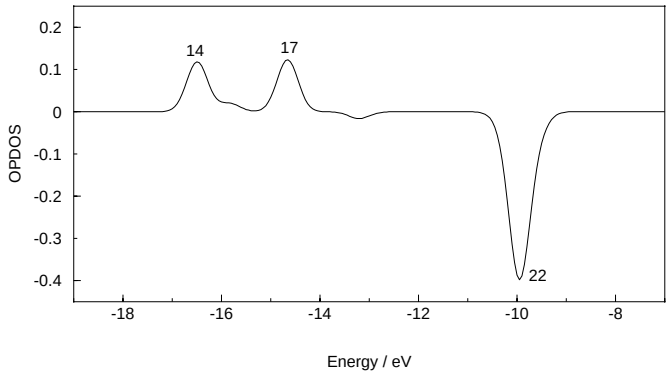

(a) Gas phase

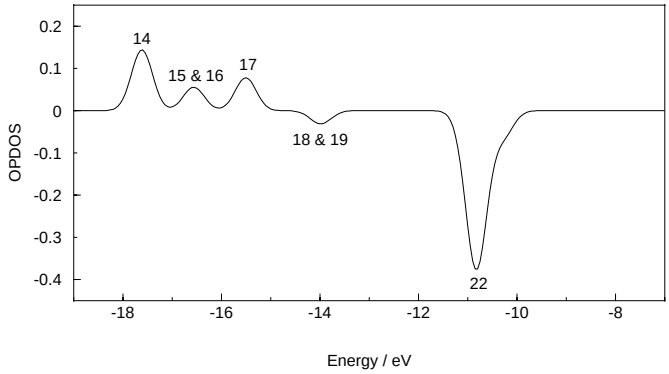

(b) 0.01 au stabilising electric field

(c) 14 (d) 15 & 16 (e) 17 (f) 18 & 19 (g) 22

Figure 6.9: OPDOS plots of the S–N bond in H_3N–SO_3 in the gas phase (a, top) and in a stabilising electric field (b, bottom). The peaks / troughs are numbered with the corresponding molecular orbitals. A selection of the important orbitals are shown (in the molecule polarised by the electric field) with the donor fragment on the right and the acceptor fragment on the left

H_3N fragment, also increases in the stabilising field. The plots also clearly show a decrease in OPDOS values for all the orbitals adding antibonding character to the B–N bond. The strengthening thus results from an increase in the bonding character of the bond, as well as a decrease in the antibonding character.

The B–N bond in H_3N–BH_3 is much less sensitive to external polarisation

and shows a small increase in bond length. This is illustrated by the OPDOS plots which show only minute changes. Orbital **6** represents the major part of donation from the amine to the borane fragment. In no electric field it is localised 52.8% on the accepting fragment, whereas in the 0.01 au field this percentage rises to 67.6%. Orbital **7** represents the antibonding contribution of the donation to the borane fragment and its OPDOS value in the region of this orbital decreases quite clearly in the stabilising field. The percentage concentration of this molecular orbital on the borane fragment drops from 68.0% to 64.7% in the electric field. The stronger bond (at least in terms of the covalent contributions) seems to be a result of a decrease in the overlap of contributions to the molecular orbital that is antibonding in the B–N bond region, rather than an increase in overlap of those strengthening the bond. This is most clearly seen by comparing the peaks corresponding to molecular orbitals **6** and **7**.

The H_3N–SO_3 molecule, which shows a clear increase in covalent interactions in the stabilising field, also shows some interesting changes. A pair of degenerate orbitals, **15** and **16**, which are only mildly contributing in the unperturbed gas phase, show some considerable additions. Molecular orbitals **18** and **19**, a degenerate pair, double in their contributions to the antibonding character. Meanwhile, molecular orbital **17** decreases in its contribution. Other changes can be disregarded. Analysis of **15** and **16** shows that they are similar to the doubly degenerate pair contributing to bonding in all the other species with amine donors, lying predominantly on the H_3N fragment (98.4%). They have a π-like shape and contain considerable involvement from the hydrogen atoms. Orbital **14** is the major lone pair donation from the nitrogen atom to the sulphur atom. Orbital **17** also corresponds to lone pair donation, but interacts more with the substituent oxygen atoms than the sulphur on the acceptor.

For the amine donors, a consistent theme is observed regarding the intramolecular interactions underlying the formation of the B/S–N bond:

- The nitrogen lone pair electron density interacts with the accepting atom.
- The lone pair density interacts with the substituents on the accepting fragment (This is absent when the substituents are hydrogen atoms, e.g. H_3N–BH_3).
- Electron density from the substituents on the donating atom interacts with the accepting fragment. This is in the form of a doubly degenerate pair.

There are of course also the equivalent antibonding interactions.

Next, the molecule which holds the most interest: HCN–BF_3. As one would expect, the electronic structure shows tremendous change. The OPDOS spectrum in the gas phase shows very little in terms of overlap in the

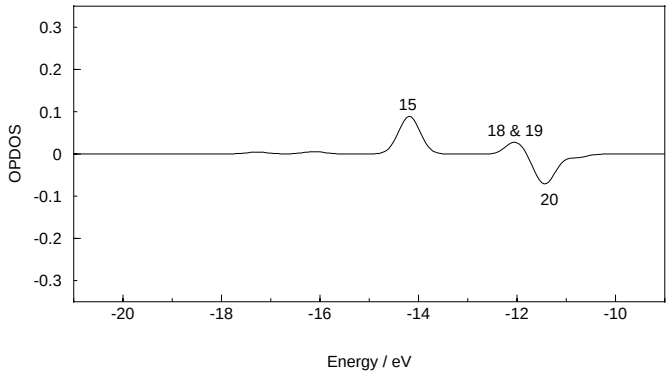

(a)

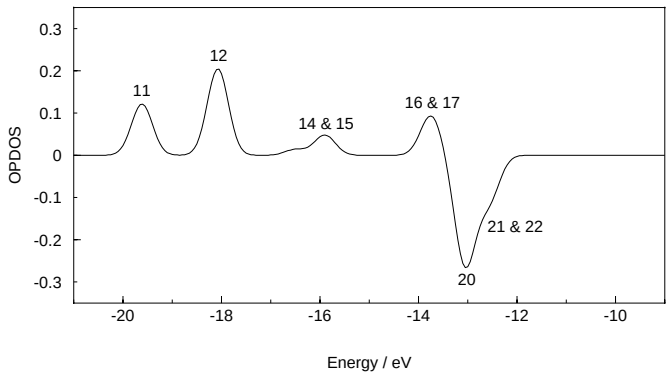

(b) 0.01 au stabilising electric field

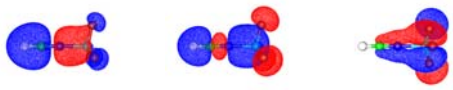

(c) 11 (d) 12 (e) 14 & 15

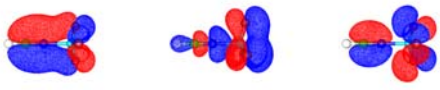

(f) 16 & 17 (g) 20 (h) 21 & 22

Figure 6.10: OPDOS plots of the B–N bond in HCN–BF_3 in the gas phase (a, top) and in a stabilising electric field (b, bottom). The peaks / troughs are numbered with the corresponding molecular orbitals. A selection of the important orbitals are shown (in the molecule polarised by the electric field) with the donor fragment on the right and the acceptor fragment on the left

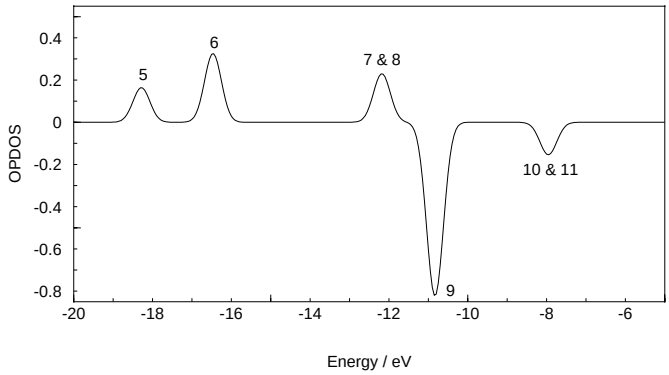

(a)

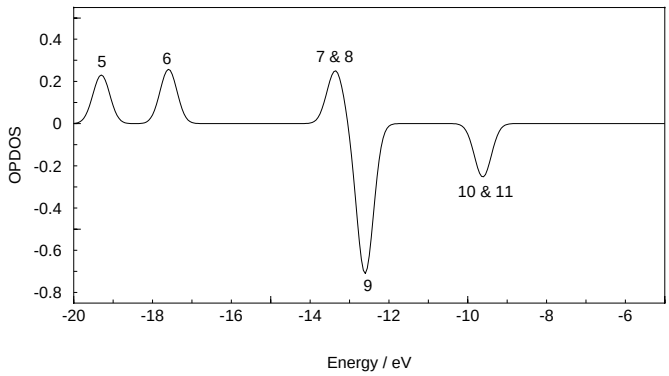

(b) 0.01 au stabilising electric field

(c) 5 (d) 6 (e) 7 & 8 (f) 9 (g) 10 & 11

Figure 6.11: OPDOS plots of the B–N bond in HCN–BH_3 in the gas phase (a, top) and in a stabilising electric field (b, bottom). The peaks / troughs are numbered with the corresponding molecular orbitals. A selection of the important orbitals are shown (in the molecule polarised by the electric field) with the donor fragment on the right and the acceptor fragment on the left

B–N bonding region. Bonding originates from orbital **15** and also the doubly degenerate **18** and **19**, antibonding from orbital **20**. The nitrogen lone pair interaction occurs in **15**, while **18** and **19** are interactions between the nitrile π-density and the fluorine lone pairs. This molecular orbital has 90.3% localisation on the BF_3 fragment, indicating very little involvement by the donor. Lone pair donation is weakened in **20** due to antibonding overlap in the ap-

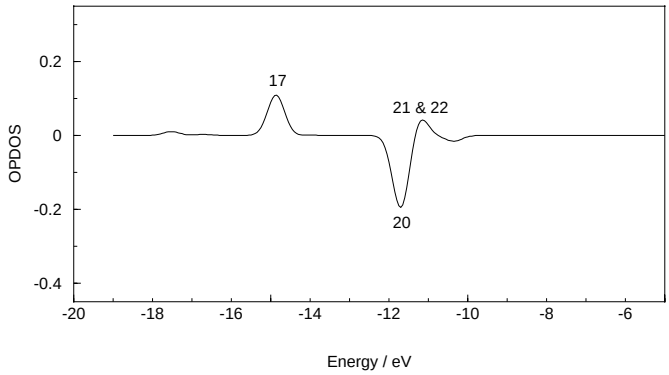

(a)

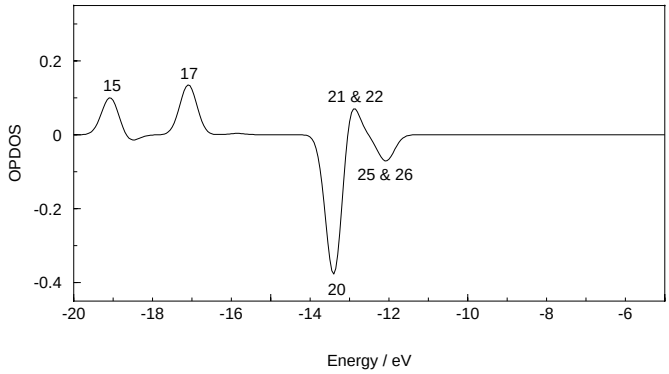

(b) 0.01 au stabilising electric field

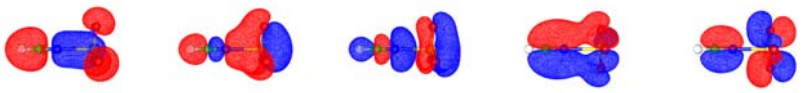

(c) 15 (d) 17 (e) 20 (f) 21 & 22 (g) 25 & 26

Figure 6.12: OPDOS plots of the B–N bond in HCN–SO_3 in the gas phase (a, top) and in a stabilising electric field (b, bottom). The peaks / troughs are numbered with the corresponding molecular orbitals. A selection of the important orbitals are shown (in the molecule polarised by the electric field) with the donor fragment on the right and the acceptor fragment on the left

propriate region. Moving on to the results in the electric field, the first two orbitals contributing to the bonding are **11** and **12**. Both constitute nitrogen lone pair donation and differ only in that one is bonding in the nitrile triple bond region and the other antibonding. The latter interaction was completely absent in the structure with a long bond. **14** and **15** are π-mixing of the nitrile with the fluorine lone pairs pointing away from the B–N bond. The better

overlap occurs between the lone pairs pointing toward the B–N bond as they overlap with the π-density of the nitrile, in **16** and **17**. As seen in all previous cases, the lone pair donation into the boron is counteracted by the antibonding interaction of **20**, as is the π-overlap between the nitrile and the lone pairs pointing toward the bond, in **21** and **22**. Interestingly, the second π-mixing does not feature in antibonding nature.

The polarised molecule thus shows a considerable increase in bonding overlap. Firstly, both π-densities of the nitrile group interacts. Secondly, donation from a lower lying nitrogen lone pair orbital also becomes important. But, since the fragments move closer and bonding interaction increases, antibonding also starts to feature more.

The HCN–BH_3 molecule is unique in these comparisons as its bond lengthens in the stabilising field. The changes are very small, and is barely noticeable in the OPDOS spectra. In terms of orbital contributions, the picture is very similar to the above, two orbitals representing donation, **5** and **6**, but with dissimilar interorbital overlap in the nitrile bonding region. This is followed by the nitrile π-density mixing with the hydrogen atoms, **7** and **8**. The second π-mixing is of course not possible, since there are no perpendicular lone pair densities in BH_3 as was the case in BF_3. Antibonding occurs once again, firstly countering the lone pair donation, **9**, and secondly the π-mixing, **10** and **11**. The question now is, where does the difference in bonding occur and does this explain why this molecule prefers polarisation that destabilises donation. The first change is that **5** has a considerable increase in bonding character to the B–N bond, whereas **6** lowers slightly. The doubly degenerate pair changes very little. The major changes in antibonding contributions cancel each other out, since in adding the electric field **9** decreases in partial overlap but **10** and **11** increases. This approach thus unfortunately produces no evidence why this molecule is different.

The final molecule under investigation is HCN–SO_3. In the gas phase orbital **17** represents lone pair donation. However, this orbital is not pure donation of the nitrogen to the sulphur, but includes substantial mixing with the lone pairs on the oxygen atoms. **21** and **22** are mixing of the π-density of the nitrile with the oxygen lone pairs, as was the case in the other HCN donors. **20** is the antibonding counterpart of lone pair mixing with the whole accepting fragment. In the electric field, **15** starts to contribute to bonding. Careful inspection shows that this orbital was also present in a nearly negligible amount in the gas phase. It corresponds to pure lone pair donation (i.e. mixing of a bonding nature with the oxygens is not present) from the nitrogen to the sulphur. The other orbitals are the same as in the gas phase. The bonding and antibonding parts of π-mixing between the nitrile and the oxygen lone pairs are represented through **21** and **22** as well as **25** and **26**.

In conclusion, the bonding interactions for the HCN donors, which also have their equivalent antibonding interactions, can be summed up as follows:

- The lone pair density of the donating atom interacts with the accepting atom.
- The lone pair density of the donating atom interacts with the *whole* accepting fragment.
- π-density of the nitrile interacts with the lone pairs of the fluorine / oxygen atoms on the accepting atom. Since the nitrile group has a triple bond it has two π-density concentrations perpendicular to each other that can both interact in doubly degenerate fashion each.

6.6 Changes in HCN–BX; X = F, Cl, Br

In the test set of nine molecules only the combination of donors with nitrile groups together with borontrifluoride show the sudden bond change, which we have seen corresponds to a complete electronic structure rearrangement and a different bond type. The question now beckons, will the other halogen substituents result in similar behaviour? A simple test is to also optimise $HCN–BCl_3$ and $HCN–BBr_3$ in increasing external electric fields. The results are shown in Figure 6.13. As expected, they both have consistently shorter

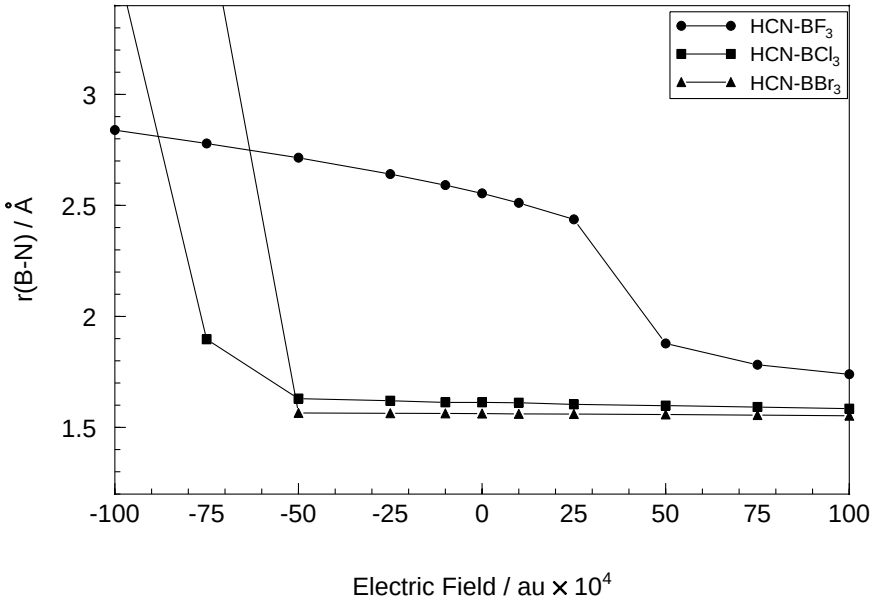

Figure 6.13: The B–N bond length as a function of the applied external electric field in $HCN–BX_3$; X = F, Cl, Br. The positive electric field stabilises the bond and is orientated against the molecular dipole moment, the negative electric field destabilises the bond and is orientated opposite the dipole moment.

B–N bonds than the BF_3 acceptor, since it is known that they are stronger Lewis acids. At no point, however, do their dative bonds show a sudden change. In destabilising fields their dative bonds rupture. So although the bonds are stronger, they are more sensitive to polarisation destabilising the bonds. Whereas the $HCN–BF_3$ molecule shows changes centred around a structure with a short bond in stabilising fields and around a different structure with a long bond in destabilising fields, the situation is not the same for the other halogenated acceptors. They do not seem to have the electrostatically bound minimum at longer separations.

6.7 Conclusions

In this chapter various molecules with dative bonds were subjected to external electric fields of varying strength. The change in dative bond length as well as the angle between the substituents of the acceptor and the donor atom were monitored. It was found that $HCN–BF_3$ and $CH_3CN–BF_3$ show sudden changes corresponding to a progression of their bonds from a partial, predominantly electrostatically bound interaction to a bond with much more covalent character. The B–N bond in $H_3N–BF_3$ and $H_3N–BH_3$ changes, the latter much less, but show no real change in bonding character. $HCN–BH_3$ and $CH_3CN–BH_3$ have the very unique behaviour that their bonds actually *decrease* in length (and strength, according to AIM analysis) in electric fields that polarise the molecules in a manner which increases interfragment donation. These bonds are very short with a high degree of orbital overlap (covalent character). $H_3N–SO_3$, $HCN–SO_3$ and $CH_3CN–SO_3$ shows considerable increases in their S–N bonds, but only a partial change in the nature of their dative bonds. In strongly stabilising fields orbital overlap starts to become a factor and adds covalent character to a bond that is otherwise dominated by electrostatics. BF_3 also seems to be unique in its behaviour since boron with the other halogens do not show similar behaviour.

Chapter 7

Conclusions and Future Work

7.1 Summary of Results and Conclusions

We have carried out a study of the effect of the surrounding molecules on the condensed phase structures of $HCN–BF_3$ and $CH_3CN–BF_3$. Several calculations were done in which dimers (with centre of inversion symmetry) of these complexes were optimised in the presence of two to six frozen surrounding molecules, whose exact atomic positions were taken from the experimentally determined crystal structure. It was found that the addition of six molecules leads to a shortening of 0.809 Å in r(B–N) of $HCN–BF_3$. Similarly, six surrounding molecules in $(CH_3CN–BF_3)_8$ reduces the B–N bond length in the central pair by 0.654 Å. The latter value is somewhat misleading, since the gas phase structure calculated has a bond length that is 0.27 Å longer than the experimental value. The N–B–F angle changes by 11.5° and 10.6°, respectively. The formation of hydrogen bonds proves influential in changes in the N–B–F angles. Both molecules show a considerable decrease in bond length in the dimer alone.

Analysis of the dipole-dipole interaction energy, based on point dipoles placed at the centre of the linear parts of the $HCN–BF_3$ and $CH_3CN–BF_3$ molecules, was done. There exists a correlation in that an increase in dipole-dipole interaction results in a shortening of the B–N bond length. However, the changes in bond length and dipole-dipole interaction energy on going from one model size to the next do not match. A large change in the interaction energy does not necessarily lead to a large change (relative to the other changes) in the B–N bond length. A correlation in terms of the magnitude of change of these two variables is thus absent. This became even more surprising when similar calculations on $H_3N–BH_3$ displayed a very good correlation.

NPA of the two complexes reveals important delocalisation of the fluorine lone pair natural orbitals into the antibonding natural bond orbital of the B–N bond. This delocalisation is dependent on both the energy of the involved

orbitals as well as their spacial overlap. The latter provides an intricate link between the N–B–F angle and the B–N bond length, something which has been noticed previously in the literature.[12,16,38]

An investigation of the changes in a $(HCN–BF_3)_2$ dimer shows that the changes in structure are dominated by a sudden jump in r(B–N). A change of just 0.02 Å (at a very specific point) in the perpendicular distance between the molecules in the dimer leads to a 0.296 Å change in r(B–N).

The effect of dipoles in the crystal structure is propagated through the polarisation caused by their reaction field (electric field). We carried out a study of the effect of electric fields of varying strength on the structure of X–Y; X = H_3N, HCN, CH_3CN; Y = BF_3, BH_3, SO_3. $HCN–BF_3$ and $CH_3CN–BF_3$ show sudden changes between electric fields of specific strengths. All the other molecules show changes, of varying magnitudes, but none display any sudden changes.

Bond composition in terms of covalent and non-covalent / ionic contributions shows that the B–N bond in $HCN–BF_3$ and $CH_3CN–BF_3$ changes from being predominantly electrostatic in the gas phase to covalent in the condensed phase. The other molecules show little change in their bond composition. The SO_3 acceptors, for instance, display a large change in their electrostatic S–N bond lengths, accompanied by only a mild introduction of covalency at very short r(S–N) values.

Analysis of the contributions to the dative bond in terms of specific atoms or fragments, based on intraorbital overlap of the MOs, reveals that the π-density of the nitrile bond plays a large role in the formation of the bond. Interactions involving the lone pairs on the fluorine atoms also contribute to the bond. Finally, replacing the fluorine atoms in $HCN–BF_3$ with the other halogens does *not* lead to a similar situation where the bond changes drastically in a field of specific strength.

We conclude that the $HCN–BF_3$ and $CH_3CN–BF_3$ molecules are unique in the magnitude of difference in structure between the gas and condensed phase. This unique nature stems from these molecules possessing *two fundamentally different phase-dependent minima* on their PES. All the other tested molecules do indeed also have two phase-dependent equilibrium structures, but these differences represent *a shift in the equilibrium distance of the same fundamental interaction*, rather than two completely different interactions. Of course, the two structures in $HCN–BF_3$ and $CH_3CN–BF_3$ are also shifted by external forces. A clear demonstration of this is Figure 6.1, which shows the changes in these molecules occurring at two different levels. The uniqueness of this behaviour becomes even more striking when it is shown that a nitrile donor with BCl_3 and BBr_3 as acceptor does not share this fate. BCl_3 and BBr_3 are known to be better acceptors than BF_3, yet the B–N bond with the former acceptors ruptures easily in the presence of a destabilising external polarisation. One can argue that the the nitrile-borontrifluoride molecule also "ruptures" in less stable polarisation, but instead of completely disintegrating just

progresses to another minimum at a longer separation where the changes can continue to happen. The dative bonds in the other complexes in the series are strong enough to remain stable in destabilising polarisation.

The weakening influence of fluorine lone pair delocalisation emphasises the importance of the initially planar borontrifluoride molecule to distort tetrahedrally. This is also illustrated by the inability of the B–N bond to progress to the stronger bound state with the N–B–F angle kept frozen at the computed gas phase value (Figure 6.2). It might thus be that the crystal field (electric field) not only promotes donation but also helps by increasing the N–B–F angle (the stabilising electric field is in the direction of N–B–F angle increase).

On the topic of the specific effects in the crystal environment that cause the bond changes: dipole-dipole interactions should surely still be considered as the main protagonist, especially in the light of the evidence that electric fields can be used satisfactorily to simulate changes of equal magnitude. However, the link between the N–B–F angle and the B–N bond length (which is further cemented by the evidence of fluorine lone pair delocalisation) provides an argument for hydrogen bonding in the crystal structure to be of some importance, since the $(HCN–BF_3)_n$ and $(CH_3CN–BF_3)_n$ models clearly show a link between H$\cdots$H contacts and the N–B–F angle. It is clear that hydrogen bonding plays no role regarding the change in fundamental nature of the bonds, but merely brings the shortening to a conclusion.

7.2 Future Work

One question that remains unanswered is why the specific combination of nitrile and borontrifluoride forms gas phase structures that are bound primarily through electrostatics. It may prove difficult to answer without a further comparison with other complexes with similar constitutions. Finding other complexes that also display these sudden changes catalysed by specific external forces might then be a priority.

Also, why does the B–N bond in nitrile-borane complexes *lengthen* in the presence of stabilising electric fields? The fact that the bond has a large covalent character explains why changes that affect electrostatic interactions cause very little perturbation. However, this does not explain why the bond in a donor-acceptor complex actually lengthens as donation increases.

Addendum A

Optimised Structures of $(HCN–BF_3)_n$; n=2,4,6,8.

The optimised structures of the $(HCN–BF_3)_n$ crystal models, calculated at B3LYP / 6-31G(d). The complete distance matrix (in Ångstrom) of one $HCN–BF_3$ molecule of the central dimer is given in each case.

$(HCN–BF_3)_2$

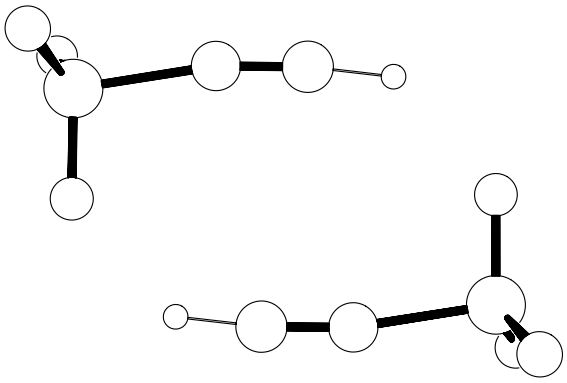

		1	2	3	4	5	6	7
1	B	0.000						
2	F	1.380	0.000					
3	F	1.342	2.298	0.000				
4	F	1.343	2.298	2.304	0.000			
5	N	1.806	2.445	2.474	2.469	0.000		
6	C	2.945	3.374	3.530	3.514	1.149	0.000	
7	H	4.008	4.297	4.570	4.542	2.226	1.080	0.000

(HCN–BF_3)$_4$

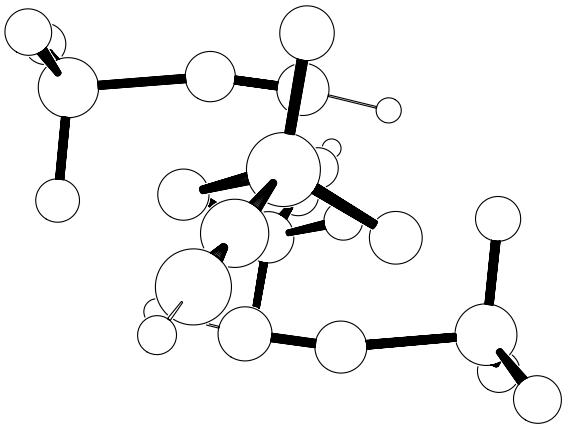

		1	2	3	4	5	6	7
1	B	0.000						
2	F	1.387	0.000					
3	F	1.349	2.303	0.000				
4	F	1.352	2.302	2.298	0.000			
5	N	1.739	2.410	2.453	2.441	0.000		
6	C	2.869	3.302	3.525	3.472	1.148	0.000	
7	H	3.928	4.204	4.580	4.483	2.227	1.083	0.000

(HCN–BF_3)$_6$

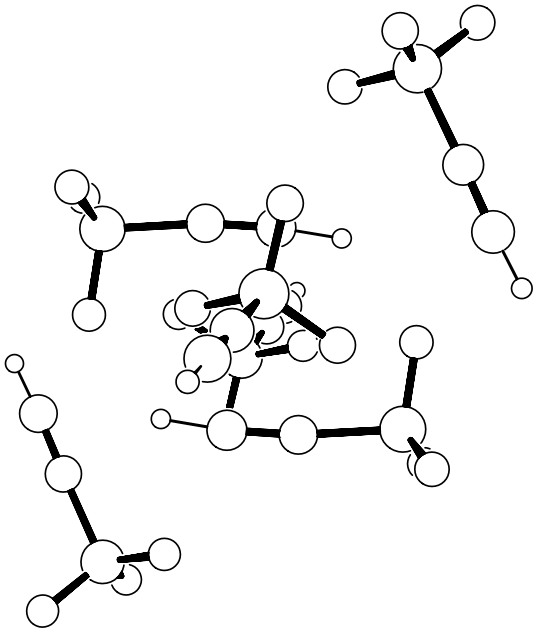

		1	2	3	4	5	6	7
1	B	0.000						
2	F	1.406	0.000					
3	F	1.360	2.294	0.000				
4	F	1.351	2.307	2.303	0.000			
5	N	1.670	2.397	2.421	2.414	0.000		
6	C	2.811	3.340	3.471	3.443	1.145	0.000	
7	H	3.875	4.270	4.505	4.466	2.218	1.076	0.000

(HCN–BF_3)$_8$

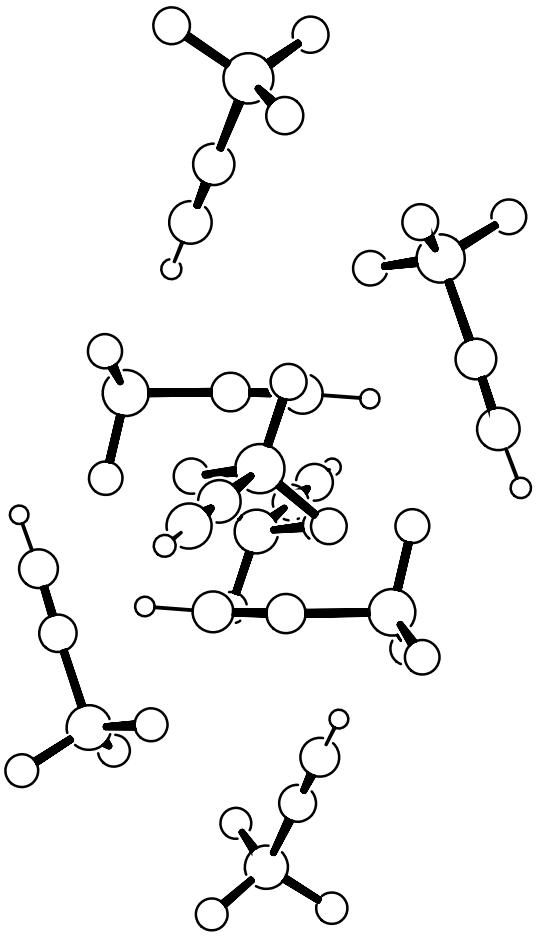

		1	2	3	4	5	6	7
1	B	0.000						
2	F	1.389	0.000					
3	F	1.355	2.293	0.000				
4	F	1.373	2.308	2.303	0.000			
5	N	1.665	2.410	2.421	2.392	0.000		
6	C	2.808	3.403	3.469	3.386	1.145	0.000	
7	H	3.877	4.380	4.503	4.385	2.216	1.072	0.000

Optimised Structures of $(CH_3CN–BF_3)_n$; n=2,4,6,8.

The optimised structures of the $(CH_3CN–BF_3)_n$ crystal models, calculated at B3LYP/6-31G(d). The complete distance matrix (in Ångstrom) of one $CH_3CN–BF_3$ molecule of the central dimer is given in each case.

$(CH_3CN–BF_3)_2$

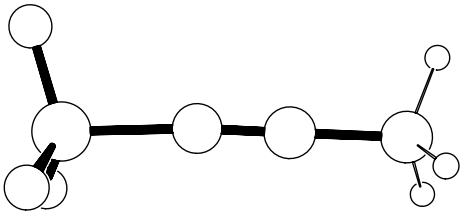

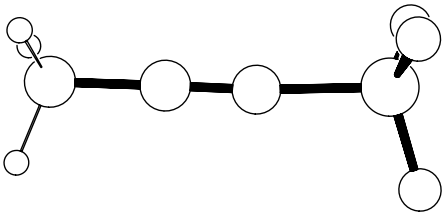

		1	2	3	4	5	6	7
1	B	0.000						
2	F	1.355	0.000					
3	F	1.376	2.305	0.000				
4	F	1.377	2.305	2.290	0.000			
5	N	1.684	2.421	2.415	2.405	0.000		
6	C	2.832	3.474	3.428	3.390	1.151	0.000	
7	C	4.284	4.863	4.802	4.738	2.603	1.452	0.000
8	H	4.784	5.089	5.450	5.306	3.144	2.095	1.094
9	H	4.767	5.416	4.999	5.356	3.142	2.084	1.093
10	H	4.706	5.428	5.279	4.857	3.115	2.069	1.093

		8	9	10
8	H	0.000		
9	H	1.797	0.000	
10	H	1.802	1.772	0.000

$(CH_3CN–BF_3)_4$

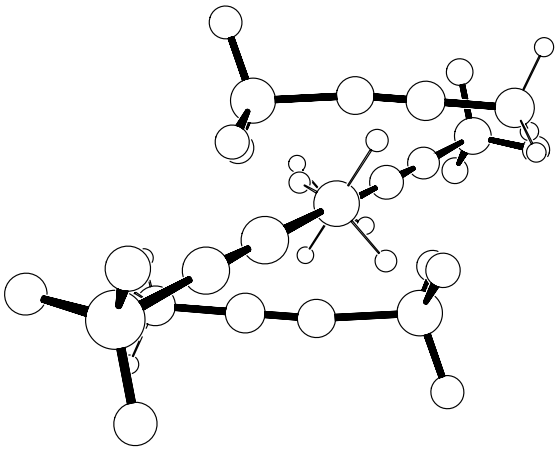

		1	2	3	4	5	6	7
1	B	0.000						
2	F	1.349	0.000					
3	F	1.387	2.307	0.000				
4	F	1.384	2.308	2.292	0.000			
5	N	1.666	2.421	2.402	2.406	0.000		
6	C	2.811	3.498	3.375	3.390	1.151	0.000	
7	C	4.260	4.906	4.712	4.743	2.602	1.452	0.000
8	H	4.792	5.179	5.301	5.435	3.151	2.097	1.094
9	H	4.669	5.465	4.817	5.189	3.113	2.069	1.094
10	H	4.733	5.432	5.331	4.924	3.143	2.088	1.094

		8	9	10
8	H	0.000		
9	H	1.799	0.000	
10	H	1.791	1.778	0.000

$(CH_3CN–BF_3)_6$

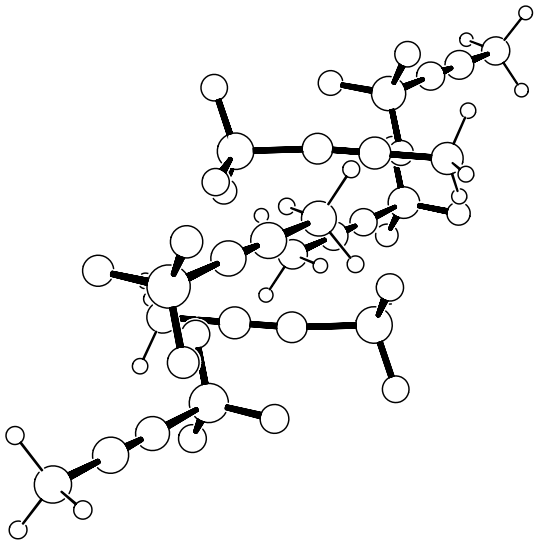

		1	2	3	4	5	6	7
1	B	0.000						
2	F	1.353	0.000					
3	F	1.389	2.304	0.000				
4	F	1.387	2.307	2.297	0.000			
5	N	1.646	2.418	2.388	2.400	0.000		
6	C	2.793	3.486	3.378	3.378	1.150	0.000	
7	C	4.241	4.887	4.728	4.726	2.600	1.450	0.000
8	H	4.745	5.125	5.387	5.298	3.130	2.078	1.092
9	H	4.705	5.416	4.893	5.323	3.134	2.085	1.092
10	H	4.656	5.441	5.200	4.834	3.107	2.058	1.092

		8	9	10
8	H	0.000		
9	H	1.807	0.000	
10	H	1.791	1.782	0.000

$(CH_3CN–BF_3)_8$

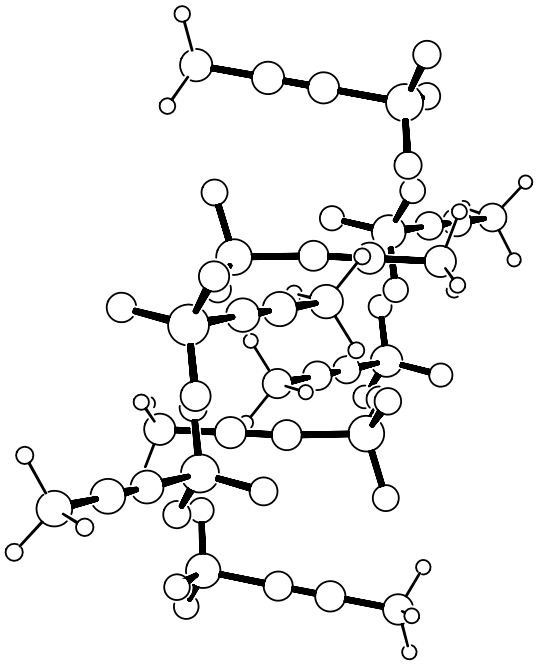

		1	2	3	4	5	6	7
1	B	0.000						
2	F	1.379	0.000					
3	F	1.385	2.301	0.000				
4	F	1.376	2.314	2.295	0.000			
5	N	1.627	2.403	2.387	2.404	0.000		
6	C	2.776	3.447	3.368	3.426	1.151	0.000	
7	C	4.222	4.830	4.706	4.798	2.598	1.447	0.000
8	H	4.707	5.028	5.307	5.384	3.121	2.070	1.093
9	H	4.653	5.353	4.827	5.335	3.117	2.072	1.093
10	H	4.679	5.406	5.259	4.961	3.112	2.061	1.092
		8	9	10				
8	H	0.000						
9	H	1.800	0.000					
10	H	1.801	1.791	0.000				

Addendum B

Molecular Orbitals of $(HCN–BF_3)_2$

Valence molecular orbitals (#13 – #46) of $(HCN–BF_3)_2$ are shown with a boron-nitrogen bond length of 1.944 Å compared to the same system with a bond length of 2.240 Å. The orbital number is given, as well as the energy in atomic units (Hartree) and the symmetry (in the C_{2h} point group). The orbitals of the two different systems are also correlated. All calculations at B3LYP / 6-311+G(2df,p).

Dimer Separation 4.42 Å, r(B–N) 1.944 Å

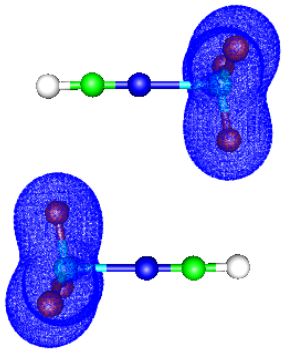

#13, -1.23521 au, A_g

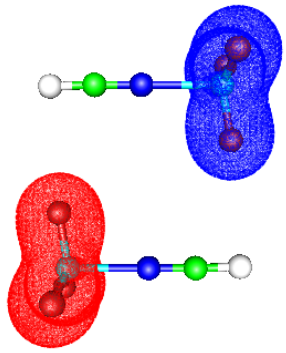

#14, -1.23520 au, B_u

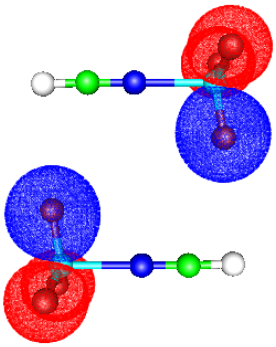

#15, -1.19620 au, A_g

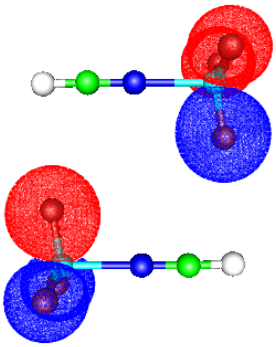

#16, -1.19618 au, B_u

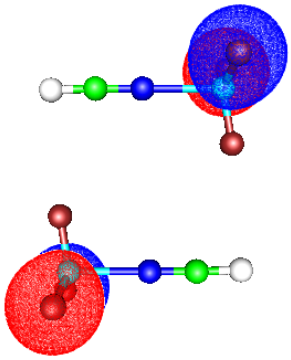

#17, -1.19452 au, B_g

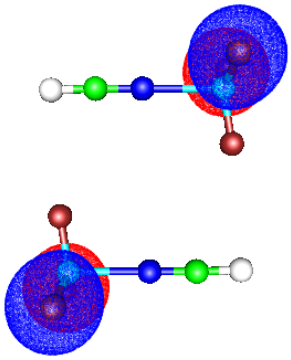

#18, -1.19451 au, A_u

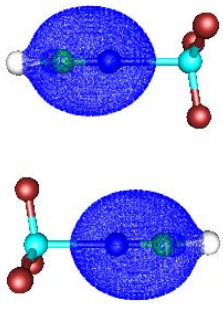

#19, -0.99310 au, A_g

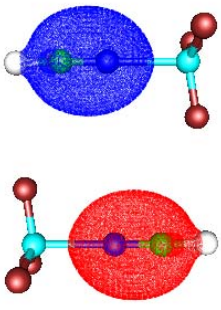

#20, -0.99305 au, B_u

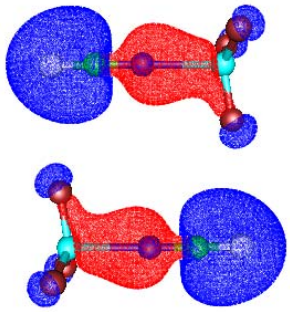

#21, -0.65933 au, A_g

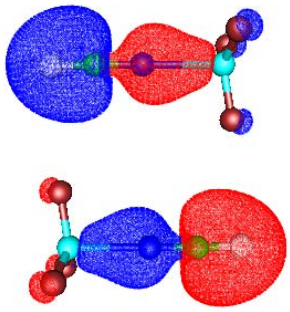

#22, -0.65836 au, B_u

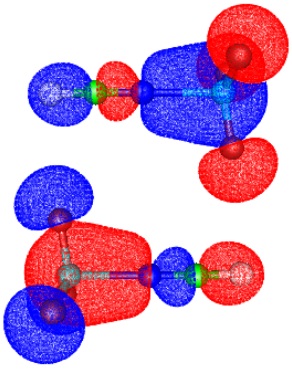

#23, -0.59422 au, B_u

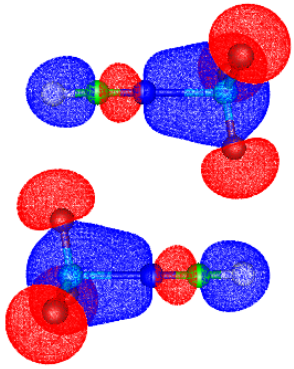

#24, -0.59212 au, A_g

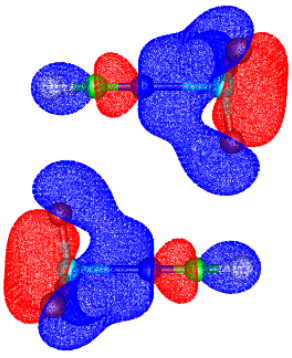

#25, -0.54588 au, A_g

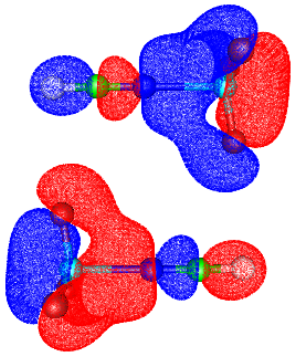

#26, -0.54445 au, B_u

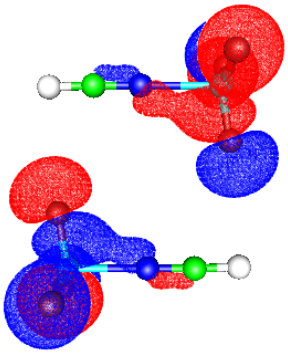

#27, -0.53901 au, B_u

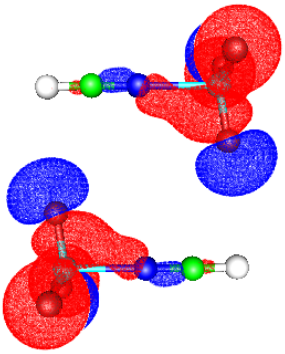

#28, -0.53822 au, A_g

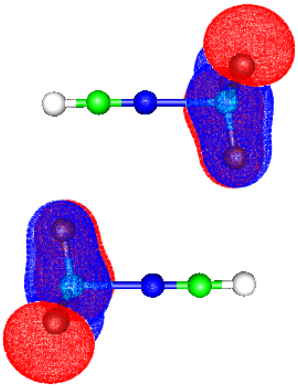

#29, -0.53627 au, A_u

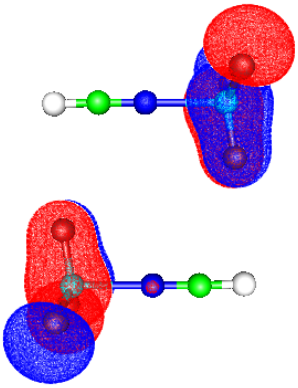

#30, -0.53618 au, B_g

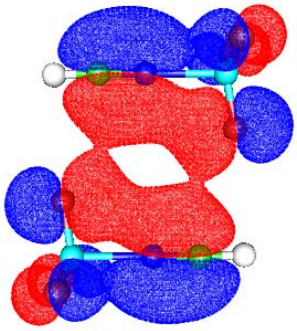

#31, -0.44645 au, A_g

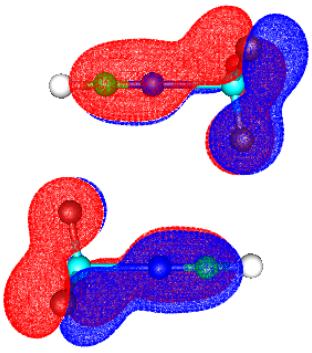

#32, -0.44345 au, B_g

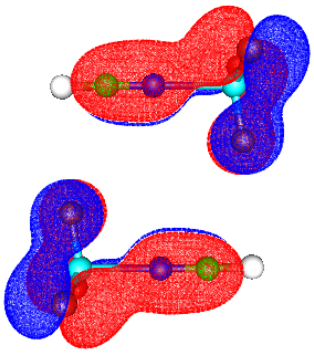

#33, -0.44245 au, A_u

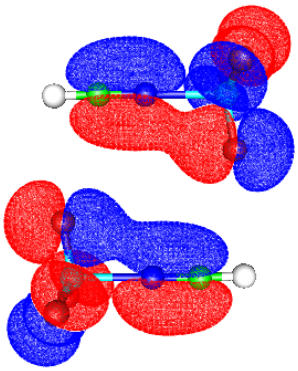

#34, -0.44189 au, B_u

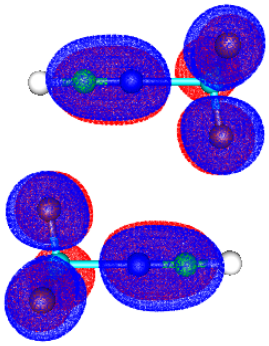

#35, -0.43823 au, A_u

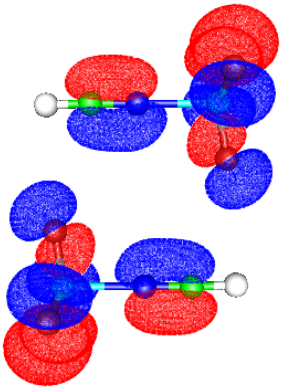

#36, -0.43696 au, A_g

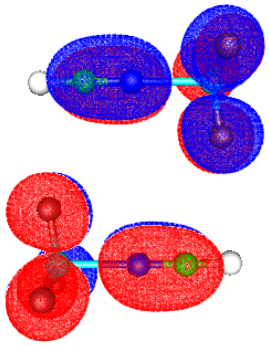

#37, -0.43652 au, B_g

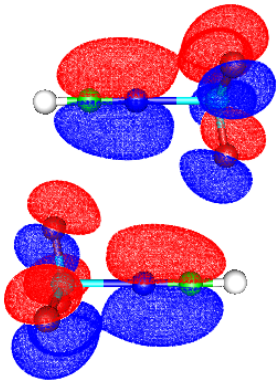

#38, -0.43218 au, B_u

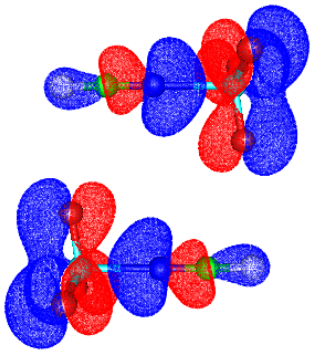

#39, -0.42680 au, A_g

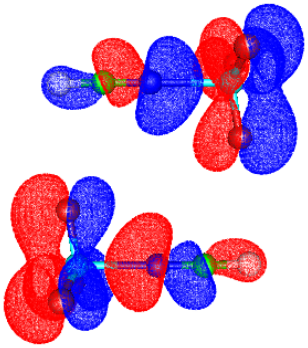

#40, -0.42676 au, B_u

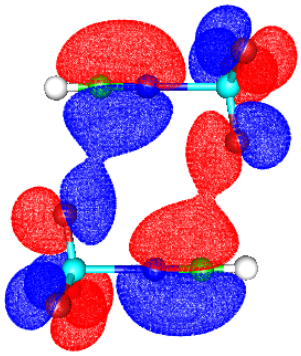

#41, -0.41653 au, B_u

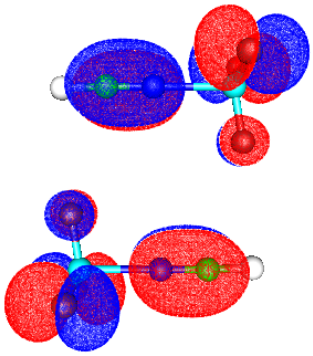

#42, -0.41240 au, B_g

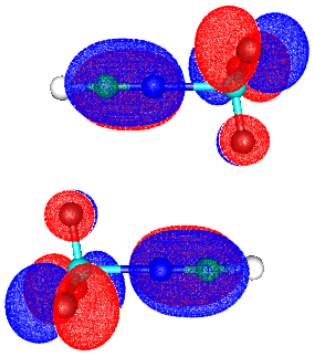

#43, -0.41182 au, A_u

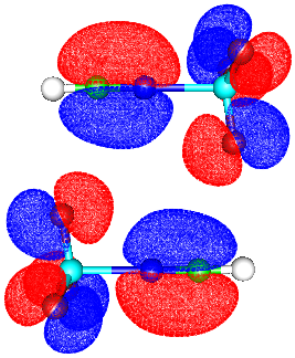

#44, -0.41052 au, A_g

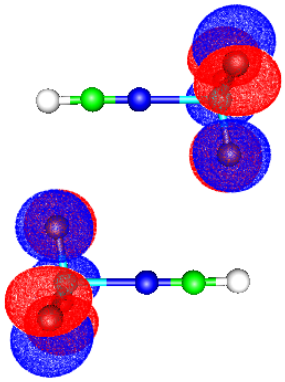

#45, -0.39655 au, A_u

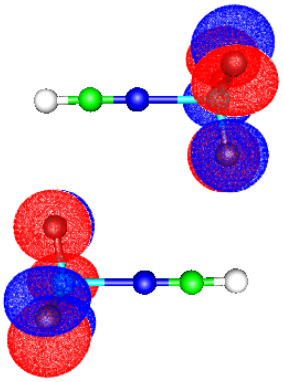

#46, -0.39648 au, B_g

Dimer Separation 4.44 Å, r(B–N) 2.240 Å

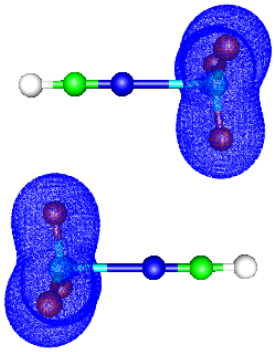

#13, -1.24914 au, A_g

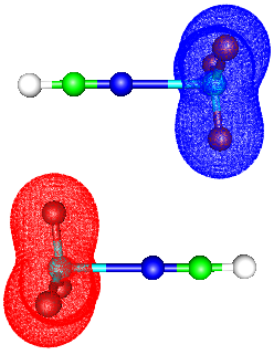

#14, -1.24913 au, B_u

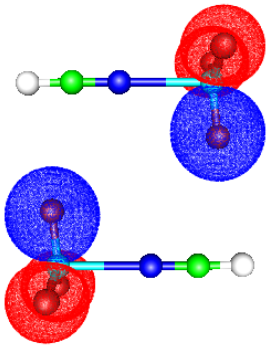

#15, -1.21126 au, A_g

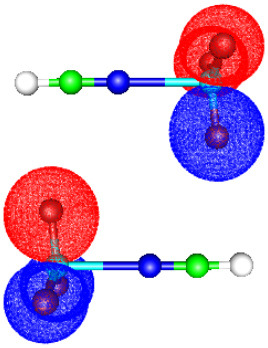

#16, -1.21124 au, B_u

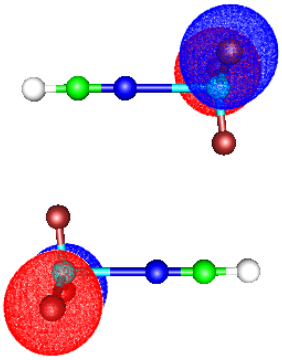

#17, -1.20968 au, B_g

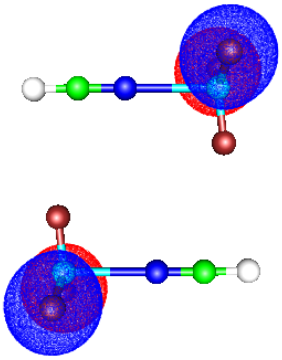

#18, -1.20968 au, A_u

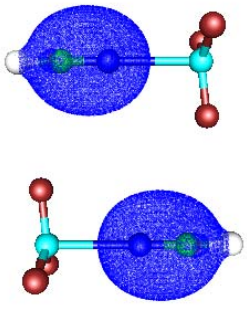

#19, -0.96494 au, A_g

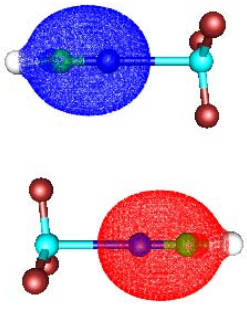

#20, -0.96491 au, B_u

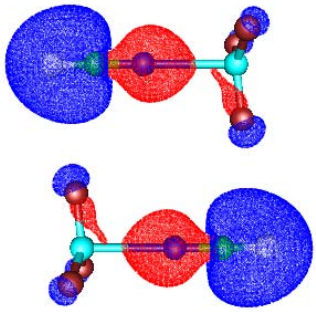

#21, -0.63793 au, A_g

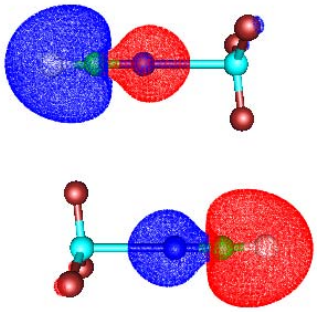

#22, -0.63713 au, B_u

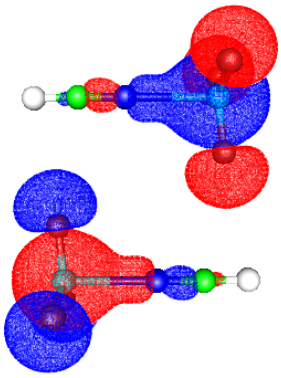

#23, -0.59263 au, B_u

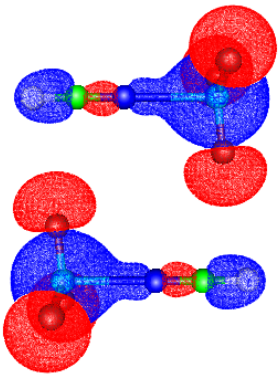

#24, -0.59156 au, A_g

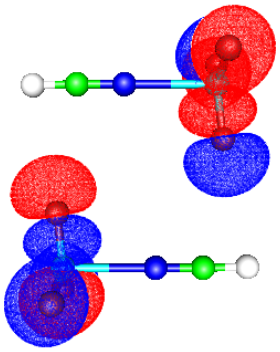

#25, -0.55194 au, B_u

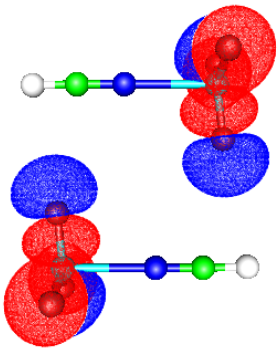

#26, -0.5518 au, A_g

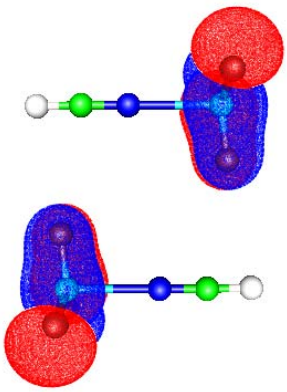

#27, -0.5497 au, A_u

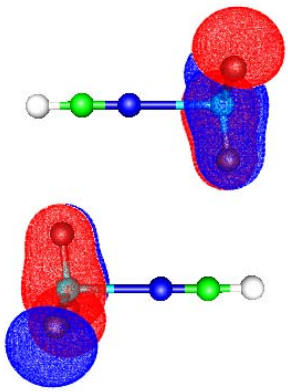

#28, -0.54966 au, B_g

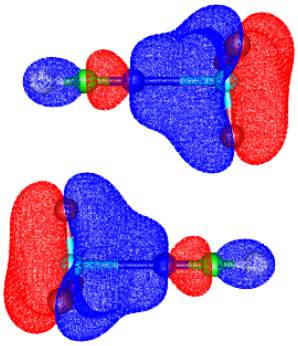

#29, -0.52894 au, A_g

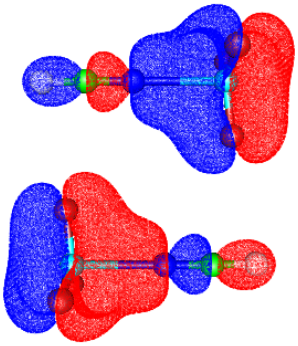

#30, -0.5285 au, B_u

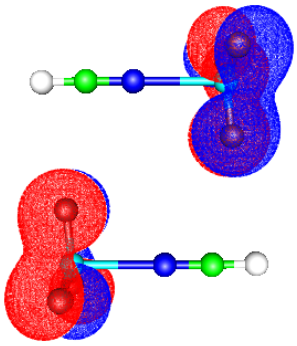

#31, -0.45056 au, B_g

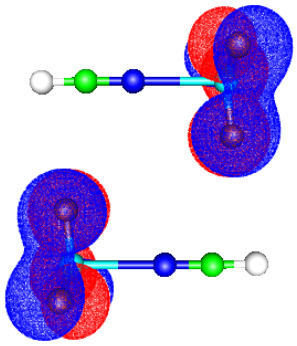

#32, -0.45055 au, A_u

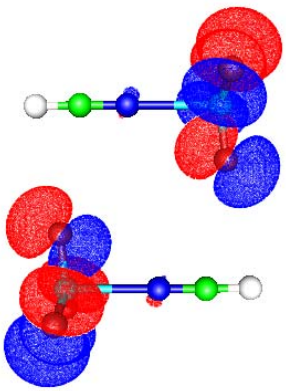

#33, -0.449 au, B_u

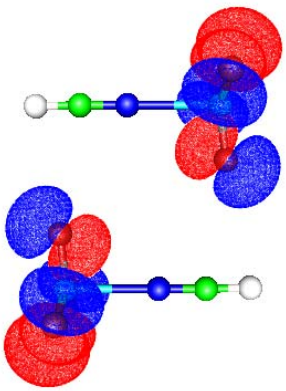

#34, -0.44883 au, A_g

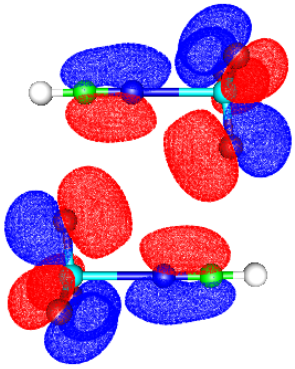

#35, -0.44247 au, A_g

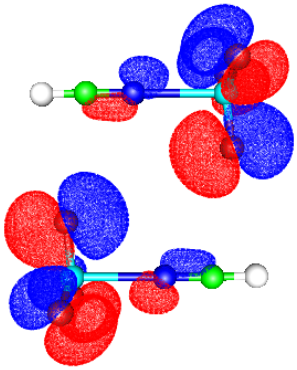

#36, -0.43889 au, B_u

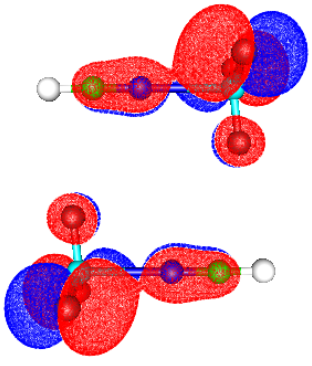

#37, -0.43846 au, A_u

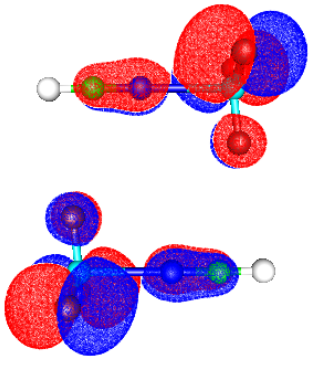

#38, -0.43813 au, B_g

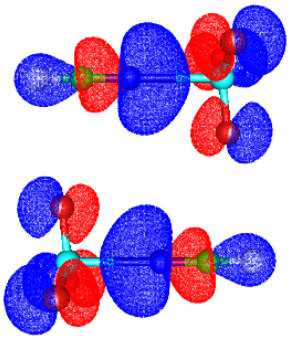

#39, -0.42402 au, A_g

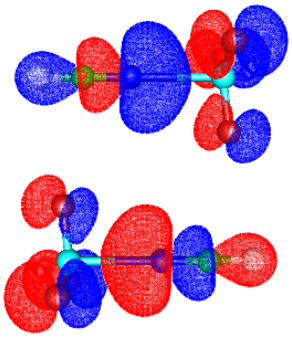

#40, -0.42357 au, B_u

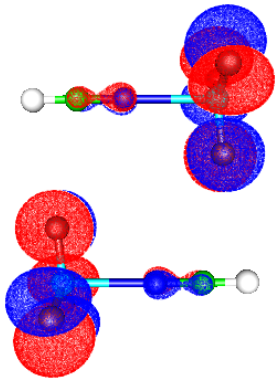

#41, -0.40822 au, B_g

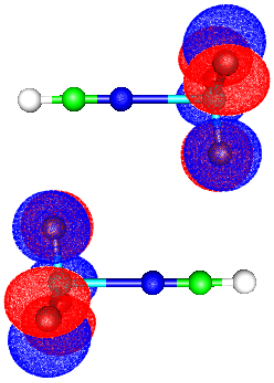

#42, -0.40817 au, A_u

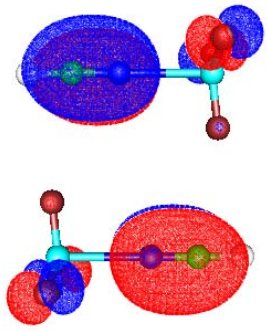

#43, -0.40129 au, B_g

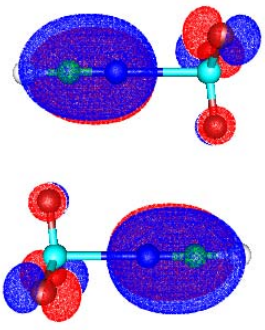

#44, -0.40124 au, A_u

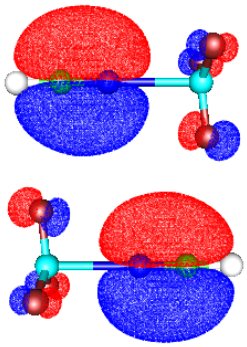

#45, -0.4009 au, B_u

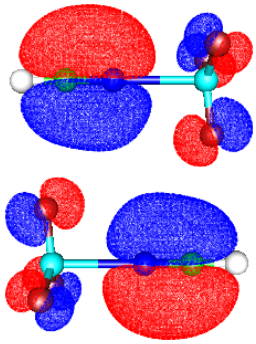

#46, -0.39965 au, A_g

Molecular Orbital Correlation

A correlation diagram, like the one given in the main text for only two times ten orbitals, is already quite cluttered. Therefore, the correlation of the complete set of occupied valence orbitals will not be given in the form of a conventional diagram, but rather simply paired off between the two systems. The orbitals are given in the order: symmetry, then the orbital number in the short-bond dimer followed by the orbital in the long-bond dimer that it correlates with.

A_g	13	⟶	13	B_g	30	⟶	28
B_u	14	⟶	14	A_g	31	⟶	35
A_g	15	⟶	15	B_g	32	⟶	38
B_u	16	⟶	16	A_u	33	⟶	32
B_g	17	⟶	17	B_u	34	⟶	33
A_u	18	⟶	18	A_u	35	⟶	32
A_g	19	⟶	19	A_g	36	⟶	34
B_u	20	⟶	20	B_g	37	⟶	31
A_g	21	⟶	21	B_u	38	⟶	36
B_u	22	⟶	22	A_g	39	⟶	39
B_u	23	⟶	23	B_u	40	⟶	40
A_g	24	⟶	24	B_u	41	⟶	45
A_g	25	⟶	29	B_g	42	⟶	43
B_u	26	⟶	30	A_u	43	⟶	44
B_u	27	⟶	25	A_g	44	⟶	46
A_g	28	⟶	26	A_u	45	⟶	42
A_u	29	⟶	27	B_g	46	⟶	41

Addendum C

Selected Molecular Orbitals of X–Y; X=H_3N, HCN, CH_3CN; Y=BF_3, BH_3, SO_3

Selected molecular orbitals of a series of datively bound complexes. They are to be studied in conjunction with the OPDOS plots and associated text of Section 6.5

H_3N–BF_3

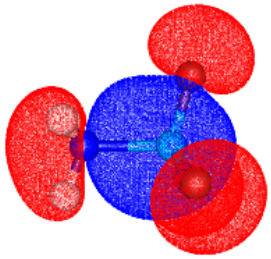

#10

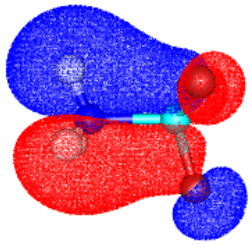

#11

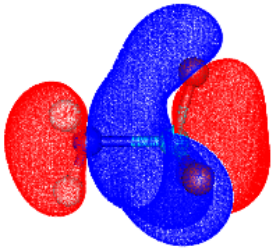

#13

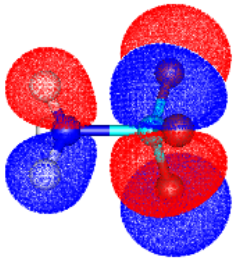

#14

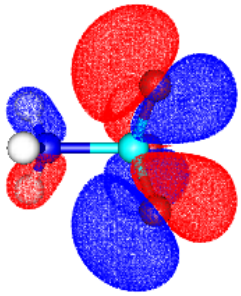

#18

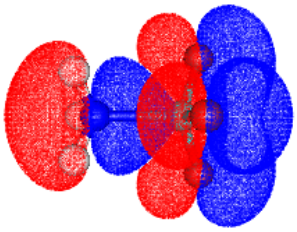

#20

H_3N–BH_3

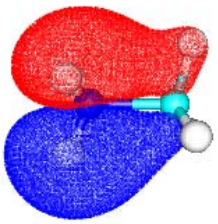

#4

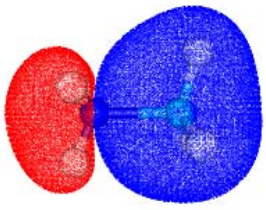

#6

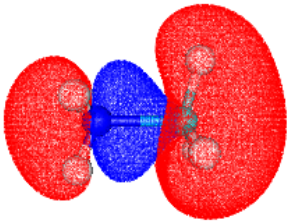

#7

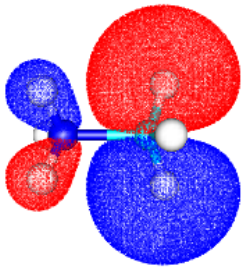

#8

$H_3N–SO_3$

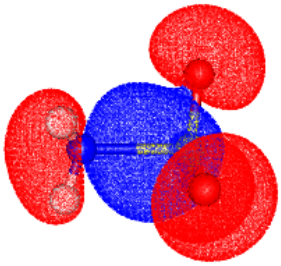

#14

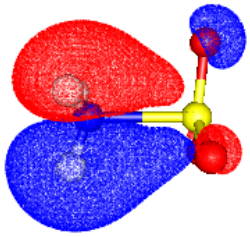

#15

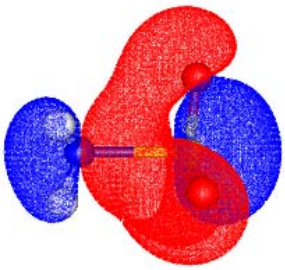

#17

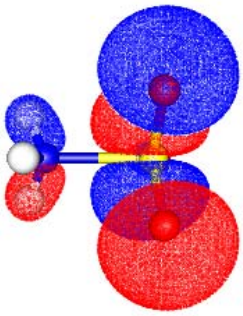

#18

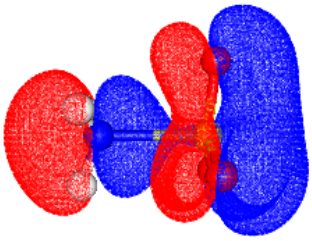

#22

HCN–BF_3

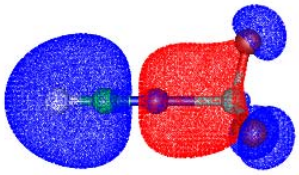

#11

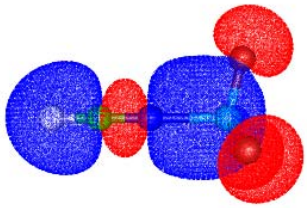

#12

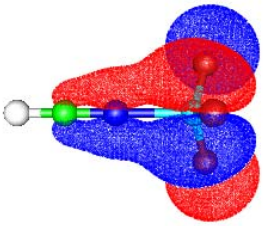

#14

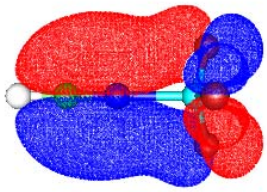

#16

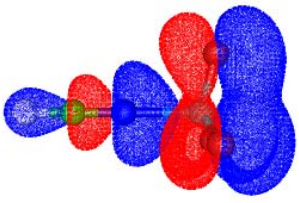

#20

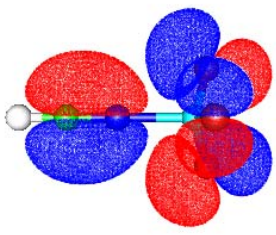

#11

HCN–BH_3

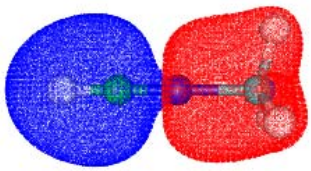

#5

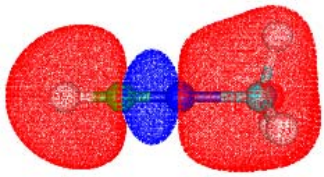

#6

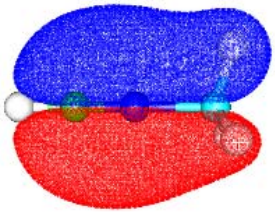

#7

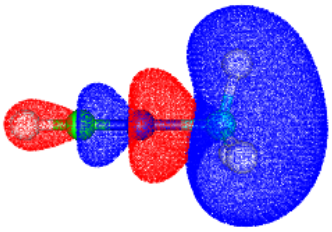

#9

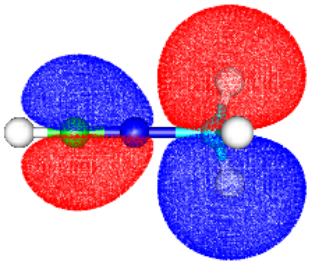

#10

HCN–SO_3

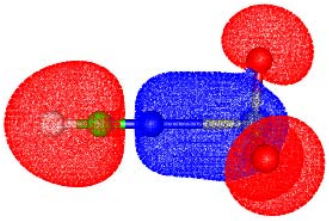

#15

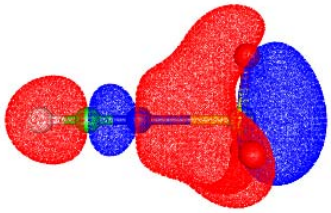

#17

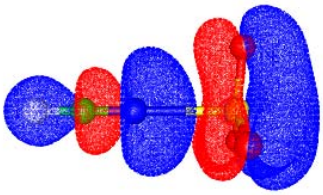

#20

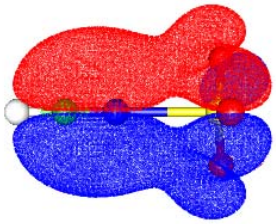

#21

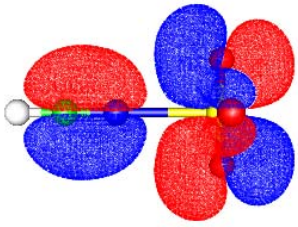

#25

Bibliography

[1] Hargittai, M.; Hargittai, I. *Phys. Chem. Miner.* **1987**, *14*, 413.

[2] Haaland, A. *Angew. Chem. Int. Ed. Engl.* **1989**, *28*, 992.

[3] Bent, H. A. *Chem. Rev.* **1968**, *68*, 587.

[4] Reeve, S. W.; Burns, W. A.; Lovas, F. J.; Suenram, R. D.; Leopold, K. R. *J. Phys. Chem.* **1993**, *97*, 10630.

[5] Burns, W. A.; Leopold, K. R. *J. Am. Chem. Soc.* **1993**, *115*, 11622.

[6] Leopold, K. R. In *Advances in Molecular Structure Research*; Hargittai, M., Hargittai, I., Eds., Vol. 2; Jai Press: Greenwich, USA, 1996.

[7] Leopold, K. R.; Canagaratna, M.; Phillips, J. A. *Acc. Chem. Res.* **1997**, *30*, 57.

[8] Thorne, L. R.; Suenram, R. D.; Lovas, F. J. *J. Chem. Phys.* **1983**, *78*, 167.

[9] Klooster, W. T.; Koetzle, T. F.; Siegbahn, P. E. M.; Richardson, T. B.; Crabtree, R. H. *J. Am. Chem. Soc.* **1999**, *121*, 6337.

[10] Fujiang, D.; Fowler, P. W.; Legon, A. C. *J. Chem. Soc., Chem. Commun.* **1995**, page 113.

[11] Hoard, J. L.; Geller, S.; Cashin, W. M. *Acta Crystallogr.* **1951**, *4*, 396.

[12] Dvorak, M. A.; Ford, R. S.; Suenram, R. D.; Lovas, F. J.; Leopold, K. R. *J. Am. Chem. Soc.* **1992**, *114*, 108.

[13] Swanson, B.; Shrivers, D. F.; Ibers, J. A. *Inorg. Chem.* **1969**, *8*, 2182.

[14] Canagaratna, M.; Phillips, J. A.; Goodfriend, H.; Leopold, K. R. *J. Am. Chem. Soc.* **1996**, *118*, 5290.

[15] Bats, J. W.; Coppens, P.; Koetzle, T. F. *Acta Crystallogr., Sect. B: Struct. Sci.* **1977**, *33*, 37.

[16] Burns, W. A.; Phillips, J. A.; Canagaratna, M.; Goodfriend, H.; Leopold, K. R. *J. Phys. Chem. A* **1999**, *103*, 7445.

[17] Muetterties, E. L. *The Chemistry of Boron and its Compounds;* Wiley: New York, USA, 1967.

[18] Janda, K. C.; Bernstein, L. S.; Steed, J. M.; Novick, S. E.; Klemperer, W. *J. Am. Chem. Soc.* **1978**, *100*, 8074.

[19] Legon, A. C.; Warner, H. E. *J. Chem. Soc., Chem. Commun.* **1991**, page 1397.

[20] Jonas, V.; Frenking, G.; Reetz, M. T. *J. Am. Chem. Soc.* **1994**, *116*, 8741.

[21] Jensen, W. B. *Chem. Rev.* **1978**, *78*, 1.

[22] Rablen, P. R. *J. Am. Chem. Soc.* **1997**, *119*, 8350.

[23] Neogrady, P.; Cernusak, I.; Urban, M.; Bartlett, R. J. *J. Mol. Struct. (Theochem)* **1992**, *90*, 261.

[24] Urban, M.; Bartlett, R. J. *J. Am. Chem. Soc.* **1988**, *110*, 4926.

[25] Marynick, D. S.; Throckmorton, L.; Bacquet, R. *J. Am. Chem. Soc.* **1982**, *104*, 1.

[26] Wong, M. W.; Wiberg, K. B.; Frisch, M. J. *J. Am. Chem. Soc.* **1992**, *114*, 523.

[27] Onsager, L. *J. Am. Chem. Soc.* **1936**, *58*, 1486.

[28] Tapia, O.; Goscinski, O. *Mol. Phys.* **1975**, *29*, 1653.

[29] Wong, M. W.; Frisch, M. J.; Wiberg, K. B. *J. Am. Chem. Soc.* **1991**, *113*, 4776.

[30] Hickling, S. J.; Woolley, R. G. *Chem. Phys. Lett.* **1990**, *166*, 43.

[31] Jiao, H.; Schleyer, P. *J. Am. Chem. Soc.* **1994**, *116*, 7429.

[32] Bühl, M.; Steinke, T.; v. R. Schleyer, P.; Boese, R. *Angew. Chem. Int. Ed. Engl.* **1991**, *30*, 1160.

[33] Jonas, V.; Frenking, G.; Reetz, M. T. *J. Am. Chem. Soc.* **1994**, *116*, 8741.

[34] Dillen, J.; Verhoeven, P. *J. Phys. Chem. A* **2003**, *107*, 2571.

[35] Iglesias, E.; Sordo, T. L.; Sordo, J. A. *Chem. Phys. Lett.* **1996**, *248*, 179.

[36] Cabaleiro-Lago, E. M.; Ríos, M. A. *Chem. Phys. Lett.* **1998**, *294*, 272.

[37] Oh, J. J.; La Barge, M. S.; Matos, J.; Kampf, J. W.; Hilling, II, K. W.; Kuczkowksi, R. L. *J. Am. Chem. Soc.* **1991**, *113*, 4732.

[38] Hankinson, D. J.; Almlöf, J.; Leopold, K. R. *J. Phys Chem.* **1996**, *100*, 6904.

[39] Fiacco, D. L.; Leopold, K. R. *J. Phys. Chem. A* **2003**, *107*, 2808.

[40] Fiacco, D. L.; Hunt, S. W.; Leopold, K. R. *J. Phys. Chem. A* **2000**, *104*, 8323.

[41] Bürgi, H. B.; Dunitz, J. D. *Acc. Chem. Res.* **1983**, *16*, 153.

[42] Eisenstein, O.; Dunitz, J. D. *Isr. J. Chem.* **1980**, *19*, 292.

[43] Murray-Rust, P.; Bürgi, H. B.; Dunitz, J. D. *J. Am. Chem. Soc.* **1975**, *97*, 921.

[44] Murray-Rust, P.; Bürgi, H. B.; Dunitz, J. D. *Acta Crystallogr., Sect. B: Struct. Sci.* **1978**, *34*, 1793.

[45] Pauling, L. J. *J. Am. Chem. Soc.* **1947**, *69*, 542.

[46] Bowden, K. H.; Leopold, K. R.; Chance, K. V.; Klemperer, W. J. *J. Chem. Phys.* **1980**, *73*, 137.

[47] Jurgens, R.; Almlöf, J. *Chem. Phys. Lett.* **1991**, *176*, 263.

[48] Giesen, D. J.; Phillips, J. A. *Phys. Chem. A* **2003**, *107*, 4009.

[49] Wong, M. W.; Wiberg, K. B. *J. Am. Chem. Soc.* **1992**, *114*, 7527.

[50] Mo, Y.; Gao, J. *J. Phys. Chem. A* **2001**, *105*, 6530.

[51] Mo, Y.; Peyerimhoff, S. D. *J. Chem. Phys.* **1998**, *109*, 1687.

[52] Mo, Y.; Zhang, Y.; Gao, J. *J. Am. Chem. Soc.* **1999**, *121*, 5737.

[53] Mo, Y.; Gao, J.; Peyerimhoff, S. D. *J. Chem. Phys.* **2000**, *112*, 5530.

[54] Pearson, R. G. *Chemical Hardness;* Wiley-VCH: Weinheim, Germany, 1997.

[55] Lewis, G. N. *Valence and the Structure of Atoms and Molecules;* The Chemical Catalog Co.: New York, USA, 1923.

[56] Cady, H.; Elsey, H. *J. Chem. Educ.* **1928**, *5*, 1425.

[57] Gay-Lussac, J. L.; Thénard, J. L. *Mem. Phys. Chim. Soc. Arcueil* **1809**, *2*, 210.

[58] Cotton, F. A.; Wilkinson, G. *Advanced Inorganic Chemistry;* John Wiley and Sons: New York, USA, fifth ed., 1988.

[59] Brinck, T.; Murray, J. S.; Politzer, P. *Inorg. Chem.* **1993**, *32*, 2622.

[60] Frenking, G.; Fau, S.; Marchand, C. M.; Grützmacher, H. *J. Am. Chem. Soc.* **1997**, *119*, 6648.

[61] Bessac, F.; Frenking, G. *Inorg. Chem.* **2003**, *42*, 7990.

[62] Deakyne, C. A.; Liebman, J. F. *J. Mol. Struct. (Theochem)* **1991**, *234*, 343.

[63] Ernst, R. D.; Freeman, J. W.; Stahl, L.; Wilson, D. R.; Arif, A. M.; Nuber, B.; Ziegler, M. L. *J. Am. Chem. Soc.* **1995**, *117*, 5075.

[64] Fischer, R. A.; Schulte, M. M.; Weiss, J.; Zsolnai, L.; Jacobi, A.; Huttner, G.; Frenking, G.; Boehme, C.; Vyboishchikov, S. F. *J. Am. Chem. Soc.* **1998**, *120*, 1237.

[65] March, J. *Advanced Organic Chemistry;* John Wiley and Sons: New York, USA, fourth ed., 1992.

[66] Gutmann, V. *The Donor-Acceptor Approach to Molecular Interactions;* Plenum Press: New York, USA, 1978.

[67] Levine, I. N. *Quantum Chemistry;* Prentice-Hall: New Jersey, USA, fifth ed., 2000.

[68] Szabo, A.; Ostlund, N. S. *Modern Quantum Chemistry;* Dover: New York, USA, 1996.

[69] Jensen, F. *Introduction to Computational Chemistry;* John Wiley and Sons: Chichester, England, 1999.

[70] Cramer, C. J. *Essentials of Computational Chemistry;* John Wiley and Sons: Chichester, England, 2002.

[71] Hurley, A. C. *Introduction to the Electron Theory of Small Molecules;* Academic Press: New York, USA, 1976.

[72] Møller, C.; Plesset, M. S. *Phys. Rev.* **1934**, *46*, 359.

[73] Koch, W.; Holthausen, M. C. *A Chemist's Guide to Density Functional Theory;* Wiley-VCH: Weinheim, Germany, 2000.

[74] Thomas, L. H. *Proc. Camb. Phil. Soc.* **1927**, *23*, 542.

[75] Fermi, E. *Rend. Accad. Lincei* **1927**, *6*, 602.

[76] Slater, J. C. *Phys. Rev.* **1951**, *81*, 385.

[77] Bloch, F. *Z. Physik* **1929**, *57*, 545.

[78] Dirac, P. A. M. *Proc. Camb. Phil. Soc.* **1930**, *26*, 376.

[79] Hohenberg, P.; Kohn, W. *Phys. Rev. B* **1964**, *136*, 864.

[80] Kohn, W.; Sham, L. J. *Phys. Rev. A* **1965**, *140*, 1133.

[81] Parr, R. G.; Yang, W. *Density-Functional Theory of Atoms and Molecules;* Oxford University Press: New York, USA, 1989.

[82] Ceperley, D. M.; Alder, B. J. *Phys. Rev. Lett.* **1980**, *45*, 566.

[83] Vosko, S. J.; Wilk, L.; Nusair, M. *Can. J. Phys* **1980**, *58*, 1200.

[84] Perdew, J. P.; Wang, Y. *Phys. Rev. B.* **1992**, *45*, 13244.

[85] Stevens, P. J.; Devlin, J. F.; Chabalowski, C. F.; Frisch, M. J. *J. Phys. Chem.* **1994**, *98*, 11623.

[86] Becke, A. D. *Phys. Rev. A* **1988**, *38*, 3098.

[87] Lee, C.; Yang, W.; Parr, R. G. *Phys. Rev. B* **1988**, *37*, 785.

[88] van Duijneveldt, F. B.; van Duijneveldt-van de Rijdt, J. G. C. M.; van Lenthe, J. H. *Chem. Rev.* **1994**, *94*, 1873.

[89] Mulliken, R. S. *J. Chem. Phys.* **1955**, *23*, 1833.

[90] Weinhold, F. In *Encyclopdedia of Computational Chemistry*; v. R. Schleyer, P., Allinger, N. L., Clark, T., Gasteiger, J., Kollman, P. A., Schaefer, III, H. F., Schreiner, P. R., Eds., Vol. 3; John Wiley and Sons: Chichester, UK, 1998; page 1792.

[91] Reed, A. E.; Curtiss, L. A.; Weinhold, F. *Chem. Rev.* **1988**, *88*, 899.

[92] Löwdin, P. O. *Phys. Rev.* **1955**, *97*, 1474.

[93] Cox, S. R.; Williams, D. E. *J. Comput. Chem.* **1981**, *2*, 304.

[94] Singh, U. C.; Kollman, P. A. *J. Comput. Chem.* **1984**, *5*, 129.

[95] Besler, B. H.; Mertz, Jr., K. M.; Kollman, P. A. *J. Comput. Chem.* **1990**, *11*, 431.

[96] Bader, R. F. W. *Atoms in Molecules. A Quantum Theory;* Oxford University Press: New York, USA, 1990.

[97] Popelier, P. *Atoms in Molecules. An Introduction;* Prentice Hall: Essex, UK, 2000.

[98] Atkins, P.; de Paula, J. *Atkins' Physical Chemistry;* Oxford University Press: New York, USA, seventh ed., 2002.

[99] Rappé, A. K.; Casewit, C. J.; Colwell, K. S.; Goddard, III, W. A.; Skiff, W. M. *J. Am. Chem. Soc.* **1992**, *114*, 10024.

[100] Castonguay, L. A.; Rappé, A. K. *J. Am. Chem. Soc.* **1992**, *114*, 5832.

[101] Rappé, A. K.; Colwell, K. S. *Inorg. Chem.* **1993**, *32*, 3438.

[102] Gaussian 98, Revision A.7. Frisch, M. J.; Trucks, G. W.; Schlegel, H. B.; Scuseria, G. E.; Robb, M. A.; Cheeseman, J. R.; Zakrzewski, V. G.; Montgomery, Jr., J. A.; Stratmann, R. E.; Burant, J. C.; Dapprich, S.; Millam, J. M.; Daniels, A. D.; Kudin, K. N.; Strain, M. C.; Farkas, O.; Tomasi, J.; Barone, V.; Cossi, M.; Cammi, R.; Mennucci, B.; Pomelli, C.; Adamo, C.; Clifford, S.; Ochterski, J.; Petersson, G. A.; Ayala, P. Y.; Cui, Q.; Morokuma, K.; Malick, D. K.; Rabuck, A. D.; Raghavachari, K.; Foresman, J. B.; Cioslowski, J.; Ortiz, J. V.; Baboul, A. G.; Stefanov, B. B.; Liu, G.; Liashenko, A.; Piskorz, P.; Komaromi, I.; Gomperts, R.; Martin, R. L.; Fox, D. J.; Keith, T.; Al-Laham, M. A.; Peng, C. Y.; Nanayakkara, A.; Gonzalez, C.; Challacombe, M.; Gill, P. M. W.; Johnson, B.; Chen, W.; Wong, M. W.; Andres, J. L.; Gonzalez, C.; Head-Gordon, M.; Replogle, E. S.; .; Pople, J. A.; Gaussian, Inc., Pittsburgh, PA, USA, **1998**.

[103] Gaussian 03, Revision B.05. Frisch, M. J.; Trucks, G. W.; Schlegel, H. B.; Scuseria, G. E.; Robb, M. A.; Cheeseman, J. R.; Montgomery, Jr., J. A.; Vreven, T.; Kudin, K. N.; Burant, J. C.; Millam, J. M.; Iyengar, S. S.; Tomasi, J.; Barone, V.; Mennucci, B.; Cossi, M.; Scalmani, G.; Rega, N.; Petersson, G. A.; Nakatsuji, H.; Hada, M.; Ehara, M.; Toyota, K.; Fukuda, R.; Hasegawa, J.; Ishida, M.; Nakajima, T.; Honda, Y.; Kitao, O.; Nakai, H.; Klene, M.; Li, X.; Knox, J. E.; Hratchian, H. P.; Cross, J. B.; Bakken, V.; Adamo, C.; Jaramillo, J.; Gomperts, R.; Stratmann, R. E.; Yazyev, O.; Austin, A. J.; Cammi, R.; Pomelli, C.; Ochterski, J. W.; Ayala, P. Y.; Morokuma, K.; Voth, G. A.; Salvador, P.; Dannenberg, J. J.; Zakrzewski, V. G.; Dapprich, S.; Daniels, A. D.; Strain, M. C.; Farkas, O.; Malick, D. K.; Rabuck, A. D.; Raghavachari, K.; Foresman, J. B.; Ortiz, J. V.; Cui, Q.; Baboul, A. G.; Clifford, S.; Cioslowski, J.; Stefanov, B. B.; Liu, G.; Liashenko, A.; Piskorz, P.; Komaromi, I.; Martin, R. L.; Fox, D. J.; Keith, T.; Al-Laham, M. A.; Peng, C. Y.; Nanayakkara, A.; Challacombe, M.; Gill, P. M. W.; Johnson, B.; Chen, W.; Wong, M. W.; Gonzalez, C.; Pople, J. A.; Gaussian, Inc., Wallingford, CT, USA, **2004**.

[104] Gilbert, T. M. *J. Phys. Chem. A* **2004**, *108*, 2550.

[105] Becke, A. D. *J. Chem. Phys.* **1993**, *98*, 5648.

[106] Becke, A. D. *J. Chem. Phys.* **1997**, *107*, 8554.

[107] Hamprecht, F. A.; Cohen, A. J.; Tozer, D. J.; Handy, N. C. *J. Chem. Phys.* **1998**, *109*, 6264.

[108] Boese, A. D.; Martin, J. M. L.; Handy, N. C. *J. Chem. Phys.* **2003**, *119*, 2005.

[109] Adamo, C.; Barone, V. *J. Chem. Phys.* **1998**, *108*, 664.

[110] Lynch, B. J.; Fast, P. L.; Harris, M.; Truhlar, D. G. *J. Phys. Chem. A* **2000**, *104*, 4811.

[111] Perdew, J. P. In *Electronic Structure of Solids*; Ziesche, P., Eschrig, H., Eds.; Akademie Verlag: Berlin, Germany, 1991; page 11.

[112] Boys, S. F.; Bernardi, F. *Mol. Phys.* **1970**, *19*, 553.

[113] Simon, S.; Duran, M.; Dannenberg, J. J. *J. Chem. Phys.* **1996**, *105*, 11024.

[114] Howard, J. A. K.; Hoy, V. J.; O'Hagan, D.; Smith, G. T. *Tetrahedron* **1996**, *52*, 12613.

[115] Merino, G.; Bakhmutov, V. I.; Vela, A. *Phys. Chem. A* **2002**, *106*, 8491.

[116] Kulkarni, S. A.; Srivastava, A. K. *Phys. Chem. A* **1999**, *103*, 2836.

[117] NBO 5.0. Glendening, E. D.; Badenhoop, J. K.; Reed, A. E.; Carpenter, J. E.; Bohmann, J. A.; Morales, C. M.; Weinhold, F.; Theoretical Chemistry Institute, University of Wisconsin, Wisconsin, USA, **2001**.

[118] Cremer, D.; Kraka, E. *Angew. Chem., Int. Ed. Engl.* **1984**, *23*, 627.

[119] Morokuma, K. *J. Chem. Phys.* **1971**, *55*, 1236.

[120] Ziegler, T.; Rauk, A. *Theor. Chim. Acta* **1977**, *46*, 1.

[121] te Velde, G.; Bickelhaupt, F. M.; van Gisbergen, S. J. A.; Guerra, C. F.; Baerends, E. J.; Snijders, J. G.; Ziegler, T. *J. Comput. Chem.* **2001**, *22*, 931.

[122] Guerra, C. F.; Snijders, J. G.; te Velde, G.; Baerends, E. J. *Theor. Chem. Acc.* **1998**, *99*, 391.

[123] ADF 2004.1. SCM, Theoretical Chemistry, Vrije Universiteit, Amsterdam, The Netherlands, **2004**.

[124] Perdew, J. P. *Phys. Rev. B* **1986**, *33*, 8822.

[125] Snijders, J. G.; Baerends, E. J.; Vernooijs, P. *At. Nucl. Data Tables* **1982**, *26*, 483.

[126] AOmix program. Gorelsky, S. I.; Stanford University.

[127] Gorelsky, S. I. *J. Organomet. Chem.* **2001**, *635*, 187.

[128] Timoshkin, A. Y.; Suvorov, A. V.; Bettinger, H. F.; Schaefer, III, H. F. *J. Am. Chem. Soc.* **1999**, *121*, 5687.